2011

Forward Error Correction in Memoryless Optical Modulation

David Rhys Jones
University of North Florida

FORWARD ERROR CORRECTION IN MEMORYLESS OPTICAL MODULATION FORMATS

by

David Rhys Jones

A thesis submitted to the

School of Engineering

in partial fulfillment of the requirements for the degree of

Master of Science in Electrical Engineering

UNIVERSITY OF NORTH FLORIDA

SCHOOL OF ENGINEERING

August 2011

The thesis "Forward error correction in memoryless optical modulation formats" submitted by David R. Jones in partial fulfillment of the requirements for the degree of Master of Science in Electrical Engineering has been

Approved by this committee: Date

Signature deleted

Aug 4, 2011

Alan Harris, PhD
Thesis Advisor and Committee Chairperson

Signature deleted

Aug. 8, 2011

Gerald Merckel, PhD

Signature deleted

Aug 4-2011

Nick Hudyma, PhD PE

Accepted for the School of Engineering:

Signature deleted

August 18, 2011

Murat Tiryakioglu, PhD
Director of the School of Engineering

Accepted for the College of Computing, Engineering, and Construction

Signature deleted

19 August, 2011

Mark A. Tumeo, PhD
Dean of the College of Computing, Engineering, and Construction

Accepted for the University

Signature deleted

Nov. 8, 2011

Len Roberson, PhD
Dean of the Graduate School

To my wife Donna, no matter how hard the storm rages,

I will always find peace by your side

ACKNOWLEDGEMENT

First I would like to thank the faculty and staff at the College of Computing, Engineering and Construction for creating an environment conducive to learning. I also would like to thank my father Dave, my daughter Kippy and my son Rhys their sacrifices have not gone unnoticed. I would also like to thank the other members of my thesis committee Gerald Merkel and Nick Hudyma.

Last but not least, this thesis would not have been completed if it had not been for the contribution, guidance and support of Alan Harris, without whom I would not be writing this acknowledgement. Words are simply inadequate to express my gratitude for what he helped me accomplish.

I learned a while ago if you don't know what to say, just say it and mean it. Alan, Thank you.

TABLE OF CONTENTS

LIST OF FIGURES

LIST OF TABLES

ABSTRACT

The unprecedented growth in demand for digital media has led to an all-time high in society's demand for information. This demand will in all likelihood continue to grow as technology such as 3D television service, on-demand video and peer-to-peer networking continue to become more common place. The large amount of information required is currently transmitted optically using a wavelength division multiplexing (WDM) network structure. The need to increase the capacity of the existing WDM network infrastructure efficiently is essential to continue to provide new high bandwidth services to end-users, while at the same time minimizing network providers' costs. In WDM systems the key to reducing the cost per transported information bit is to effectively share all optical components. These components must operate within the same wavelength limited window; therefore it is necessary to place the WDM channels as close together as possible. At the same time, the correct modulation format must be selected in order to create flexible, cost-effective, high-capacity optical networks. This thesis presents a detailed comparison of Differential Quadrature Phase Shift Keying (DQPSK) to other modulation formats. This comparison is implemented through a series of simulations in which the bit error rate of various modulation formats are compared both with and without the presence of forward error correction techniques. Based off of these simulation results, the top performing modulation formats are placed into a multiplexed simulation to assess their overall robustness in the face of multiple filtering impairments.

Chapter 1

INTRODUCTION

Optical communication systems can support terabit per second capacities over great distances, which make them ideal for high-capacity line based networks. The major impetus driving the expansion of the information carrying capacity of current wavelength division multiplexing (WDM) systems is society's increased demand for information. The key to meeting these demands for data in a cost effective manner is to create effective sharing by all channels of all optical components within a WDM network. This effectively creates a cost reduction in the cost per transported information bit. Advanced modulation formats are essential to the cost effective transport of data through the network.

The purpose of this thesis is to evaluate the performance of an advanced modulation format, differential quadrature phase shift keying (DQPSK). This performance comparison is implemented by evaluating DQPSK against two other modulation formats, differential phase shift keying (DPSK) and carrier suppressed return to zero (CSRZ). DPSK has been selected due to recent research focus on memoryless modulation formats. CSRZ will be used for a comparison of a format with memory and is considered a pseudo-multilevel intensity format. DQPSK has been selected based on current research focuses in the area of memoryless multilevel formats.

The remainder of this thesis is organized as follows. Chapter 2 presents an overview of optical communication networks, along with impairments to transmission within optical networks with the identification of the most detrimental impairments to cost effective transmission. The two most detrimental impairments identified will be the focus of the research.

Chapter 3 contains an explanation of the advanced modulation formats to be studied, The components necessary in the design of these transmitters to provide stable and accurate data transmission, an explanation of alphabet size and a mathematical description of the formats to be studied and their merits.

Chapter 4 presents a discussion of the types of common forward error correction (FEC) algorithms being applied in optical networks long with the justification of their choice for the work presented in this thesis.

Chapter 5 describes the simulations designed to test the identified network impairments and to effectively measure their impact on the modulation method being tested. Furthermore, it describes the sequence of steps followed to demonstrate the unbiased generation of data to be analyzed.

Chapter 6 describes the results of the simulations conducted and the methodology used to determine the most effective formats.

Chapter 7 contains concluding remarks, as well as recommendations for future research areas identified by this thesis work.

Appendix A contains a list of acronyms used in this thesis, and Appendix B contains the tables of the raw data collected prior to analysis.

Chapter 2

OVERVIEW OF FIBER OPTIC COMMUNICATION SYSTEMS

This chapter will define a fiber optic communication system. It contains a discussion of the advantages of fiber optic communication systems, the structure of fiber, how light propagates within a fiber, the benefits of wavelength division multiplexing, impairments to efficient communication within a fiber network and finally how the efficiency of one fiber optic network can be compared to another.

2.1 Overview of Fiber System

Fiber optic communication systems contain the same basic elements as other communication systems. As shown in Figure 2.1, a fiber optic communication system consists of a transmitter, an information channel and a receiver. In a fiber network the message enters the transmitter which consists of a modulator, a carrier source and a channel coupler. The information channel is the fiber optic cable which contains the glass transmission core and is encased in cladding to protect the glass and copper wire for powering necessary electronic components.

Fiber optic networks like all communication networks operate utilizing the same classification of components as other networks. They are comprised of transmitters, receivers, amplifiers, filters and the medium that connect them together to form the

network. The transmitter consists of a light source, its associated drive technology (optoelectronics), a cable which protects the fiber, optical amplifiers to increase transmission distance, filters to route signals to their intended destinations, a receiver which contains the photodetector device, and signal decoding circuitry as is shown in Figure 2.1.

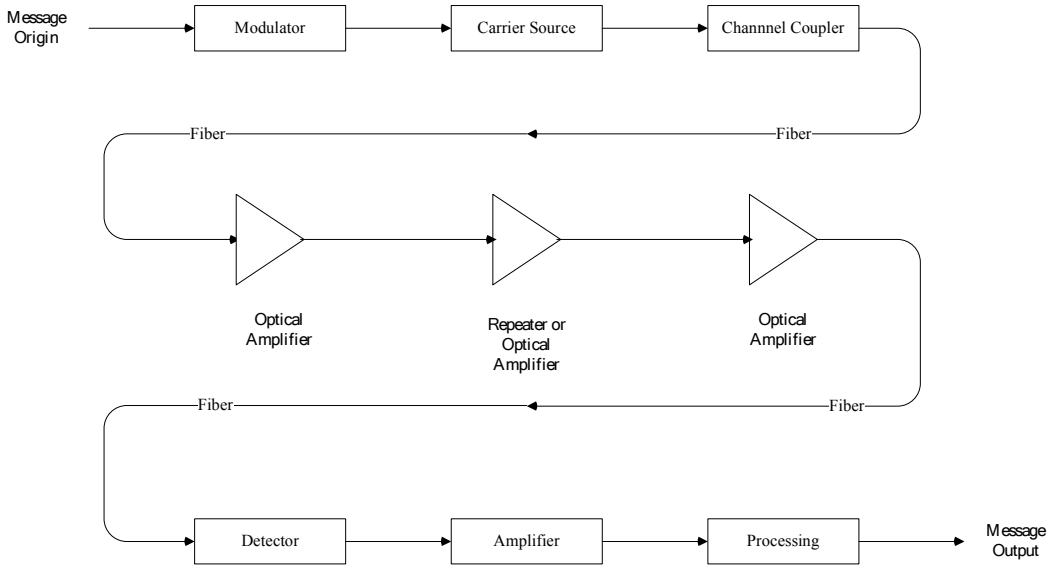

Figure 2.1 Fiber optic network [1]

Just as with other transmission mediums, such as wire and coaxial cable, optical fibers can be installed above or below ground, underwater, through existing ducting or aerially along with power lines. Actual length of fiber cable is primarily determined by practical considerations such as reel size and weight.

2.1.1 Advantages of Optical Fiber Networks

The basic material for fiber is silicon dioxide which is plentiful; fiber is small and light therefore easy to install, and fiber can be produced that has very low transmission losses. Despite the fragility associated with glass, optical fiber is made very rugged and serviceable by encasing the glass in a polymer material. No electrical current travels within the optical fiber so there is no electromagnetic radiation emanating from the fiber; the light is trapped within the glass. Therefore light cannot accidently couple into the fiber from outside. Because of these reasons fiber has excellent rejection of radio frequency interference (RFI) and electromagnetic interference (EMI). It also does not pick up and propagate electromagnetic pulses (EMP) caused by nuclear blasts. Fiber by the very nature of how the light propagates offers a degree of security and privacy and a fiber can be repaired without powering down the network.[1]

2.2 Structure of Optical Fiber

Optical fiber is a dielectric waveguide that operates at optical frequencies. It is normally cylindrical; it confines the electromagnetic energy of the light to within the fiber and directs the propagation of the light in a direction parallel to the fibers axis.

Many configurations of the optical waveguide can be used. The most widely used structure is the single solid dielectric cylinder of radius a and a refractive index of n_1 which is approximately 1.48 as shown in Figure 2.2. The cylinder of radius a is known as

the core. The core is surrounded by another solid dielectric material the cladding which has a refractive index of n_2 which is slightly less than n_1. The difference in range between the refractive indexes is between 1 and 3 percent for multimode fiber and 0.2 to 1.0 for single mode fiber [2].

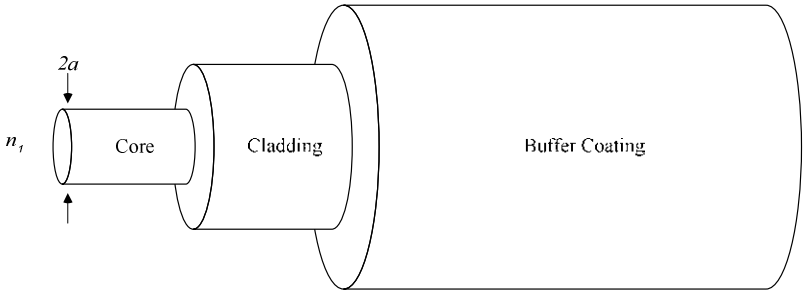

$$n_{core} > n_{cladding}$$

Figure 2.2 Structure of fiber optic cable[1].

2.3 Light Propagation in Fiber

Light has both wave and particle properties. To describe the propagation of the light along the waveguide both must be addressed. A ray of light travels along the core of a step index fiber at an angle such that total internal reflection occurs. The refractive index of the core is larger causing the fiber to act as a waveguide and propagate the electromagnetic field along the fiber core. While fibers are manufactured in various forms one of the most common is a step-index fiber. The second form is manufactured so the refractive index varies as a function of radial distance from the center of the fiber, this is known as graded index fiber. In step-index fiber total internal reflection occurs when the light ray strikes the core-cladding interface at the angle is defined by Snell's law. The

result of reflection causes the light ray to follow a zigzag path along the fiber core crossing the axis of the core after each reflection. With graded index fiber the light is repeatedly bent toward the greater refractive index located at the center of the fiber's core. This process is repeated as the ray crosses the central axis of the fiber allowing the light to propagate along the fibers core, as shown in Figure 2.3.

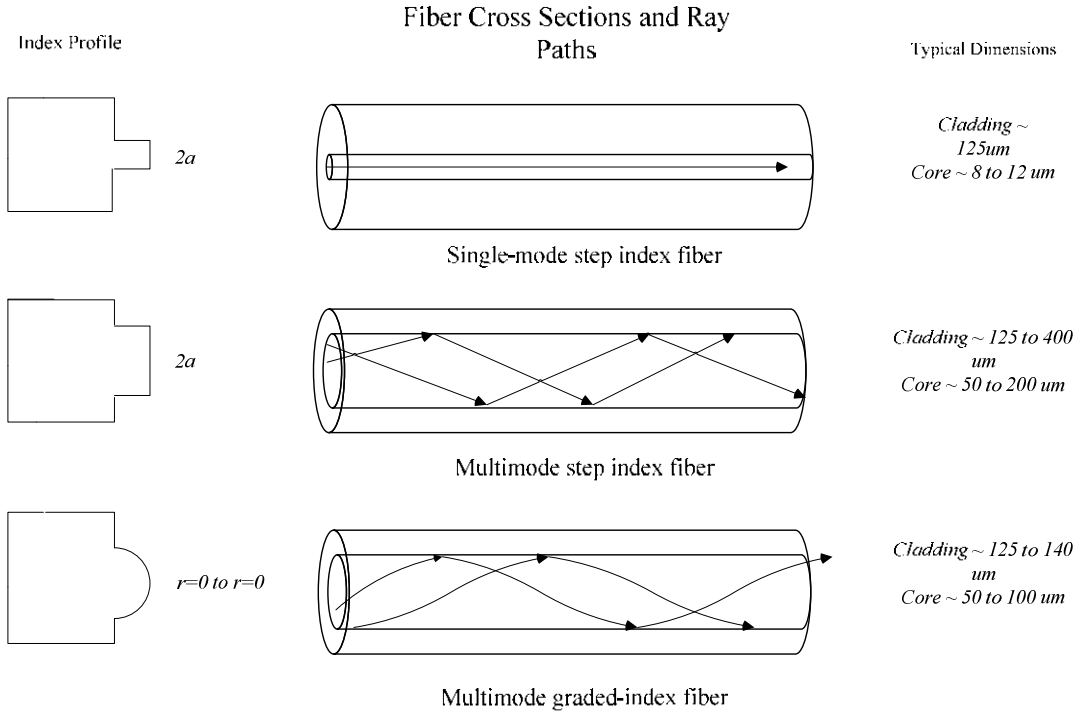

Figure 2.3 Fiber Index profiles [2]

The propagation can also be described as a set of guided electromagnetic waves called modes of the waveguide (fiber core). A closer look at an optical fiber reveals how light waves travel through the core. The optical signal travels through the fiber as an electromagnetic wave. The standard wave equations for this journey are derived from Maxwell's equations, assuming a linear, isotropic dielectric material having no currents or free charges. The propagation of an electromagnetic field along the z axis in cylindrical

coordinates (r, φ, z) takes the form of Equations 2.1 and 2.2. The electric field E and magnetic field H are

$$\vec{E} = \overrightarrow{E_0}(r,\varphi)e^{j(\omega t-\beta z)} \tag{2.1}$$

$$\vec{H} = \overrightarrow{H_0}(r,\varphi)e^{j(\omega t-\beta z)} \tag{2.2}$$

By inserting Equation 2.1 and 2.2 into Maxwell's curl Equations 2.3 and 2.4 respectively

$$\nabla \times \vec{E} = -\frac{\delta \vec{B}}{\delta t} \tag{2.3}$$

$$\nabla \times \vec{H} = \frac{\delta \vec{D}}{\delta t} \tag{2.4}$$

Mathematical manipulation yields Equations 2.5 and 2.6 which describe the transverse fields of an electromagnetic field.

$$\frac{\delta^2\overrightarrow{E_z}}{\delta r^2} + \frac{1}{r}\frac{\delta\overrightarrow{E_z}}{\delta r} + \frac{1}{r^2}\frac{\delta^2\overrightarrow{E_z}}{\delta \varphi^2} + q^2\vec{E} = 0 \tag{2.5}$$

$$\frac{\delta^2\overrightarrow{H_z}}{\delta r^2} + \frac{1}{r}\frac{\delta\overrightarrow{H_z}}{\delta r} + \frac{1}{r^2}\frac{\delta^2\overrightarrow{H_z}}{\delta \varphi^2} + q^2\vec{H} = 0 \tag{2.6}$$

These fields can be visualized as shown in Figure 2.4.

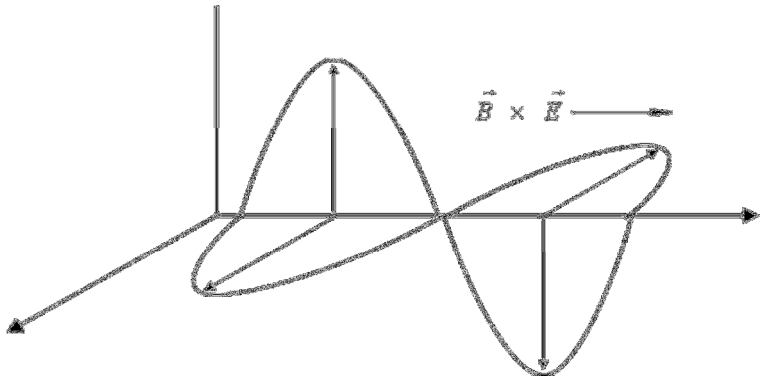

Figure 2.4 Propagation of light along the z axis of fiber optic cable [2]

2.4 Wavelength Division Multiplexed (WDM) Systems

In standard point-to-point links, a single fiber line has one optical source and a photodetector at the receiving end. Since optical light sources can be generated with a very narrow linewidth this type of transmission utilizes a very small portion of the available bandwidth of the fiber. A very powerful benefit of fiber optic communication systems is the ability to send many wavelengths along a single fiber simultaneously; generally in the 1270 nm to 1350 nm spectral band and the 1480 nm to 1600 nm spectral band. The technology of combining a number of wavelengths onto a single fiber is known as wavelength division multiplexing (WDM) as shown in Figure 2.5. Conceptually WDM is essentially frequency-division multiplexing only at optical frequencies. Proper spacing of the different wavelengths is needed to avoid interchannel interference. Current optical networks are operating at bitrates of 40GHz and spectral spacing of 0.4nm [2]with an available bandwidth of approximately 27nm. This translates into terabits of data transmitted at one time on a single network. Literature often uses the term dense wavelength division multiplexing (DWDM) in contrast to WDM. This term does not denote a precise operating condition, in general it refers to spacing's denoted by ITU_T.692 (International Telecommunications Union-Telecommunication Standardization Sector) [2].

They also suffer from essentially the same impairments to their operation such as attenuation, noise and distortion albeit generated differently so the design to compensate for their impact also differs.

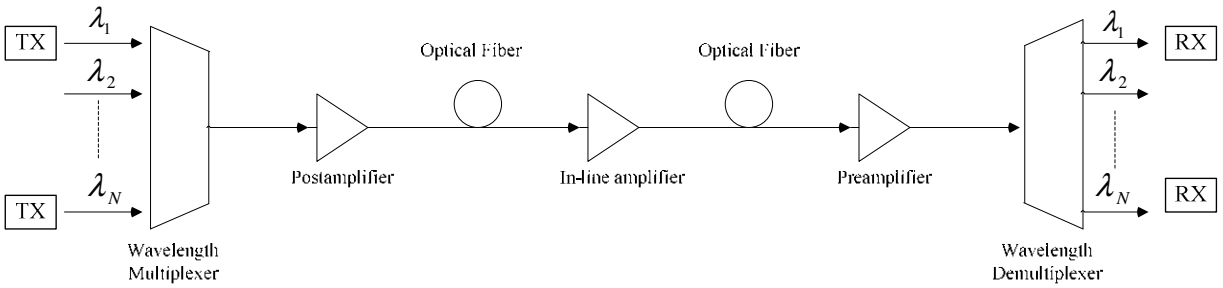

Figure 2.5 WDM network [2]

2.5 Impairments to Communication Signals with Fiber Optics

A principal characteristic of fiber is that the attenuation is a wavelength dependent phenomenon as shown in Figure 2.6 [3][2]. The basic attenuation mechanisms present in an optical fiber are absorption, scattering and radiative losses of optical energy. Absorption is related to the fiber material, scattering is caused by both the fiber material and imperfects created in manufacture of the fiber and radiative losses originate from perturbations of fiber geometry.

2.5.1 Chromatic Dispersion

Chromatic dispersion (CD) has been the focus of extensive research in the past where the optical field *E(t)* propagating along the z-axis in a fiber is described by Equation 2.7. This equation applies to a fiber with uniform loss, where $\alpha(z) = \alpha_0$ (the fiber loss coefficient) and with distributed amplification. [4];

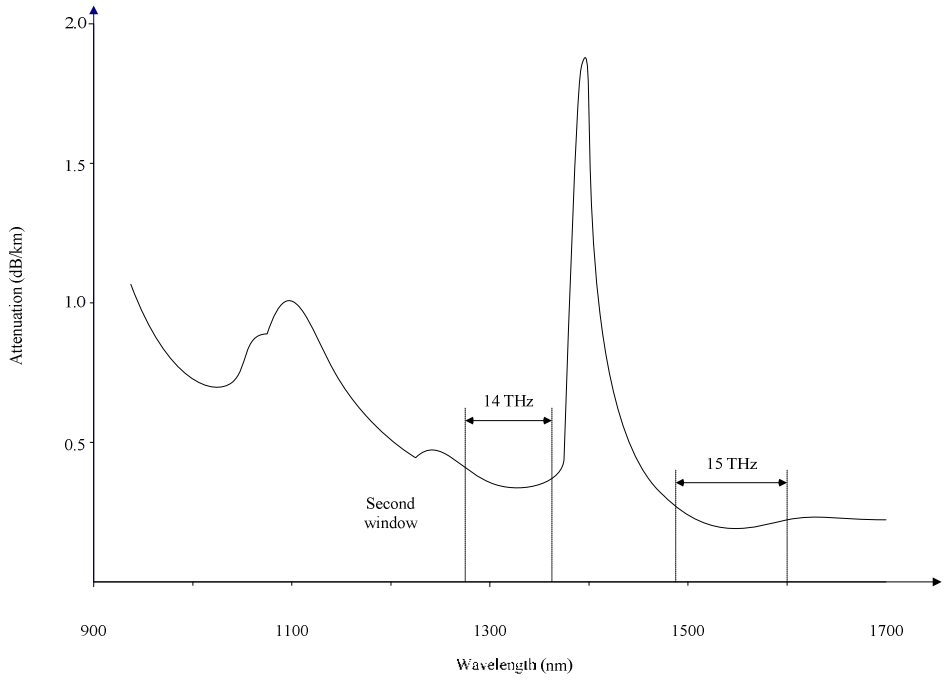

Figure 2.6 Transmission bandwidth versus attenuation [2].

$$\frac{\delta E}{\delta t}+\frac{i}{2}\beta_2(z)\frac{\delta^2 E}{\delta t^2}-\frac{1}{6}\beta_3(z)\frac{\delta^3 E}{\delta t^3}+\frac{\alpha(z)}{2}E(t)=0 \qquad (2.7)$$

The parameter $\beta_2(z)$ is called the group velocity dispersion (GVD), or chromatic dispersion (CD) denoted as D(z) in Equation2.8 [2].

$$D(z)=\ -\frac{2\pi c}{\lambda^2}\beta_2(z);\ [ps/(km*nm)] \qquad (2.8)$$

$\beta_3(z)$ accounts for the change in GVD with angular frequency, it is referred to as the third-order CD parameter, it is related to the dispersion slope $S(z)$ by Equation 2.9

$$S(z)\equiv\frac{dD}{d\lambda}=\frac{4\pi}{\lambda^3}\beta_2(z)+\left(\frac{2\pi c}{\lambda^2}\right)^2\beta_3(z) \qquad (2.9)$$

In Equation 2.9 the term β_3 can be thought of as the effective change of β_2 between channels in a WDM system, rather than an impact from the WDM channel itself.CD produces a spread in the propagation speed of the differing spectral components

contained with the optically modulated signal, Figure 2.9. That results in signal distortions and typically by pulse broadening.

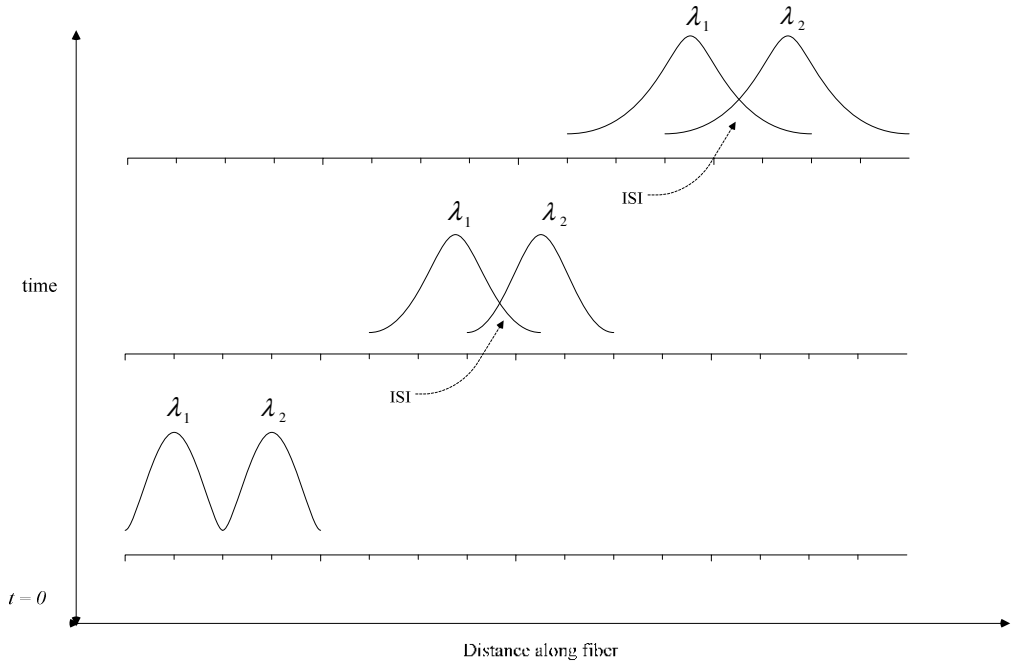

Figure 2.7 Effect of chromatic dispersion on optically modulated signal

This pulse spreading can result in intersymbol interference (ISI), which degrades the signal quality by corrupting the amplitude of the 1-bit or 0-bit through optical interference between the periodic wave form created by the symmetrical and periodic transfer function of the CD. CD can have a positive or negative value associated with it based upon the fibers material composition and geometry. This property is used during the manufacture of fibers to produce dispersion compensating fiber. This fiber is used to counteract the chromatic dispersion accumulated along the optical pathway [4].

2.5.2 Attenuation Fiber, Propagation Losses and Amplification

Single mode fibers are a very transparent medium with attenuation coefficients of approximately $0.2\ dB/km$ across a bandwidth of multiple terahertz. The attenuation experienced over long distances does require the use of optical amplifiers (OA) every 40 to 100 km depending on the system Figure 2.8. In contrast to many RF amplifiers many OA do not introduce distortion to the amplified signal. They do, however, exhibit constant gain across the transmitted spectrum even at bitrates of 40 GHz. The primary impact is amplified spontaneous emission (ASE) beat noise [5, 6].

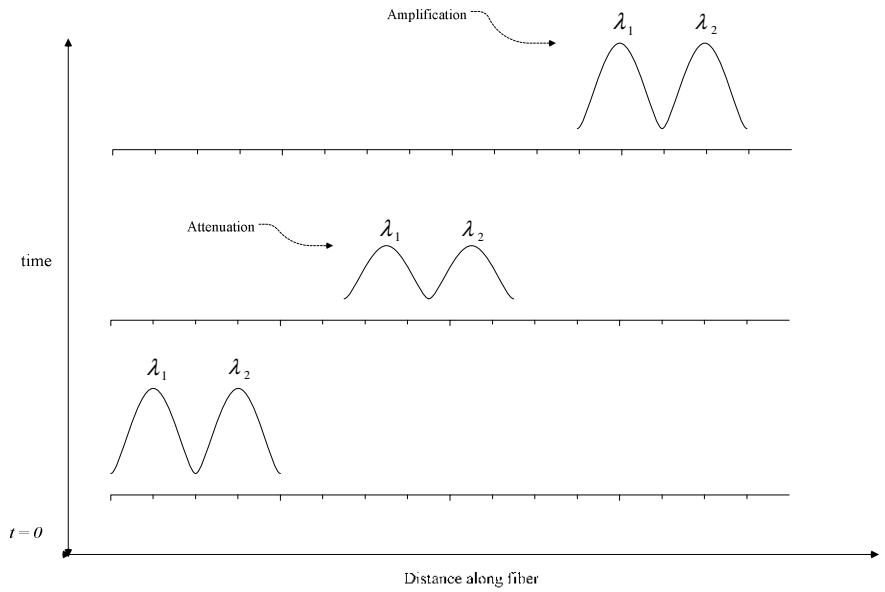

Figure 2.8 Attenuation and amplification along an optical fiber

2.5.3 Amplified Spontaneous Emission

Amplified Spontaneous Emission (ASE) will be discussed in the context of crosstalk in optical add-drop multiplexers (OADMs), which is not the same phenomenon as ASE beat noise encountered during fiber propagation of information. Fiber induced beat-noise is Gaussian noise. The Gaussian noise generated within a fiber is typically constant "white" noise across the spectrum. Unlike the ASE beat noise from coherent DWDM crosstalk which is strongly correlated to the number of bits [7] and occurs as error bursts. This will be discussed further in section 2.5.7.2

2.5.4 Multipath Interference

Multipath interference (MPI) is the coherent interference of a signal with the residual of signals with the same wavelength [8]. These signals can create multiple reflections of the desired signal due to imperfect fiber connections of more fundamentally double Rayleigh back scattering in Raman-Amplified systems. In optically routed networks, MPI can also arise from OADMs. In a complete analogy to ASE beat noise and DWDM crosstalk, MPI beat noise manifests itself at the square-law detection. The impact of MPI depends on a number of interferers causing MPI. In general RZ and chirped modulation formats are less susceptible to MPI due to reduced signal-MPI beat noise[9].

2.5.5 Polarization Mode Dispersion

Polarization mode dispersion (PMD) results from the fact that light signal energy at a given wavelength in single mode fiber occupies two orthogonal polarization states or modes. In an ideal fiber the polarization states propagate in perfect alignment, Figure 2.9.

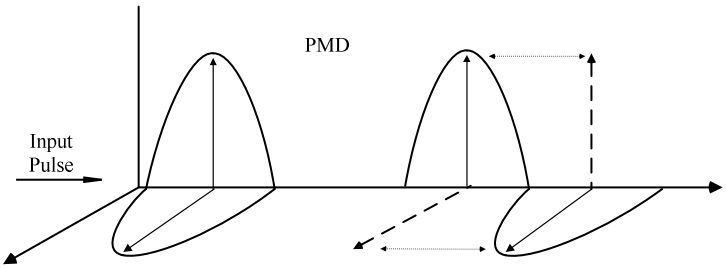

Figure 2.9 Effects from polarization mode dispersion [10]

In practice minute fiber asymmetries cause the two states to exhibit different group velocities and different group dispersion (DGD). This is another source of pulse broadening as shown in Figure 2.9. For many applications DGD can be considered constant across a single WDM channel but varying across multiple channels [8].

2.5.6 Kerr Nonlinearities

Light transmission within an optical fiber is confined highly to the fiber core. The range of the modes range from $20\ \mu m^2\ to\ 100\ \mu m^2$. Light intensities exceeding MW/cm^2 are a result of the very strong confinement At such high intensities the fiber's index of refraction is affected by the optical signals through the Kerr effect, these changes in the

refractive indexes translate into changes of the transmissions optical phase , resulting in waveform distortions that increase with signal power thus hampering transmission [8].

Fiber nonlinearities for advanced modulation formats are still an active topic of research, numerical and experimental investigations have suggested the types of nonlinear effects that typically limit transmission. Intensity-modulated formats above 10 GHz are limited by intrachannel cross-phase modulation and intrachannel four-wave mixing. For phase-modulated formats above 40 GHz intrachannel nonlinearities dominate, even though phase noise can become a limiting factor at low optical to signal noise ratio (OSNR)[8].

2.5.7 Other Adverse Effects

Two most dominant impairments created from densely packed channels in WDM optically routed networks are coherent WDM crosstalk and filter narrowing [8].

2.5.7.1 Filter Narrowing

Filter narrowing is also referred to as WDM filter concatenation; this filter impairment is unique to transparent optical networks. Any given signal can be multiplexed and demultiplexed at many network elements and components before it finally reaches its intended destination. The effective spectral transfer function of the filter set is the product of all the individual transfer functions that the signal passes through. The effective transfer function is can therefore be much narrower in spectral width than a signal filter. The effective transfer function results in attenuation and distortion lead to ISI. In

networks with high SE, the impairments created by the ISI is even more dramatic and results in limiting the maximum number of elements that can be cascaded [8] [11].

A difference between a concatenated 33% DQPSK signal and a non-concatenated 33% DQPSK signal after passing through a series of cascaded OADMs simulated with and without distortion created by crosstalk are shown in Figure 2.10.

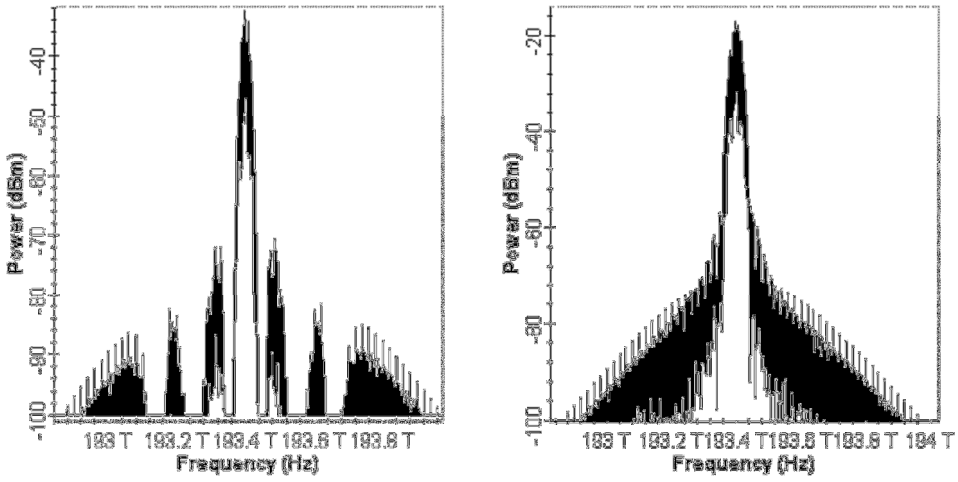

(a) (b)

Figure 2.10 (a) DQPSK Non-concatenated Signal, (b) DQPSK Concatenated Signal

2.5.7.2 OADM Cross Talk

The other principal impairment that is present in a DWDM in transparent optical networks is coherent WDM crosstalk [11]. Crosstalk can classified as either coherent or incoherent [12].

Coherent WDM crosstalk manifests itself in a way that is very similar to ASE beat noise. Coherent WDM crosstalk is the interference between an optical field and the residual

field of and adjacent WDM channel after demultiplexing it produces interference during the square-law detection. Unlike the ASE beat noise, noise from coherent DWDM crosstalk is strongly correlated to the number of bits and occurs as error burst [7]. In Equation 2.10, $E(t)$ is the optical signal field, $R(t)$ is the residual optical field of the neighboring WDM channel. The first two terms arise from the signal field and the residual field exclusively.

$$S(t) \propto |E(t) + R(t)|^2 = |E(t)^2| + |R(t)^2| + 2Re\big(E(t) \cdot R^*(t)\big) \qquad (2.10)$$

The third term comes from the polarization between adjacent WDM channels called beat interference. In co-polarized WDM channels, degradations arise mostly from the $2Re(E(t) \cdot R^*(t))$ term, which can be suppressed by polarization-interleaving. Polarization interleaving is achieved by transmitting adjacent WDM channels in orthogonal polarizations. The beat interference term also depends on the optical waveform of the interfering channel, carrying a randomly different data stream, as well as on the random carrier-phase difference between WDM channels [8].

Careful multiplexing and demultiplexing design has to ensure that WDM crosstalk is suppressed as much as possible [13-15]. Signals that pass through OADMs are contaminated more by coherent crosstalk due to the loop-back paths [12]. The intrinsic analog nature of optical networks exacerbate the crosstalk problem, because the crosstalk generated inside each node accumulates as the signal corresponding to a given channel traverse multiple OADMs within nodes [12]. In DWDM networks with a number large of nodes and a high wavelength density this impairment can become the main source of performance degradation and a main scaling limitation factor. It has been shown in [12] if

the delay τ_i is much larger than bit period, then $u(t-\tau_i)$ become completely uncorrelated, which can be used to reduce the impact of coherent crosstalk in OADMs[12].

Figure 2.11 illustrates visually the impairments from filter-narrowing and coherent crosstalk in OADMs. The effects from crosstalk on the performance of DPSK, DQPSK and CSRZ signals will be examined in this thesis.

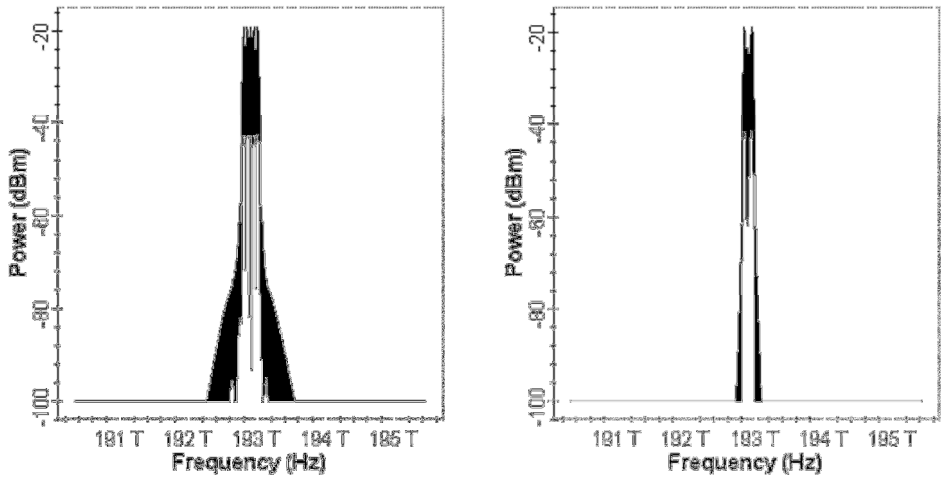

(a) (b)

Figure 2.11 33% RZ DQPSK Signal (a) prior to crosstalk, (b) after crosstalk

2.6 Spectral Efficiency

Spectral efficiency (SE) is a term used to assess the overall capacity of a DWDM transmission system. The system is governed by the available bandwidth and by the achievable SE. SE is the ratio of a networks transmission rate and channel spacing. For example, a 40 GHz network transmitting optical channels spaced at 50 GHz is therefore

operating at a spectral efficiency of $0.8(bits/s/Hz)$. The limits of systems spectral efficiency is determined by the information-theoretic capacity per unit bandwidth [16].

It is readily apparent that one way of increasing network efficiency is by increasing the rate at which data is transmitted. A four-fold increase in data transmission rate typically results in a two-and-a-half-fold increase in transponder costs. So quadrupling the per-channel data rate results in a 40% reduction in cost [8]. The other way to increase SE is to space the optical channels as closely together as possible. With the advent of improvements in optical filtering technology, channel spacing has been reduced to 50 GHz. Based upon these advances networks operating at SE of 0.8 and above have, been demonstrated. Currently networks operating at 40 GHz are operating commercially [8].

These advances, combined with a further effort to increase the capacity of optically routed networks by increasing the point-to-point capabilities and expanding upon broadband optical technology, will increase network functionality and reduce the cost of transmission. These benefits are being achieved by the increased use of reconfigurable optical add/drop multiplexers (ROADM) and optical cross-connects (OXC) the combination of which allow the delivery, addition switching or rerouting of channel wavelengths at nodes were necessary. These two components are becoming the major building blocks of the next generation of optically routed networks [8].

High SE, flexibility and capacity within optical networks which are the prime movers in fiber-optic communications research today they are:

- Low-loss optical components, which minimizes the need for amplification.
- Low-noise optical amplifiers, which results in a lower amount accumulated noise.
- Advances in fiber technology, which leads to a reduction in nonlinear distortions and facilitates higher optical launch powers.
- Forward Error Correction (FEC), which allows for operation at a higher bit error rate (BER).
- Advances in modulation formats, which allows for compensation of fiber characteristics and resilience to filtering producing during routing through OADMs.

The spectral limit is dependent on a number of specifics of the given optical communications network. These include choice of modulation format, detection technique and propagation regime [17]. For a system that has constant-intensity, coherent detection and a linear regime formats such as differential phase shift keying (DPSK) allow for a SE greater than the SE of a format which utilizes binary modulation and direct detection such as carrier suppressed return to zero (CSRZ). Formats that do not rely on the detection of changes in intensity, but rather in coherent detection of phase or polarization shifts have been computed[18]. Non-binary modulation formats such as differential quadrature phase shift keying (DQPSK) and coherent detection are necessary to approach the fundamental limits of spectral efficiency described above [17]. For DPSK and DQPSK signals with high OSNR the theoretical SE limit is 1.1 more than half the Hartley-Shannon limit (Equation 2.4) [17].

$$SE = (Bitrate/Channel\ spacing) \cdot 0.5 \cdot (log_2 SNR + 1.1) \qquad (2.11)$$

Chapter 3

ADVANCED MODULATION FORMATS

This chapter will describe the advanced modulation formats discussed in this thesis. The formats described are differential phase shift keying (DPSK), differential quadrature phase shift keying (DQPSK) and carrier suppressed return to zero (CSRZ).

3.1 Return to Zero and Non-return to Zero (RZ and NRZ)

Whether information is imprinted based upon intensity, phase, or polarization of optical pulses the format is further classified as either return to zero (RZ) or nonreturn to zero (NRZ). If a pulse is characterized as RZ this indicates the pulse intensity will return to zero within each bit period, if it is an NRZ format the optical intensity will remain constant over several bit periods until the information bit changes Figure 3.1. The differentially encoded relationship between phase shifts will be explained further in the descriptions of DPSK and QPSK modulation formats.

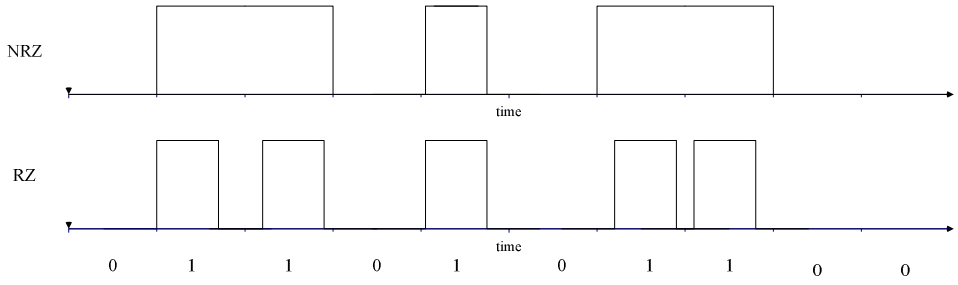

Figure 3.1 NRZ versus RZ modulation

RZ transmitters are generally constructed from NRZ transmitters by inserting a pulse carver at the output of the NRZ transmitter. RZ formats therefore typically require a slightly more complex transmitter design than their NRZ counterparts, but are generally more robust to ISI caused by imperfections in frequency response and the limited bandwidth of optoelectronic transmitter and receiver hardware, RZ formats also tend to be more robust in the face of many nonlinear propagation distortions as well as multipath interference (MPI) [8].

As stated previously RZ transmitters are created by the conversion of NRZ transmitters with the addition of a pulse carver. A pulse carver consists of a sine wave generator, a Mach Zehnder modulator and depending upon the format desired a gain inverter. A typical pulse carver and some of the specifications used in the formats examined in this research are depicted below in Figure 3.2 and Table 3.1.

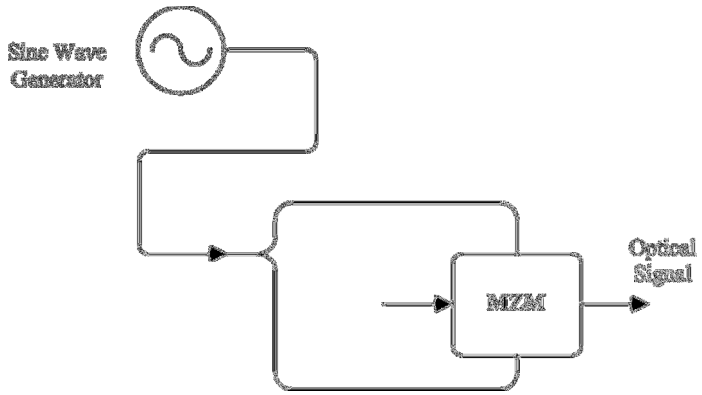

Figure 3.2 Schematic representation of a pulse carver

Extinction ratio	50 dB
Switching bias/RF Voltage	4V/4V
Insertion loss	0 dB
Modulation Voltage	4V/-4V
Bias Voltage	0V/0V
Phase	-90deg, 45deg, 0 deg

Table 3.1 Sample Pulse Carver Specifications

3.2 Modulator Technologies

It is vital to consider practical aspects of modulation and detection hardware when designing optical modulation format transmitters. Finding the most cost-effective technique for a particular system involves aspects of both modulation format and modulator technology. The three basic modulator technologies include: directly modulated lasers (DML), Mach Zehnder Modulators and Electroabsorption Modulators.

3.2.1 Directly Modulated Lasers

Directly modulated lasers (DMLs) are the easiest way to imprint data on an optical pulse, the data to be transmitted is modulated onto the laser drive current, which then switches the light emerging from the laser on and off as shown in Figure 3.3. The resulting modulation format is a binary intensity modulation, also known as on/off keying (OOK). The main drawback of DMLs for high-bitrate transmission beyond short-reach access applications is their highly component-specific “chirp”.

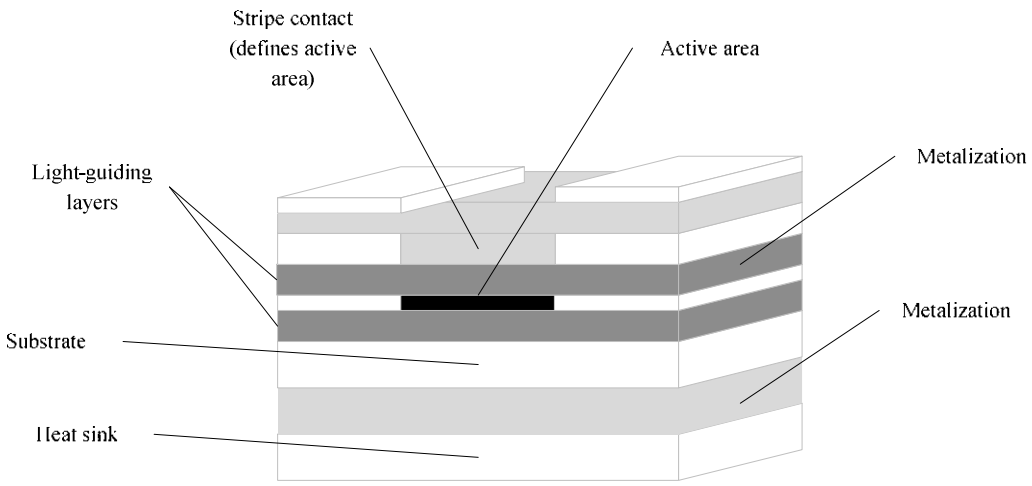

Figure 3.3 Directly modulated laser

A chirp is a residual phase modulation accompanying the desired intensity modulation. Laser chirp broadens the spectrum which is not desirable for WDM and can lead to an increase in signal distortions cause by fiber interactions. [8]. The limitation of DMLs makes them unsuitable for inclusion as components in the construction of the modulation simulations investigated here.

3.2.2 Electroabsorption Modulators

Electroabsorption Modulators (EAMs) are on-off optical devices. They are compact and stable devices that can be easily integrated with other optical devices. EAMs are transparent until an external voltage is applied which causes the bandgap of the semiconductor to absorb the light at the wavelength they are designed for. By turning the external voltage off and on the information can be modulated onto the light. They are constructed using a pin semiconductor technology. The term pin describes the manner in

which the semiconductor material is doped, in this instance it stands for positive-intrinsic-negative. Similar to DMLs they also produce some residual chirp. They also have dependent absorption characteristics, dynamic extinction ratios, and limited optical power capabilities[8]. Like the DMLs the aforementioned characteristics make them undesirable as components to be utilized.

3.2.3 Mach Zehnder Modulators

Mach Zehnder modulators (MZMs) are external modulators, however, unlike EAMs they operate on the principal of interference. They are also more costly and bulkier than their counterparts, but do not have the problem of chirping. It is therefore the modulator of choice for high performance systems. Figure 3.4 shows a schematic representation of a MZM. The external modulator uses a constant laser source also referred to as a continuous wave laser (CW laser).

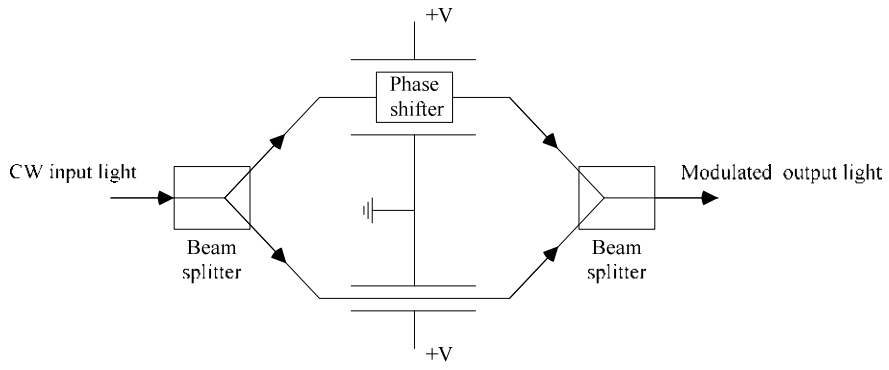

Figure 3.4 Mach Zehnder modulator

The MZM is inserted between the CW Laser and the fiber link to create the desired transmitter. In the MZM the CW light is split equally into two parallel waveguides on the

surface of the substrate, generally $LiNbO_3$ and then recombined at the output. A control voltage is applied to the electrodes which creates a small change in the refractive index through an electro-optic effect. This causes a change in the propagation constant and a relative phase shift where the two waves combine. When no voltage is applied the relative phase shift is zero and the combined signal exits the modulator without attenuation, except the constant loss caused by the waveguides. When a voltage is applied that produces a phase shift of π between the two paths then the signal at the output is zero.

The behavior of the MZM is described by the equations below. E_{out} is the electromagnetic field emitted at the output of the MZM while E_{in} is the electromagnetic field injected into the MZM.

$$E_{out}(t) = E_{in}(t) \cdot \cos\big(\Delta\theta(t)\big)e^{j\Delta\emptyset(t)} \tag{3.1}$$

Where the $\Delta\theta$ is the phase difference between the two branches and is defined as

$$\Delta\theta(t) = \frac{\pi}{2}\big(0.5 - ER(M(t) - 0.5)\big) \tag{3.2}$$

with

$$ER = 1 - \frac{4}{\pi}\tan^{-1}\left(\frac{1}{\sqrt{extrat}}\right) \tag{3.3}$$

and

$$\Delta\emptyset(t) = SC \cdot \Delta\theta(t) \cdot (1 + SF)/(1 - SF) \tag{3.4}$$

The parameter SC is –1 if negative signal chirp is true, or 1 if negative signal chirp is false, extract is the extinction ratio, SF is the symmetry factor, and M(t) is the electrical input signal. The electrical input signal is normalized between 0 and 1[19].

MZMs are readily implemented using one of three structures: $LiNbO_3$, GaAs, or InP. $LiNbO_3$-based devices are bulkier than their semiconductor counterparts, but offer more efficient fiber to chip coupling and no residual intensity modulation accompanying the desired phase modulation. MZMs especially $LiNbO_3$ based devices have wavelength-independent modulation characteristics, excellent extinction performance and typically lower insertion losses. Their characteristics of having well-controlled modulation performance and the possibility of independently modulating intensity and the phase of the optical field, MZM form the basis of many advanced modulation format transmitters [8].

The application of voltage on both waveguides, results in a device called a dual drive MZM Figure 3.4. This device allows for the generation of quadrature signals. These external modulators can also be used to generate phase modulation in coherent systems [3]. Based upon these characteristics a dual drive $LINbO_3$ MZMs will be used in the simulations developed for this thesis.

The optical field at the output of the Lithium Niobate Mach-Zehnder modulator is given by Equation 3.5,

$$E_o(t) = \frac{E_{in}(t)}{10^{\frac{\text{insertionloss}}{20}}} \cdot \left(\gamma \cdot e^{\left(\frac{jnv_{2(t)}}{V_{nRF}} + \frac{j\pi v_{bias2}}{V_{\pi DC}} \right)} + (1-\gamma) e^{\frac{jnv_1(t)}{VnRF} + \frac{j\pi v_{bias1}(t)}{V_{\pi DC}}} \right) \qquad (3.5)$$

Where $E_{in}(t)$ is the input voltage $v_1(t)$ and $v_2(t)$ are the RF modulating voltages, and v_{bias1} and v_{bias2} are the DC bias voltage applied to arm 1 and arm 2, respectively γ

denots the power combining ratio of arm 2 for the input Y- branch waveguide, and is defined by Equation 3.6.

$$\gamma = \left(1 - \frac{1}{\sqrt{\varepsilon_r}}\right)/2 \tag{3.6}$$

where $\varepsilon_r = 10^{\mathrm{ExtRatio}/10}$. The DC bias voltages v_{bias1} and v_{bias2} are included separately because $V_{\pi DC}$ the switching bias voltage can be different than the switching RF voltage. The optical power and phase of the modulator output are determined in response to the modulating voltage waveforms. The modulator transfer function relates the effective drive voltage to the applied voltage [19].

3.3 Symbol Alphabet Size

Figure 3.5 illustrates the relationship between the categories of optical modulation formats. Figure 3.5(a) is the intensity modulation family and Figure 3.5(b) shows the differential phase family. Multilevel signaling uses $\log_2(M)$ data bits encoded on M symbols and transmitted at a symbol rate $R/\log_2(M)$, R is the bit rate. Symbols are in general assigned without regard to the symbols sent before or after it (memoryless modulation). Multilevel signaling offers the benefits of higher spectral efficiencies at the cost of a reduced tolerance to noise [16]. Multilevel signaling allows single-channel data rates to exceed the limits of high-speed optoelectronics technology. Alternatively, multilevel signaling allows for lower symbol rates at a fixed data rate, which is beneficial in the presence of dispersive signal distortions, such as CD or PMD, as well as for implementing digital electronic signal processing [8].

Multilevel intensity modulation (MASK) and multilevel phase modulation have been investigated for use in multigigabit transmission [20-22]. MASK has not proven beneficial for many fiber optic transmissions to date. This is attributed to the back-to-back receiver sensitivity penalties when judged beside a format like OOK[20]. One of the most promising formats is Differential Quadrature Phase Shift Keying (DQPSK), which is discussed in detail in Section 3.4.2 [8].

Within the classification of multilevel signaling are modulation formats that use more than two symbols, they are known as correlative coding and pseudo-multilevel modulation. For these formats the number of symbols is not increased to increase the data rate or to reduce the symbol rate at a fixed rate; instead all symbols are transmitted at the bitrate, and additional degrees of freedom are gained by using the two or more symbols generated to shape the spectrum and improve the tolerance of a format to specific propagation impairments by introducing memory into the modulation scheme, this is also referred to as line coding[16][23-25]. If more than two symbols are used to represent a bit, and if the transmission of redundant bits is data-independent, this is called pseudo-multilevel Data Modulation Format (DMF). If the assignment of symbols is based upon the information contained in the transmitted data the DMF is referred to as correlative-coding. The most commonly used pseudo-multilevel format is carrier suppressed return to zero (CSRZ) [8].

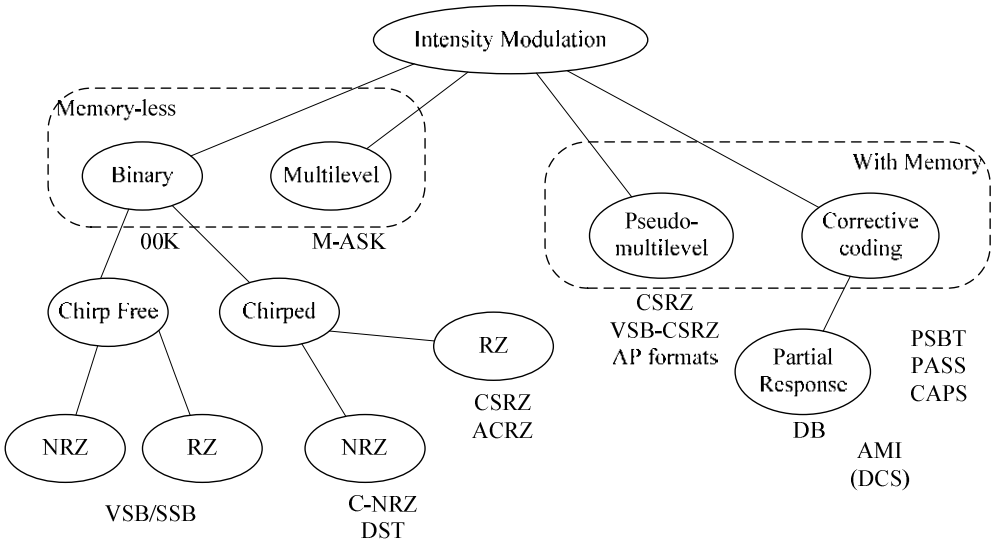

(a)

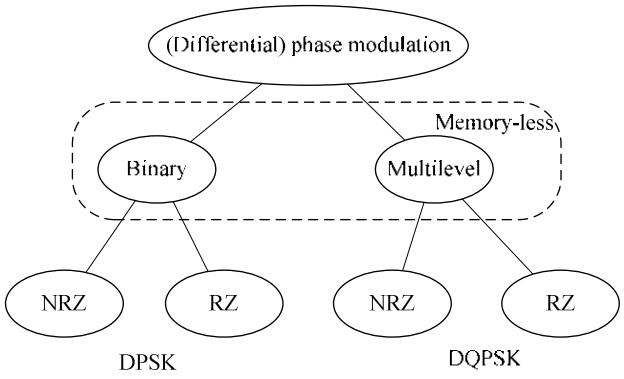

(b)

Figure 3.5(a) Modulation format classified as intensity modulation and

(b) Modulation formats classified as phase modulation

The four most important symbol diagrams used when discussing optical modulation formats are OOK, CSRZ (which is also identical to DB and AMI), DPSK and DQPSK These formats are shown in shown in Figure 3.6 [8]. Two formats are intensity modulated one memoryless, and the other two are phase modulated with DQPSK being multilevel as shown in Figure 3.6.

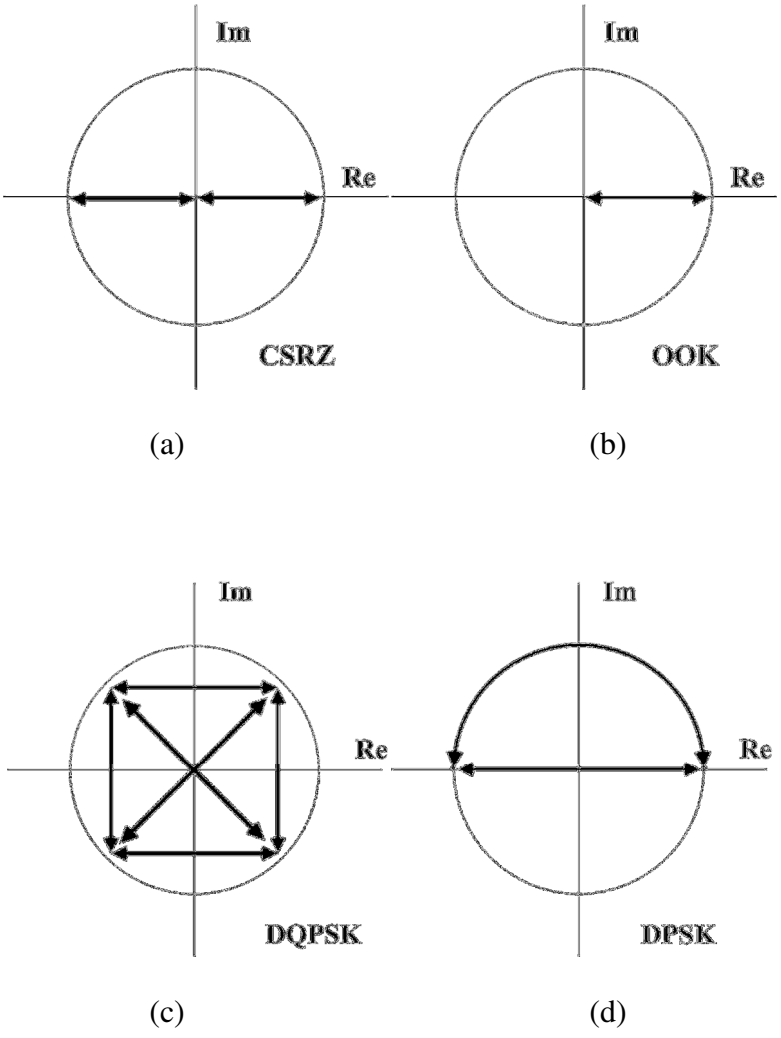

Figure 3.6 Symbol diagrams of modulation formats for (a) CSRZ, (b) OOK, (c) DQPSK and (d) DPSK

In WDM systems the key to reducing the cost per transported information bit is to effectively share all optical components. These components must operate within the same wavelength limited window; therefore it is necessary to place the WDM channels as close together as possible. The ratio of net per-channel information data rate to the WDM channel spacing is referred to as spectral efficiency (SE) and is measured in bits per second per Hertz (b/s/Hz)[26] or as information spectral density (ISD)[27]. Another way

to decrease the cost per information bit is to increase per-channel data rates. These considerations, among others, led to the development of 40 Gbit/s per-channel rates[28]. One way of comparing these technologies is to look at the maximum data rates they support for a given, regeneration-free transmission distance. The regeneration free transmission distance is defined as the distance that can be bridged without detecting and retransmitting the digital information anywhere along the propagation path[8]. The physical properties of high-SE, high-capacity optically routed transport networks, which drive fiber-optic communications research today, are enabled by several key technologies.

- Low-loss optical components (including transmission fiber, dispersion-compensating devices, and optical switching/routing elements) minimize the need for optical amplification and reduce the associated amplification noise.
- Low-noise optical amplifiers (such as distributed Raman amplifiers) lower the noise accumulated along transmission lines.
- Advanced optical fibers reduce nonlinear signal distortions and enable higher signal launch powers
- FEC allows for operation at poorer channel bit error ratio (BER), which relaxes the requirements on the OSNR at the receiver.
- Advanced modulation formats are used to trade off noise resilience, fiber propagation characteristics, and resilience to narrowband optical filtering due to multiple passes through OADMs [8].

3.4 Modulation Formats

Recalling the coherent signal detected at the receiver is in the form of Equation 3.7 below.

$$S(t) \propto |E(t) + R(t)|^2 = |E(t)^2| + |R(t)^2| + 2\mathrm{Re}\big(E(t) \cdot R^*(t)\big) \tag{3.7}$$

Where E(t) is the optical signal field, R(t) is the residual optical field of the neighboring WDM channel. In co-polarized WDM channels, degradations arise mostly from the $2\mathrm{Re}(E(t) \cdot R^*(t))$ term. For the simulations presented in this thesis, co-polarization of signals will not be used in an effort to assess the most robust formats. The beat interference term also depends on the optical waveform of the interfering channel, carrying a randomly different data stream, as well as on the random carrier-phase difference between WDM channels [8]. The use of multiple OADMs, which are combinations of multiplexers and demultiplexers, in networks with high SE cause concatenation which narrows the overall optical filter bandwidth and thus distorts the signal transmitted with designated format[8].

Phase Modulation of data can be described by the following equations:

An angle or phase modulated signal can be written as

$$u(t) = A_c \cos\big(\theta(t)\big) \tag{3.8}$$

$\theta(t)$ is the phase angle and

$$f_i = f_c + \frac{1}{2\pi}\frac{d\theta(t)}{dt} \tag{3.9}$$

if $x(t)$ is a bandpass signal then it has the following form and, therefore;

$$x(t) = A_c \cos\big(2\pi f_c t + \emptyset(t)\big) \tag{3.10}$$

if $m(t)$ is the message then in a phase modulated (PM) signal where k_p is the phase deviation constant.

$$\emptyset(t) = k_p m(t) \tag{3.11}$$

If the carrier is phase modulated with the integral message it is the same as frequency modulating the carrier with the original message, or conversely if the carrier is frequency modulated with the derivative of the message, the result is equivalent to the phase modulation of the carrier with the message [16].

With PM the maximum phase deviation is given by

$$\Delta\emptyset_{max} = k_p \max[|m(t)|] \tag{3.12}$$

The message signal

$$m(t) = A_m \cos(2\pi f_m t) \tag{3.13}$$

is now used to phase modulate the carrier

$$x_c(t) = A_c \cos(2\pi f_m t) \tag{3.14}$$

resulting in

$$\emptyset(t) = k_p A_m \cos(2\pi f_m t) \tag{3.15}$$

and the phase modulated signal becomes

$$u(t) = A_c \cos\left(2\pi f_c t + k_p A_m \cos(2\pi f_m t)\right) \tag{3.16}$$

$$u(t) = \mathrm{Re}\left(A_c e^{j2\pi f_c t} e^{jA_m \sin(2\pi f_m t)}\right) \tag{3.17}$$

The above equations give rise to two of the advanced modulation formats to be studied, Differential Phase Shift Keying (DPSK) and Differential Quadrature Phase Shift Keying (DQPSK).

3.4.1 Differential Phase Shift Keying

The transmission of a DPSK formatted signal encodes each bit with the information on the binary phase of adjacent bits and the binary phase information acts as a phase reference for another bit, this is the fundamental principal of DPSK formats [29].

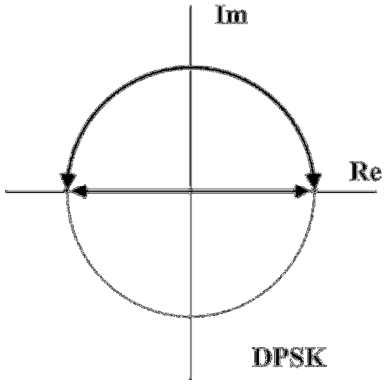

Figure 3.7 DPSK symbol diagram

A 1-bit is encoded onto the π phase change, and a 0-bit is represented by no phase change as shown in Figure 3.7. DPSK can be implemented in RZ or NRZ format. DPSK is defined by Equation 3.18.

$$s(t) = A\cos\left(2\pi f_c t + \theta(k)\right), \quad kT \le t < (k+1)T$$

$$\theta(k) = \begin{cases} 0 = 1 \\ \pi = 0 \end{cases} \tag{3.18}$$

DPSK's advantage over other OOK formats is from the improvement in the 3dB receiver sensitivity [30][29]. For fixed optical power the symbol spacing of a DPSK and an OOK are $\sqrt{2}$ and 1 respectively. The increase in symbol distance makes DPSK accept a $\sqrt{2}$ larger standard deviation incurred by the optical field noise than its OOK counter-part for

an equal BER. This translates into a 3-dB reduction in OSNR. A DPSK transmitter can be constructed as shown in Figure 3.8, with its specifications listed in Table 3.2. The data signal can be differentially encoded at the transmitter which avoids error propagation that can occur by differential decoding at the receiver[31].

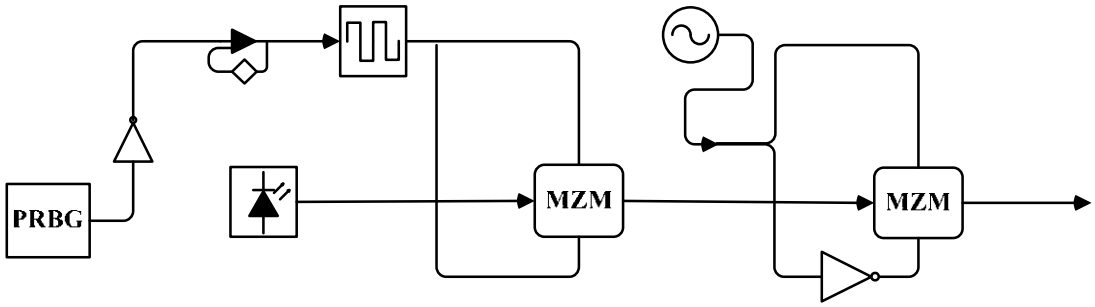

Figure 3.8 Schematic representation of a DPSK transmitter

Power	0 dBm
Extinction ratio	20 dB
Linewidth	10 MHz
Initial Phase	0 deg
Duty Cycle	33%; 50%; 66%; NRZ

Table 3.2 DPSK transmitter specifications

Encoding is performed by a relatively simple logic circuit preceding the modulator [16]. The following is an example of the precoding of a data sequence. The data sequence 0 1 0 1 1 0 enters the precoder then after the data exists the precoder it is transformed to 0 1 1 0 1 0.

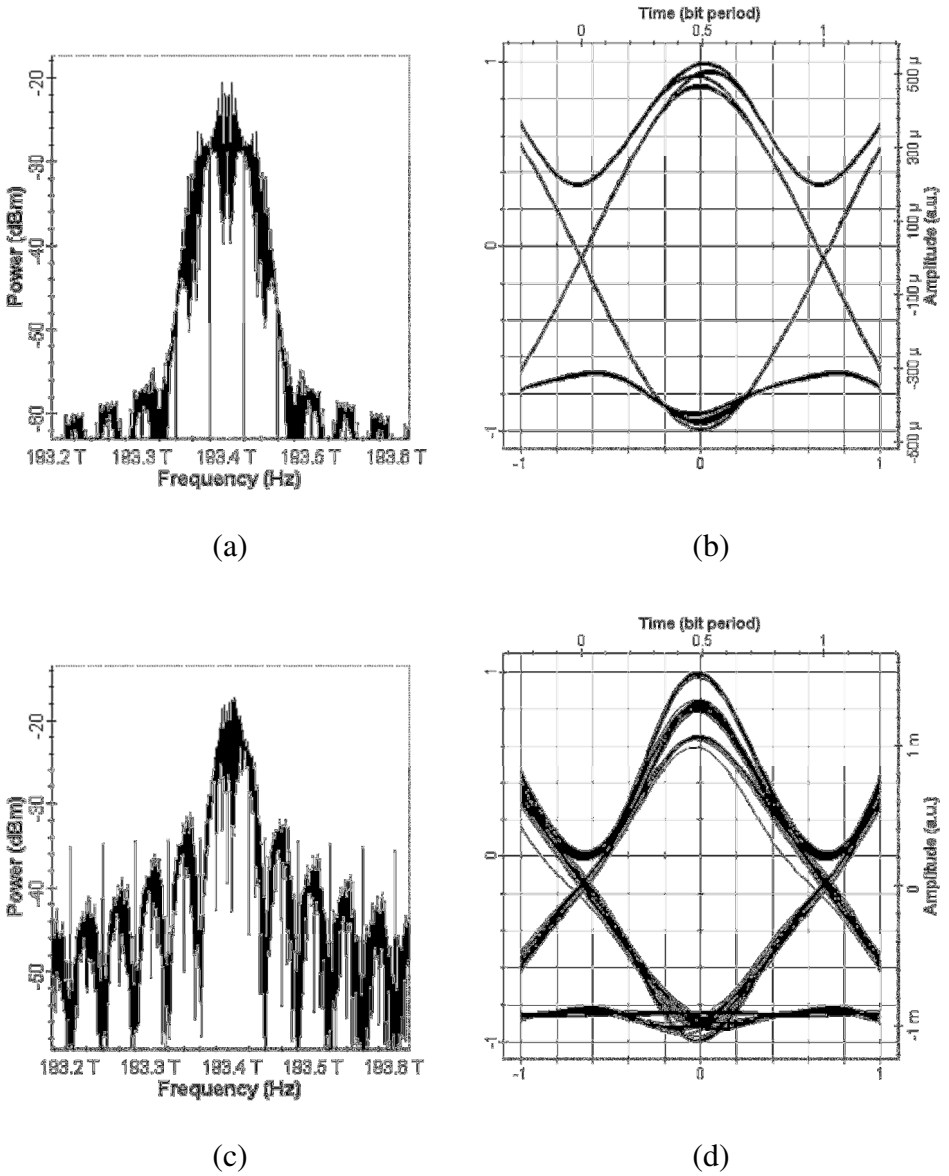

Figure 3.9 (a) RZ DPSK optical spectrum, (b) RZ DPSK eye diagram, (c) NRZ DPSK optical spectrum, (d) NRZ DPSK eye diagram

The phase of the optical field of a narrow-linewidth laser source is flipped between 0 and π using the precoded sequence. This generalization is straightforward and can be extended to higher phase modulation. DPSK can be implemented in either RZ or NRZ

format. The eye diagrams and optical spectrum for RZ DPSK and NRZ DPSK formats are shown in Figure 3.9.

The modulation of a data signal can be accomplished using either a straight-line phase modulator (PM) or a MZM. Because the optical phase directly follows the electrical drive signal, the speed of transition is limited by the bandwidth of the driver amplifier and the phase modulator.

Overshoot and ringing in the drive waveform appear as phase distortions. The difference between the two modulators manifests itself when the phase changes position on the unit circle. The MZM is driven around the zero transmission through the origin of the complex optical field plane, this always produces an exact phase jump of π, but produces residual intensity drops during the phase transitions. With a PM modulated signal the phase is changed by traveling back and forth between 0 degrees of phase 180 degrees of phase change. The phase change can travel by two routes one on the unit circle thus preserving the intensity of the signal, but also taking more time and increasing the probability of errors in the phase changes as bitrates increase.

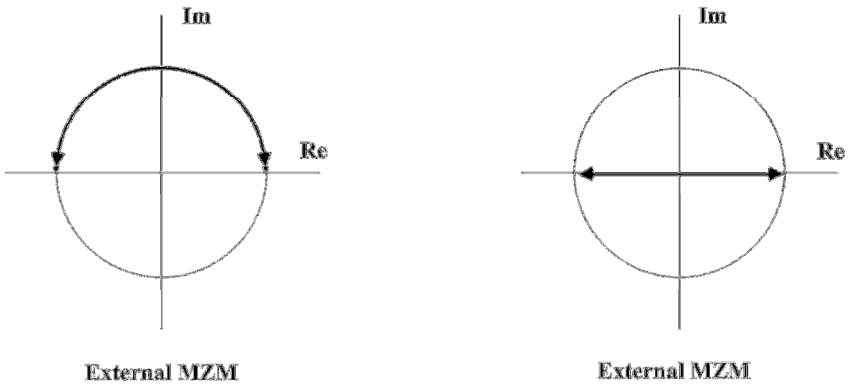

Figure 3.10 Different phase shift operation between types of MZM

Alternatively, the change in phase can travel back and forth through the origin. Both of these phase change possibilities are shown in Figure 3.10. Since very accurate phase modulation is a higher priority than intensity in phase modulation formats, the transmitters need to be more precise, so they are easier to implement with a MZM as a phase modulator [29].

To achieve differentially encoded coherent phase modulation and demodulation the carrier signal must be filtered out from the received signal. The differential encoding allows for the received data to be decoded in the presence of phase ambiguities. In differential encoding the information is transmitted via phase shifts between any two successive signal intervals [16]. DPSK signals cannot be directly received by square-law detection. For the information contained within the optical field of a differential phase modulated signal utilizing a square-law detector, like the one in Figure 3.11. A Mach Zehnder Interferometor (MZI) acts as a Delay Interferometer (DI) and must be inserted to convert the phase modulation into intensity modulation. The absence of an optical phase

reference at the square-law detector also requires that the phase reference be provided by the actual signal.

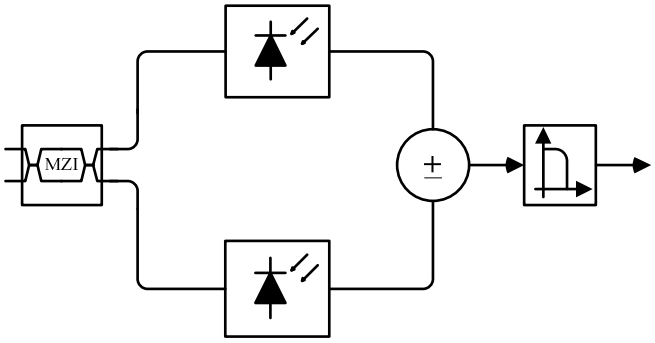

Figure 3.11 Schematic DPSK receiver

The encoded phase information is detected is when the DI splits the optical signal into two paths. They experience a delay differential equal to the bit duration τ which is approximately 25 ps at 40 Gb/s, this allows the two neighboring bits to interfere at the output. At the output port the two optical fields interfere destructively whenever there is no phase change, and constructively whenever there is a phase change between bits in accordance with the differential precoding. The output of either port is sufficient to fully detect the DPSK signal, the 3-dB sensitivity advantage is not seen unless balanced detection is used. The reason the increased performance is realized is the non-Gaussian noise statistics, characteristics of beat noise limited system [29] [32] [33].

3.4.2 Differential Quadrature Phase Shift Keying

DQPSK is the only true multilevel modulation format that has received much attention in optical communications thus far [22, 34]. It transmits four phase shifts at a symbol rate of half the aggregate bit rate, as shown in Figure 3.12

The DQPSK signal can be represented by Equation 3.19.

$$s(t) = A\cos\left(2\pi f_c t + \theta(k)\right), \quad kT \le t < (k+1)T$$

$$\theta(k) - \theta(k-1) = \begin{cases} \pi & \text{if } (I(k), Q(k)) = (0,0) \\ \frac{3\pi}{2} & \text{if } (I(k), Q(k)) = (1,0) \\ 0 & \text{if } \left(I(k), Q(k)\right) = (1,1) \\ \frac{\pi}{2} & \text{if } \left(I(k), Q(k)\right) = (0,1) \end{cases} \tag{3.19}$$

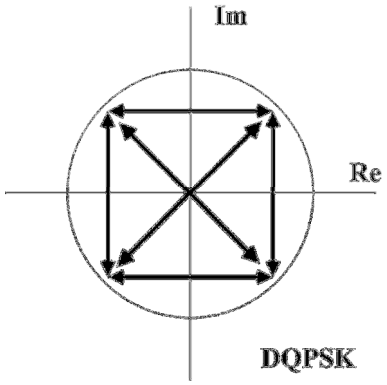

Figure 3.12 Symbol diagram for a DQPSK signal

For the purposes of this thesis the DQPSK transmitters will be designed and tested using two different configurations, series and parallel. Figure 3.13 and Table 3.3 depict the configuration and specifications for series RZ DQPSK transmitter. The spectrum of

advanced modulation formats vary dramatically. Because of this some formats perform better than others in DWDM networks as defined by SE. Optically routed networks are currently being pushed to spectral efficiencies of 0.8 and above.

The normalized output signal for a series MZM DQPSK signal is given by Equation 3.20.

$$E_t(V_a, V_b) = \frac{1}{2}\left(e^{j\frac{\pi}{V_\pi}V_a} + e^{j\frac{\pi}{V_\pi}V_b}\right) \tag{3.20}$$

Where V_π is the voltage necessary to change the output intensity from maximum to minimum and V_a and V_b are the drive voltages for the two arms.

CW Laser	
Power	0 dB
Linewidth	0 MHz
Initial Phase	0 deg
Azimuth & Ellipticity	0 deg
LiNb MZM 1 & 2	
Extinction ratio	100 dB
Switching Bias/RF	4V/4V
Insertion loss	0 dB
Modulation voltage	-4V/-4V
Bias Voltage	0V/0V
LiNb MZM Pulse Carver	
Sine Wave Generator frequency	Bitrate/4
Phase	0 deg, -45 deg, -90 deg
Extinction ratio	50 dB
Switching Bias/RF	4V/4V
Insertion loss	0 dB

Modulation voltage	-4V/-4V
Bias Voltage	0V/0V
NRZ Pulse Generator	
Amplitude	1 a.u.
Bias & position	0 a.u.
Rise & Fall time	0.01 bit
4-DPSK precoder	Serial

Table 3.3 DQPSK Transmitter Specifications (series)

In the series configuration the CW laser is sent directly into the first of two MZMs. The MZMs are configured identically with the only exception being the modulation voltage. MZM 1 sets the modulation voltages to be -4V and -4V while MZM 2 sets the modulation voltages at 2V and 2V respectively; this difference generates the phase modulation and eliminates the necessity of the phase shift at the output of one of the MZM as noted in the design of the parallel configuration.

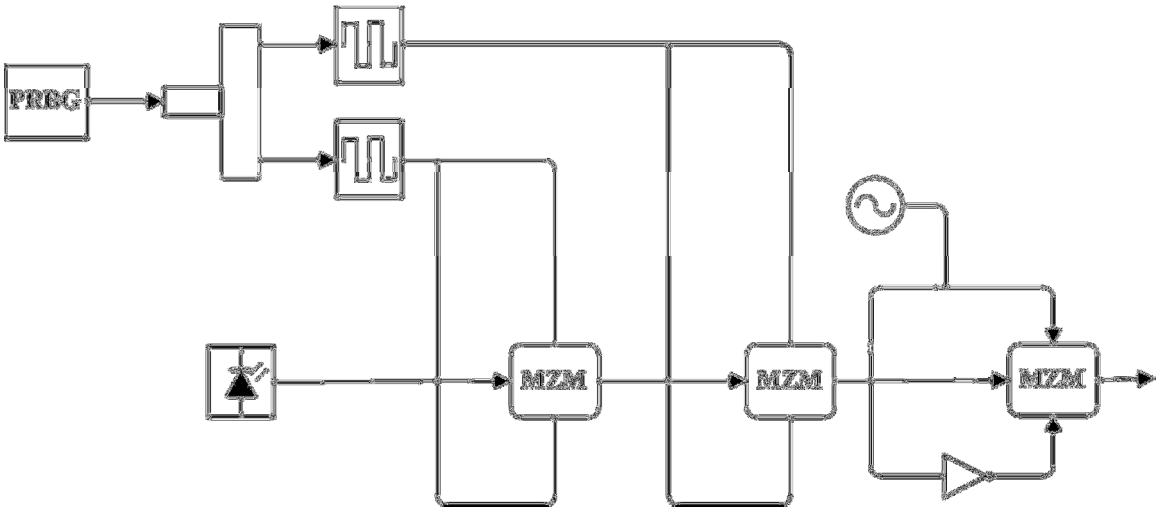

Figure 3.13 Schematic of a DQPSK transmitter (series)

The normalized output signal for a Parallel MZM DQPSK signal is given by Equation 3.21.

$$E_t(V_a, V_b) = \sin\left(\frac{\pi}{V_\pi} V_a\right) + j \sin\left(\frac{\pi}{V_\pi} V_b\right) \tag{3.21}$$

Where V_π is the voltage necessary to change the output intensity from maximum to minimum and V_a and V_b are the drive voltages applied to the two parallel MZMs.[35]

Figure 3.14 along with Table 3.4 illustrate the specifications and configuration for the parallel RZ DQPSK transmitter.

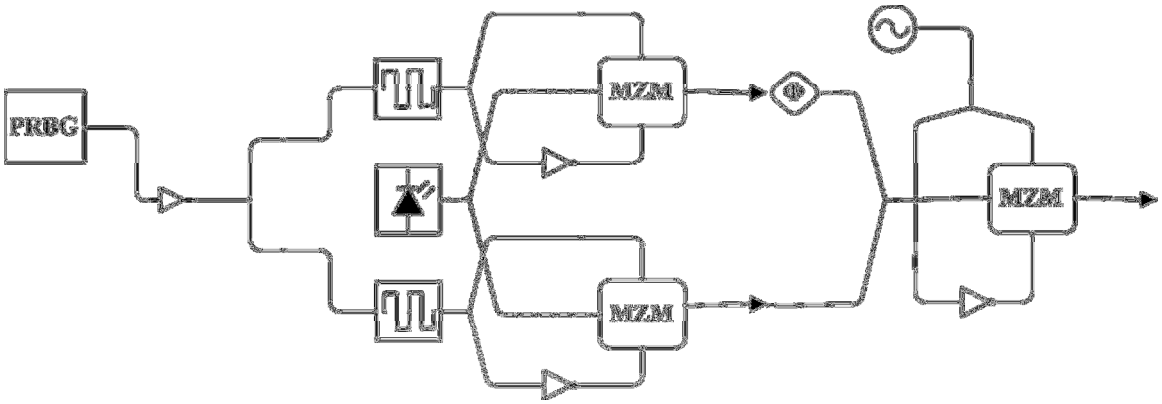

Figure 3.14 Schematic DQPSK transmitter (parallel)

CW Laser	
Power	0 dB
Linewidth	0 MHz
Initial Phase	0 deg
Azimuth & Ellipticity	0 deg
LiNb MZM 1 / 2	
Extinction ratio	100 dB
Switching Bias/RF	4V / 4V
Insertion loss	0 dB
Modulation voltage	-4V / -4V
Bias Voltage	0V / 0V
Electrical Gain	-1
MZM 1 output phase shift	90 deg
LiNb MZM Pulse Carver	
Sine Wave Generator frequency	Bitrate/4
Phase	0 deg, -45 deg, -90 deg
Extinction ratio	50 dB
Switching Bias/RF	4V/4V
Insertion loss	0 dB
Modulation voltage	-4V/-4V
Bias Voltage	0V/0V
NRZ Pulse Generator	
Amplitude	1 a.u.
Bias & position	0 a.u.
Rise & Fall time	0.01 bit
4-DPSK precoder	Serial

Table 3.4 Parallel DQPSK Transmitter Specifications (parallel)

In the parallel configuration the CW laser is launched into an optical splitter to divide the light into to equal intensities and then into two MZMs which function as phase modulators and at the output of one of the MZMs is a $\pi/2$ phase shift. This transmitter structure takes advantage of the exact π-phase shifts produced by the MZMs. This design also only requires binary electronic drive signals. These signals are much easier to generate at high speeds than multilevel drive waveforms.

Utilizing this transmitter structure takes advantage of the exact π-phase shifts produced by the MZMs. To generate a RZ format the combined output from the LINb MZM is passed through a pulse carver. By varying the phase of the sine wave generator, within the pulse carver, the desired RZ modulation format can be produced. This structure also requires only binary electronic drive signals. These signals are much easier to generate at high speeds than multilevel drive waveforms.

The eye diagrams, constellation diagrams and optical spectrum for both configurations of transmitters are shown below in Figures 3.15 and 3.16 respectively. The eye diagrams, constellation diagrams and optical spectrum for both configurations of the NRZ transmitters are also shown below in Figures 3.17 and 3.18 respectively.

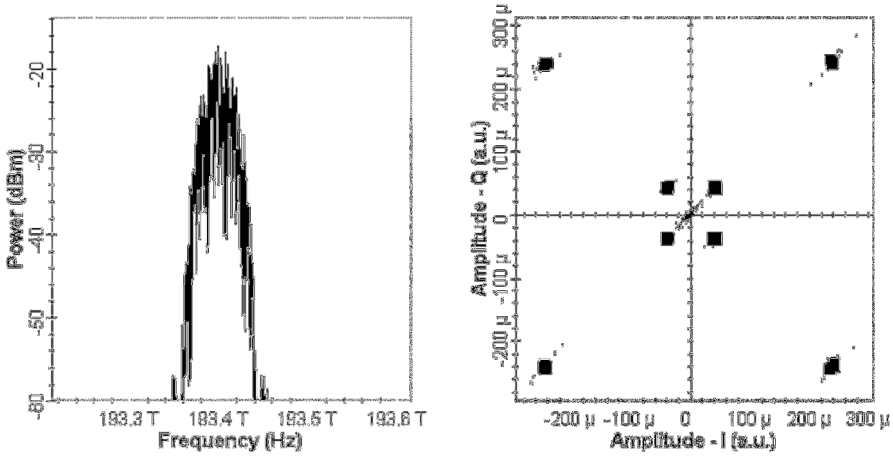

(a) (b)

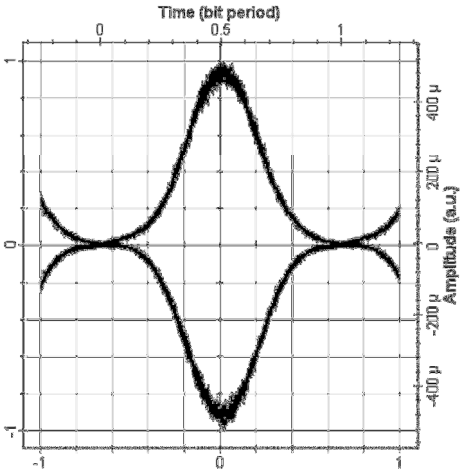

(c)

Figure 3.15 (a) Spectrum DQPSK (series), (b) Constellation diagram DQPSK (series), (c) Eye diagram RZ DQPSK (series)

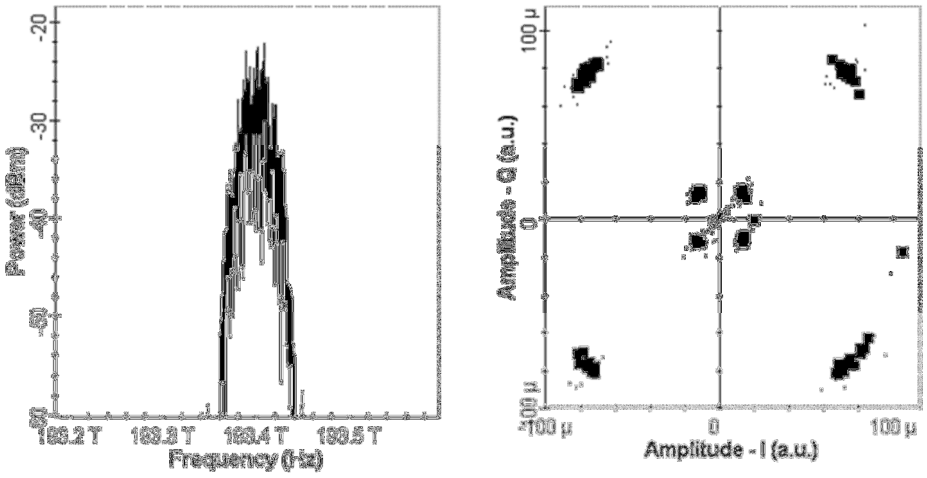

(a) (b)

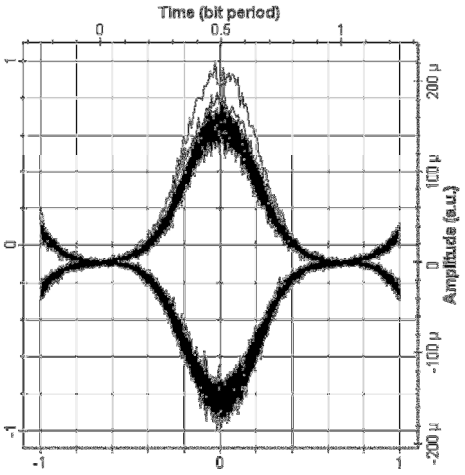

(c)

Figure 3.16 (a) Spectrum DQPSK (parallel), (b) Constellation DQPSK (parallel),

(c) Eye diagram DQPSK (parallel)

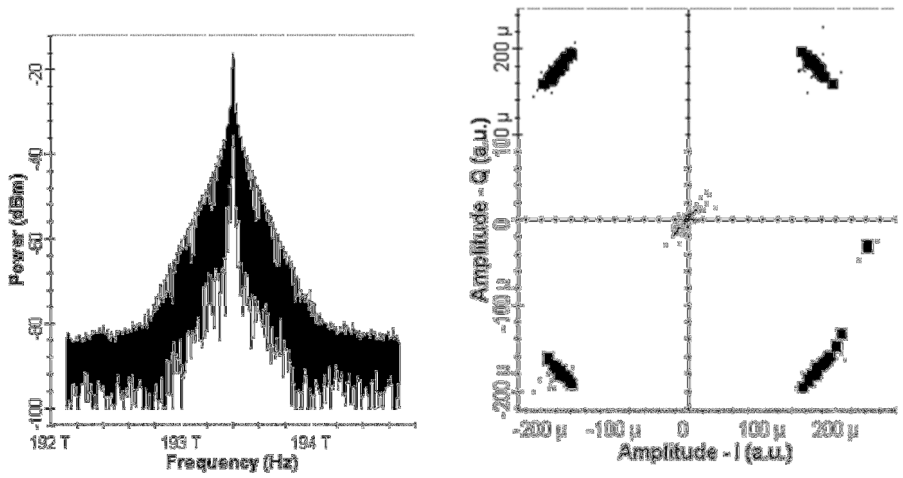

(a) (b)

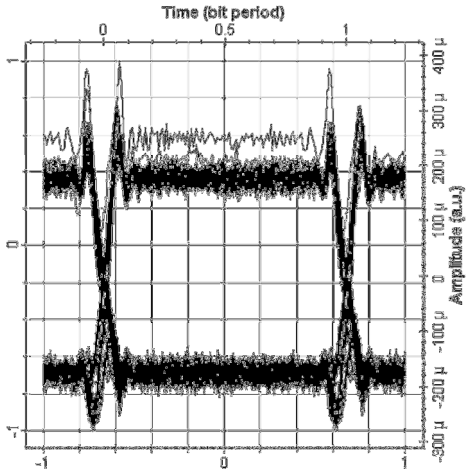

(c)

Figure 3.17 (a) Spectrum NRZ DQPSK (parallel), (b) Constellation diagram NRZ DQPSK (parallel), (c) Eye diagram NRZ DQPSK (parallel)

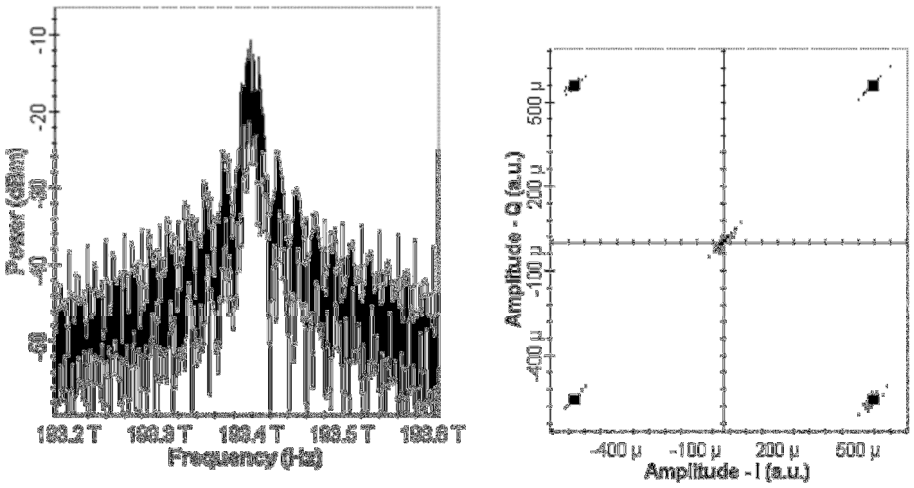

(a) (b)

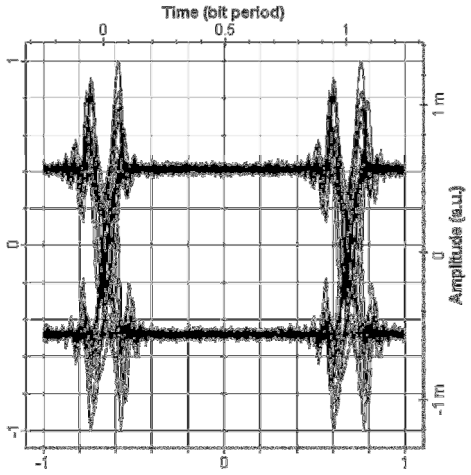

Figure 3.18 (a) Spectrum NRZ DQPSK (series)

(b) Constellation diagram NRZ DQPSK (series), (c) Eye diagram NRZ DQPSK (series)

Since differential quadrature phase-shift-keying (DQPSK) format only transmits two bits per symbol resulting in the symbol rate that is half the bit rate and a less complex system. DQPSK is tolerant to chromatic dispersion (CD), polarization-mode dispersion (PMD), and has a high spectral efficiency, and thus can be used in ultra long haul transmission. Although the configuration of a DQPSK system is less complex when compared to a

QPSK system, large size and high power consumption of the optical transceivers still pose challenges to designers [8].

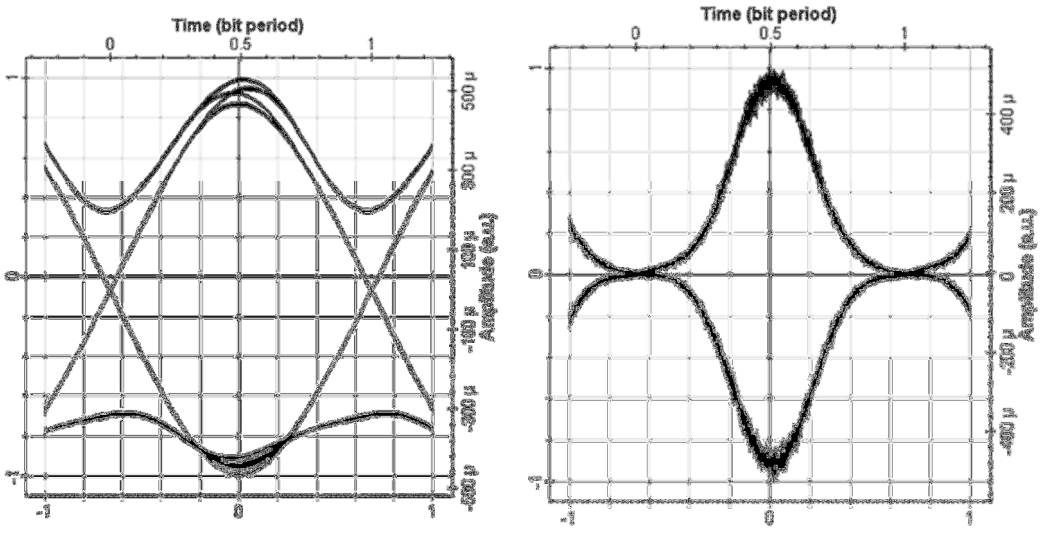

(a) (b)

Figure 3.19 (a) Eye diagram DPSK, (b) Eye diagram DQPSK

The shape of the eye diagrams of the DPSK and DQPSK can be remarkably similar. They will however differ in that the spectrum of the DQPSK is compressed in frequency by two times because of the halved symbol rate for transmission at a fixed bit rate, as shown in Figure 3.19(a) and (b) respectively. This compressed spectrum is most useful in achieving high spectral efficiency (SE) [21, 36] and an increased resistance to the negative impacts caused by chromatic dispersion (CD) [21, 37]. These two characteristics of DQPSK make it a very robust.

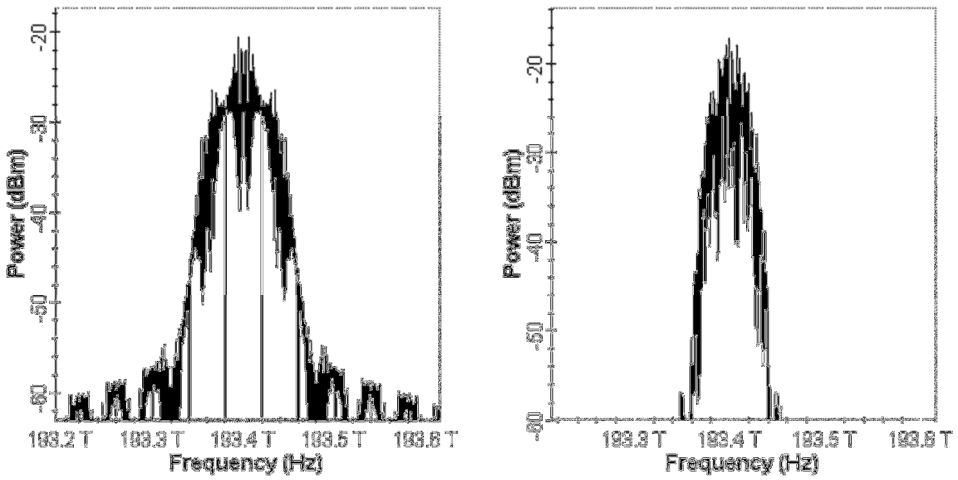

(a) (b)

Figure 3.20 (a) Spectrum of RZ DPSK signal (b) Spectrum of DQPSK formatted signals

3.4.3 Carrier Suppressed Return to Zero

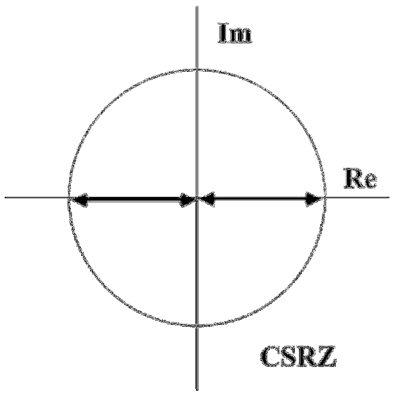

Figure 3.21 CSRZ symbol diagram

CSRZ is a pseudo-multilevel modulation format that is characterized first by the information being encoded on the intensity levels {0, 1}, and secondly where the phase is changed by π every bit, regardless of the data information, as shown Figure 3.21. In

contrast to the correlative coding formats where the sign reversal occurs with every bit transition, and are completely independent of the information-carrying section of the signal.

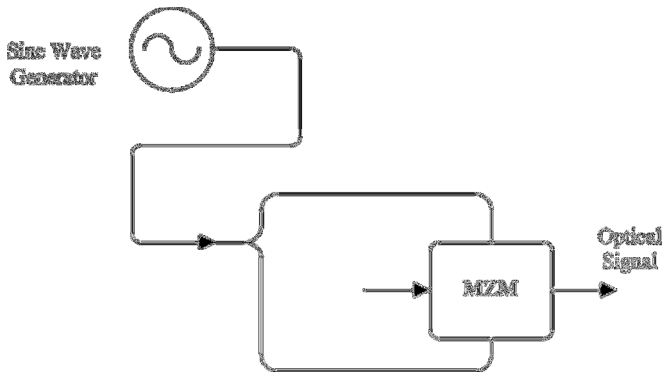

Figure 3.22 Schematic for a pulse carver

CSRZ signals can be generated by sinusoidally driving a MZM pulse carver at half the data rate between its transmission maxima, as shown in Figure 3.22. The CSRZ transmitter is constructed by coupling the output from a dual drive MZM to a pulse carver as shown in Figure 3.23. Since the optical field transfer function of the MZM changes its sign at the transmission minimum, phase inversions between adjacent bits are produced.

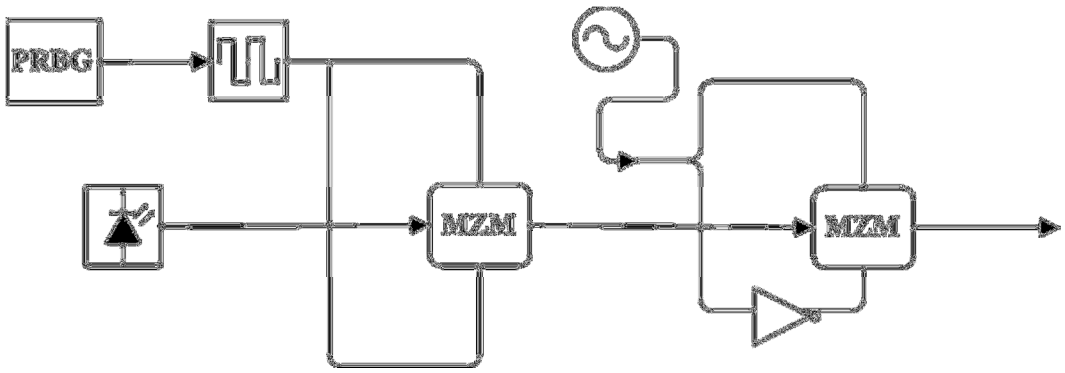

Figure 3.23 Schematic for a CSRZ transmitter

On average the optical field of half the 1-bits have a positive sign associated with them, while the other half have a negative sign. This results in an optical field envelop with zero mean. The consequence of the zero mean is the suppression of the carrier frequency, giving CSRZ it name. The period of the signals' phase is periodic at half the data rate. The CSRZ spectrum therefore exhibits a characteristic tone at $\pm \mathrm{R}/2$ [8] Figures 3.24(a) and (b). The CSRZ transmitter used in the simulations utilized the specifications in Table 3.5.

CSRZ Laser Settings	
Power	0 dBm
Linewidth	0 MHz
Initial Phase	0 deg
MZM1	
Extinction ratio	100 dB
Switching bias/RF Voltage	4V/4V
Insertion loss	0 dB
Bias Voltage	-2V/2V

Table 3.5 CSRZ Transmitter and Specifications

All of the preceding technologies can be further enhanced by the utilization of forward error correction (FEC) techniques. Their use allows for operation at higher channel bit error rates (BER) which in turn decreases the cost of the receiver due to less stringent optical signal-to-noise ratio (OSNR) requirements. The required value for the measured input BER for application of FEC is 3.8×10^{-3}[38]. Advanced modulation formats are

used to trade off noise resilience, fiber propagation characteristics and resilience to narrowband filtering due to multiple passes through optical add-drop multiplexers (OADMs) [8].

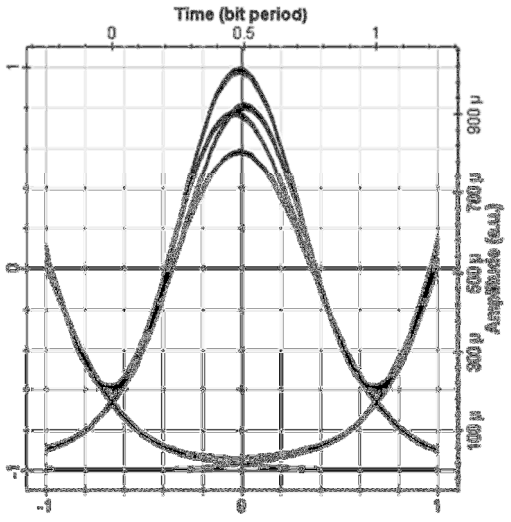

(a)

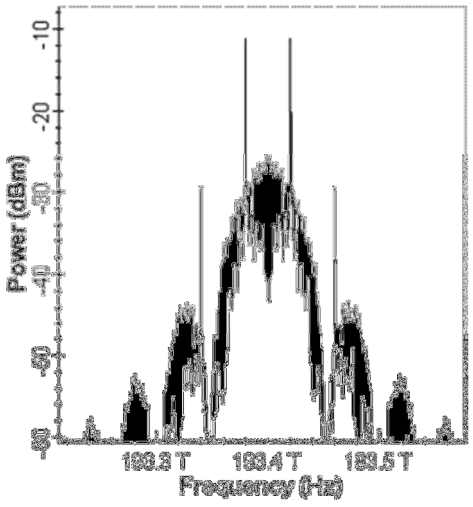

(b)

Figure 3.24 (a) Eye diagram CSRZ, (b) Spectrum CSRZ

Chapter 4

FORWARD ERROR CORRECTION

There are many factors which can cause the output from a channel to differ from its input. Among them are nonlinearities, attenuation, noise, and dispersion to name a few. The errors generated can be overcome through an increase in signal energy; however, this is not always feasible. Coding the input signal can increase the performance of the channel close to capacity and when coding coincides the use of orthogonal signals, channel capacity can be reached as the number of signals approach infinity [16, 39]. In this chapter coding more specifically forward error correction coding, will be reviewed with the intention of improving BER caused by OADM crosstalk and filter narrowing.

4.1 Channel Capacity

The channel capacity of an additive white Gaussian noise channel is defined by Shannon's formula, which is given by Equations 4.1 through 4.5 [40].

$$C = W\ log\left(1 + \frac{P}{N_o W}\right) {}^{bits}/_{sec} \tag{4.1}$$

$$W = bandwidth; P = signal\ power$$

As can be seen from Equation 4.1, a trade-off between $P\ and\ W$ exits in that one compensates the other. By increasing the signal power the channel capacity is increased. The increase in capacity by increasing power is logarithmic and therefore slow.

Increasing channel bandwidth has an immediate impact; it dramatically increases capacity yet at the same time increases noise and it follows that performance is decreased.

Through simple manipulation of Equation 4.1, the following relation is realized, defined as the spectral bit rate.

$$r = log\left(1 + r\frac{\mathcal{E}_b}{N_o}\right) \tag{4.2}$$

The graph of this function defines reliable communications. Above the curve reliable communications is not possible, below the curve reliable communications can be achieved and optimal communications exist on the curve. The point where approaches zero is called the absolute minimum point that reliable communications are possible. This point is where

$$\frac{\mathcal{E}_b}{N_o} > 0.693 \tag{4.3}$$

In binary signals that have an equal probability of transmitting a one or zero, the error probability in the binary antipodal case can be expressed as,

$$P_b = Q\left(\sqrt{\frac{2\varepsilon_b}{N_0}}\right) \tag{4.4}$$

where

$$SNR = \frac{\mathcal{E}_b}{N_o}\ ; \mathcal{E}_b = signal\ energy\ and\ N_o = Noise\ power \tag{4.5}$$

Referring back to Equation 4.1 now provides an expression for probability can be obtained that intuitively leads to the following: to decrease the error probability the signal

power has to be increased. This can be accomplished in one of two ways; by either increasing the transmitter power, or by increasing the transmission duration. It is not always feasible or practical to increase the transmitter power enough to achieve the desired result. Increasing the transmission duration decreases the transmission rate, which also is not desirable. Therefore, in order to eliminate error probability the transmission rate must be allowed to reach zero. However, while this is the case, reliable communications can be achieved only if Equation 4.4 is satisfied.

Orthogonal signals can achieve reliable communications but the price is considerable in bandwidth. In order to reliably transmit signals over a noisy AWGN channel at a rate without an exponential increase in bandwidth, coding must be implemented.

4.2 Linear Block Codes

An (n, k) block code is completely defined by $M = 2^k$ binary sequences of length n called code words. A code **C** consists of **M** code words $\boldsymbol{c}_i$ for $1 \leq i \leq 2^k$.

$$\boldsymbol{C} = \{\boldsymbol{c_1}, \boldsymbol{c_2}, \ldots . \boldsymbol{c}_M\} \tag{4.5}$$

where each $\boldsymbol{c}_i$ is a sequence of length n with components equal to 0 or 1[39].

A block code is linear if any linear combination of two code words is also a code word. In the binary case this requires that if $\boldsymbol{c}_i \; and \; \boldsymbol{c}_j$ are code words then are $\boldsymbol{c}_i \oplus \boldsymbol{c}_j$ is a code word, where $\oplus$ denotes component-wise modulo-2 addition. This definition produces a linear block code that is k-dimensional subspace of an n-dimensional space, also all zero

sequence **0** is a code word of any linear block code. According to the above definition linearity of code words only depend on the code words and not on the way the information sequence is mapped to the code words[39].

Hamming codes are a class of linear block codes with $n = 2^m - 1, k = 2^m - m - 1 \; and \; d_{min} = 3, for \; some \; integer \; m \geq 2$.The parity checks for these codes are a very simple structure. Hamming codes are very high rate codes with small relative distance ($d_{min} = 3$). The minimum distance of a code is closely related to its error-correcting capability. Therefore Hamming codes have a limited error-correcting capability[39].

4.2.1 Cyclic Codes

Cyclic codes are subset of linear block codes that use easily implemented encoders and decoders. A cyclic code is a linear block code with an extra condition imposed, that being if a $\boldsymbol{c}$ is a code word a cyclic shift of $\boldsymbol{c}$ is also a code word. An example of a cyclic code is $\{000, 111, \; 011, 101\}$ this code is a cyclic code because it is linear and any cyclic shift of the code words is a code word. An example of a code word that is not a cyclic code is $\{000, 010, 101, 111\}$ it is linear but not cyclic because the cyclic shift of $\{101\}$ is not a code word. Compared to the general class of linear block codes, cyclic codes have greater structure and are easier to implement.

Bose, Chaudhuri, and Hocquenghem (BCH) codes are a subset of cyclic codes that can be designed for the correction of *t* errors. The versatility and the existence of efficient

decoding algorithms make these codes widely used. For any *m* and *t*, there exists a BCH code with parameters;

$$n = 2^m - 1, n - k \leq mt, and\ d_{min} = 2t + 1 \tag{4.6}$$

Since *m* and *t* are arbitrary, the designer of the system has a large number of combinations to choose from[39].

4.2.2 Reed-Solomon Codes

Reed-Solomon codes are a subset of BCH codes also making them a member of the family of cyclic codes. They are nonbinary codes; an example of a code word $\boldsymbol{c} = \{\boldsymbol{c_1}, \boldsymbol{c}_2, \ldots . \boldsymbol{c}_n, \}$ with elements $\boldsymbol{c}_i$ for $1 \leq i \leq n$ are members of a *q*-ary alphabet. Generally q is chosen to be a power of 2, such as $q = 2^k$. In this instance *k*-information bits would be mapped into an element from the *q*-ary alphabet, then using a Reed-Solomon(*N, K*) code, *K, q*-ary symbols are mapped into *N, q*-ary symbols and transmitted over the channel. Reed-Solomon codes are defined by Equations 4.7 to 4.11 [39]

$$N = q - 1 = 2^k - 1 \tag{4.7}$$

$$K = 1, 3, \ldots . , N - 2, \tag{4.8}$$

$$D_{min} = N - K + 1 \tag{4.9}$$

$$R_c = \frac{K}{N} \tag{4.10}$$

Reed-Solomon codes can correct up to *t* symbol errors where *t* is equal to

$$t = \frac{D_{min} - 1}{2} \tag{4.11}$$

Reed-Solomon codes have very good distance properties and are well suited for using in q-ary modulation and adept at handling errors when they tend to occur in bursts. The latter is a result of burst errors only effecting a relatively few errors in the coding. On the other hand in binary codes, a burst would result in many bits in error, which may not be easily corrected. Reed-Solomon codes can be concatenated with binary codes to provide more robust correction capability. The binary encoder is located directly after the modulator and after the demodulator [39]. Recalling that errors generated within OADMs are burst errors makes the use of REED-Solomon FEC algorithms the logical choice [8].

4.3 Convolutional Codes

Convolutional codes are different from block codes by the existence of memory in the encoding scheme. In block codes k input bits are mapped into a block of length n output bits by a rule defined by the code regardless of the previous bit. Convolutional codes are generated by passing the information sequence through a linear finite-state shift register. The register consists of K (k-bit) stages and n linear algebraic function generators. The binary input into the encoder is shifted into and along the shift register k bits at a time. The number of output bits for each k-bit input sequence is n-bits. The code rate is therefore $R_c = k/n$, which is consistent with the code rate for block codes. K is also known as the constraint length of the convolutional code. Convolution codes can be described by not only the state space machine but also with a trellis diagram[39].

4.3.1 Complex Codes based upon Combinations of Simple Codes

The performance of block and convolutional codes is primarily determined by the distance properties of the code, in particular the minimum distance in block codes and the free distance in convolutional codes. To design block codes for great distance at a given R_c the value of n has to be increased thereby increasing the length of the code. This results in an increase in the complexity of the decoding. With block codes the decoding complexity increases exponentially as the block length increases. Convolutional codes decoding complexity is increased by an increase in trellis length which is a direct result of increasing the constraint length of the code. Three widely used methods of combining codes are Product codes, concatenated codes and turbo codes[39].

Product codes (code arrays) are similar in structure to a crossword puzzle. They are generated by using a linear block codes arranged in a matrix form. Decoding is accomplished by using the rows to guess the correct bit value then the column codes improve on these guesses. This process is done in an iterative process improving with each iteration. Decoding that generates soft outputs are employed in Turbo codes[39].

Concatenated codes are two codes one inner the other outer that are connected serially. Typically the inner code is a block code or a convolutional code, the outer code is generally a Reed-Solomon code. This has the effected of correcting a signal that is now an input array for the Reed-Solomon code, providing further error correction protection.

Turbo codes are a special class of concatenated codes where an interleaver exists between parallel or serial encoders. This results in very large word lengths with excellent performance at very low SNRs but makes their use to increase SE is limited[39]. This thesis will concentrate on the improvement in performance and increase in SE upon memoryless advanced modulation formats on optical networks by utilizing a cyclic, linear block code: Reed-Solomon product code and concatenated code.

Performance analysis of a communication system cannot be graded unless a quantifiable method of measuring the information and the modeling of the information. Hartley, Shannon and Nyquist pioneered the defining of these quantitative we utilize today. What is common among communication sources is they are all band limited and therefore meet the criteria for sampling at the Nyquist rate or greater and can be reconstructed from the sampled values [39].

Chapter 5

METHODOLOGY

Four different simulations were developed to assess the impact of filter narrowing and WDM crosstalk generated within OADM on memoryless advanced formats. Then the improvement that forward error correction (FEC) can have in addressing the decrease in BER. The intent of these simulations is to determine which format(s) are more tolerant to the adverse effects of transmission within an optical network that contains multiple OADMs. The modulation formats studied are 33% RZDPSK, 50% DPSK, 66% DPSK, NRZDPSK, 33% DQPSK, 50% DQPSK, 66% DQPSK, NRZDQPSK and CSRZ. CSRZ is described as a format that has pseudo-memory and will be used as a comparison to the other formats that are memoryless. To actually measure the impact of filter narrowing and WDM crosstalk, simulations were designed to test each of these effects separately.

5.1 Repeated Filtering of the Two Adjacent Channels

To measure the effect of filter narrowing, banks OADMs each containing four optical add/drop filters were constructed. The OADMs simulate the transmission of an optical signal λ_2 through a network and the repeated reuse of λ_1 and λ_3 by adding and dropping them onto the network. To measure the impact on λ_2 from filter narrowing the simulated OADMs were configured to the specifications shown in Table 5.1 and Figure 5.1.

Insertion Loss	0 dB
Attenuation	0 dBm
Bandwidth	50 GHz or 100GHz
Depth	100 dB
Filter type	Bessel
Filter order	2
Delay	0
Channel Spacing	Varied based upon SE 0.4 (0.1 THz) 0.08 THz, 0.05 THz)

Table 5.1 Specifications for Repeated Filtering of the Two Adjacent Channels.

The first scenario tested an optical transmission $\lambda_2 = 192.9$ THZ passing through multiple OADMs without being dropped and added to the network. This simulated the transmission of λ_2 passing through a network of multiple OADMs before the signal reaches its final destination. This configuration allowed for an effective method to measure the impact on the desired channel. To simulate the effect of the adjacent channels each bank of OADMs contained four separate filters designed to repeated add and drop the two channel frequencies on each side of $\lambda_2 = 192.9$ THz $\lambda_1 = 192.9 +$ [(channel spacing)] THz and $\lambda_3 = [192.9 -$ (channel spacing)] THz. The OADMs had their channel spacing based upon the SE under investigation and the filter bandwidth being assessed. The channel spacing's where 0.1 THz, 0.08 THz and .05 THz, the two OADM filter bandwidths tested were 100GHz and 50GHz.

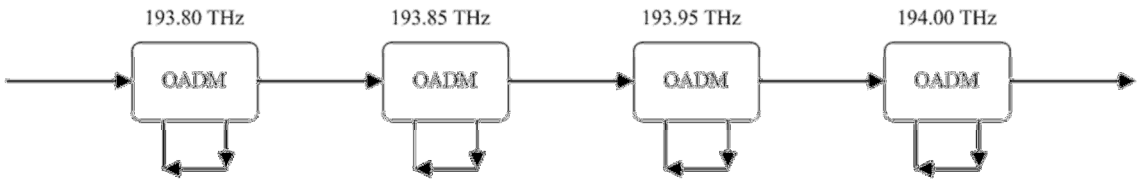

Figure 5.1 OADM node for repeated filtering by the two adjacent channels.

Each modulation format was tested by starting the simulation with one bank of OADMs each containing the four filters. The simulations were run and an OADM was added to each modulation format simulation until the BER received was less than 10^{-3} or the Reed Solomon FEC could not improve the received transmission to a BER of 10^{-6} or greater as shown in Figure 5.2. Then the total number of OADMs resulting in a satisfactory BER was recorded along with the maximum uncorrected BER and the resulting corrected BER. The simulations were stopped when a modulation format was able to transmit successfully through five sets of OADMs or twenty total filters. The BER and corrected BER received at the end of the five OADMs was recorded.

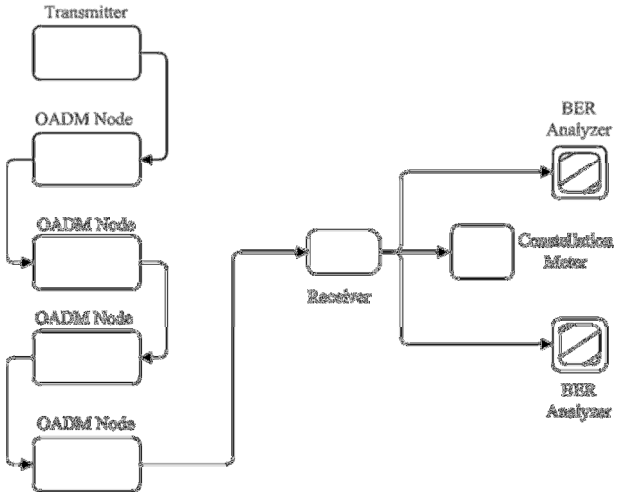

Figure 5.2 Typical configuration for simulation #1

The preceding experiment was repeated for each of the 9 modulation formats under investigation and each of the nine formats was tested at SE=0.4 and SE=0.8. For SE of 0.4 the simulations were set up using a bitrate of 40 GHz a WDM channel spacing of 0.01 THz. For a SE of 0.8, a bitrate of 40 GHz and a WDM channel spacing of 0.05 THz was tested and then repeated with a bitrate of 100 GHz and a WDM channel spacing of 0.08 THz. All three of the above simulations were run twice, first with an OADM comprised of second order Bessel filters with bandwidths of 100 GHz and then the same second order Bessel filters with bandwidths of 50 GHz.

5.2 Repeated Dropping and Adding of a Channel to Another Network

The next set of simulations was conducted to establish the effect a transmitted modulation format using $\lambda_2 = 193.4$ THz would experience if passed through a series of OADMs in which it was repeatedly dropped the added to another network. To simulate these phenomena, banks of OADMs were constructed comprising of four second order Bessel filters all tuned to the transmission frequency of $\lambda_2 = 193.4$ THz. The OADMs specifications are in Table 5.2 below.

Insertion Loss	0 dB
Attenuation	0 dBm
Bandwidth	50 GHz or 100GHz
Depth	100 dB
Filter type	Bessel

Table 5.2 Specifications for OADMs for Simulation #2

As in the previous simulation, to measure the effect of the multiple OADMs on a specific modulation format a signal, the prescribed modulation format was generated and launched through the multiple banks of OADMs. Each OADM was comprised of four second-order Bessel filters all tuned to the same frequency as the transmitted optical signal $\lambda_2 = 193.4$ THz Figure 5.3 and using the specifications in Table 5.3.

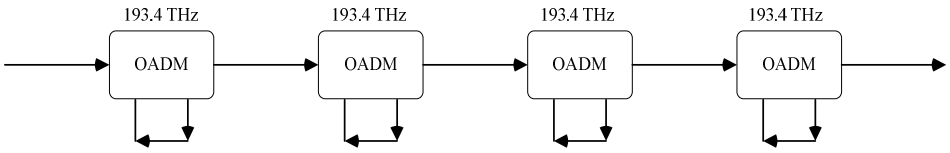

Figure 5.3 OADMs to simulate the repeated dropping and adding λ_2 to other networks.

Add Drop Frequency	193.4 THz
Insertion Loss	0 dB
Attenuation	0 dBm
Bandwidth	50 GHz or 100GHz
Depth	100 dB
Filter type	Bessel
Filter order	2
Delay	0
Channel Spacing	Not applicable

Table 5.3 Simulation Configuration for the Repeated Dropping and Adding of λ_2

This simulated the transmission of an optical signal repeatedly undergoing the process of being dropped and added to another network through an OADM without undergoing any amplification or processing until it reached its final destination. This configuration, as shown in Figure 5.4, presented a simple yet effective method to measure the impact on the desired channel caused by repeatedly filtering with the same filter frequency and the subsequent filter narrowing could then be assessed. To simulate the effect each bank of OADMs contained four separate filters designed to drop and add the channel frequency that was transmitted, $\lambda_2 = 193.4$ THz.

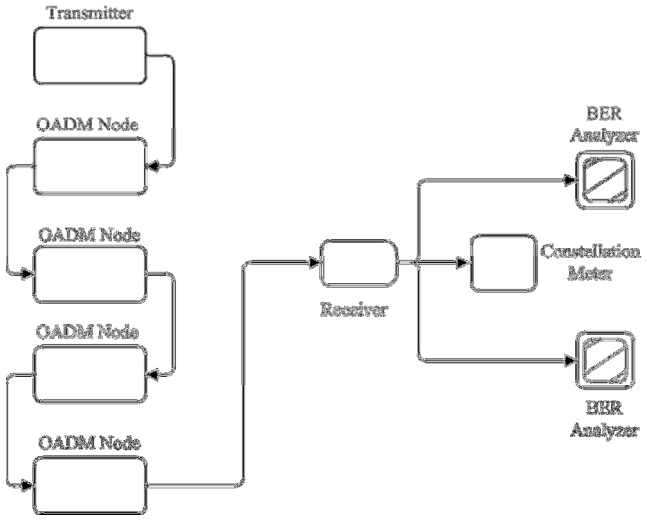

Figure 5.4 Simulation configuration for repeated adding and dropping of a channel λ_2

Each modulation format was tested by starting the simulation with one bank of OADMs which contained four identical filters. An OADM was added to each modulation format simulation until the BER received was less than 10^{-3} or the Reed Solomon FEC could not improve the received transmission to a BER of 10^{-6}, at which point the total number of OADMs resulting in either a satisfactory BER was recorded along with the maximum uncorrected BER and the resulting corrected BER. The simulations were stopped when a modulation format was able to transmit successfully through five banks of OADMs or twenty total filters. If the modulation format tested successfully transmitted through five banks of OADMs the BER and corrected BER received at the end of the five banks of OADMs was then recorded. This process was repeated for all nine modulation formats at a bitrate equal to 100 GHz and a filter bandwidth of 100 GHz then again at a bit rate of 100 GHz and a filter bandwidth of 50 GHz. Then the nine modulation formats were tested again at a bitrate of 40 GHz and a filter bandwidth of 100 GHz and then again at 40 GHz and a filter bandwidth of 50GHz.

5.3 OADM Crosstalk

The next simulation was designed to measure the effect of crosstalk generated within an OADM by adjacent channels. The channel spacing of the WDM network is predicated on the SE being investigated.

The simulation was designed to measure this phenomena consisted of three pairs of OADMs located at nodes in a WDM optical network, as shown in Figure 5.5. Only three channels are transmitted, the two adjacent channels and the channel to be measured were launched into the network. To estimate the full impact from the coherent crosstalk within the OADM only the adjacent channels need be transmitted, all other channels are spaced too far away to give rise to beat frequencies that fall within the electrical detection bandwidth[7]. The channels were not copolarized for worst-case scenario performance. Channel spacing and bitrate were based upon the desired SE.

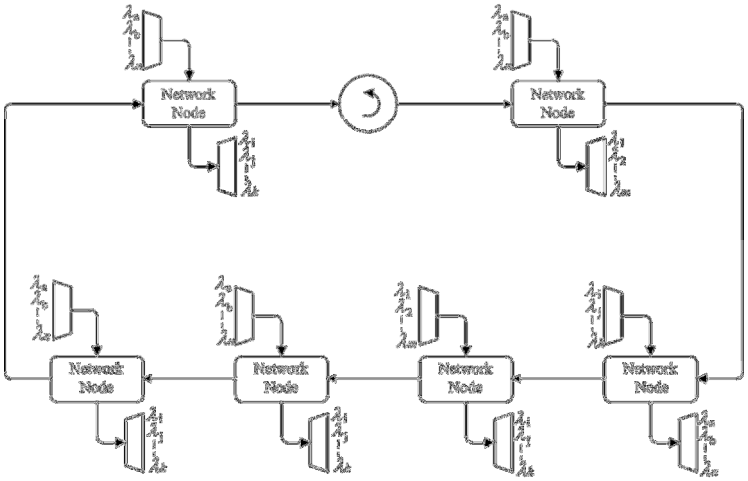

Figure 5.5 Crosstalk simulation configuration

Each node in Figure 5.5 contained the following components listed below:

- One OADM set to one of three transmitted frequencies
- optical attenuator set to 0 dB
- optical interleaver
- serial and parallel

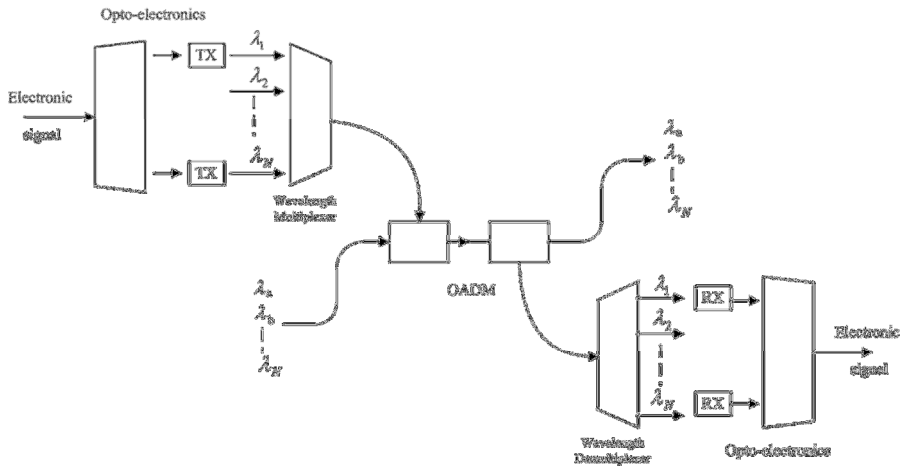

Figure 5.6 Typical node used in simulation # 3

Each component within the node that was not specifically linked to the generation of a particular modulation format was tuned to the specifications outlined in Table 5.4.

CW Laser	
Initial Phase	0 deg
Azimuth	0 deg
Ellipticity	0 deg
OADM	
Add Drop Frequency	193.4 THz
Insertion Loss	0 dB
Attenuation	0 dBm
Bandwidth	50 GHz or 100GHz
Depth	100 dB
Filter type	Bessel
Filter order	2

Table 5.4 Specification for Simulation #3

The simulation was designed such that the channel experiencing the adverse effects from the crosstalk passed through each of the OADMs contained within each node while it was under the influenced of the adjacent channel as shown in Figure 5.5 and Figure 5.6. The BER and FEC BER were measured at the final node after the channel that had been subject to the crosstalk and been dropped from the network. In this way the maximum impact from the OADM crosstalk could be assessed. Each of the modulation formats were placed into the simulation for SE of 0.4 and SE of 0.8. The simulation for SE of 0.4 was created utilizing a bitrate of 40 GHz and a channel spacing of 0.1 THz. The SE of 0.4 was simulated utilizing both OADM filter bandwidths of 100 GHz and 50 GHz. The resulting BER and FEC BER for each of the aforementioned scenarios was recorded. The same procedures were then applied to the transmitted format at a SE of 0.8. The SE of 0.8

was generated two ways, first by using a bitrate of 40 GHz and channel spacing of 0.05 THz and then again using a bit rate of 100 GHz and a channel spacing of 0.08 THz, each of the SE 0.8 simulations were repeated for OADM filter bandwidths of 100 GHz and 50 GHz.

The BER and the FEC BER where recorded for each format under each scenario. If the minimum BER of 10^{-3} was not obtained or the Reed Solomon FEC could not generate a predicted BER of 10^{-6} the results were recorded as 10^{-2}.

5.4 Multiplexed Simulation

The top performing modulation formats will be determined based upon their overall performance during the three preceding simulations. The top formats will then be subjected to one final simulation. This simulation will address their overall robustness in the face of multiple filtering impairments. This simulation will test the ability of the format to operate in an environment that not only combines the adverse effects from first three simulations but adds the impairments introduced by the filter narrowing caused by multiplexing and demultiplexing as shown in Figure 5.7.

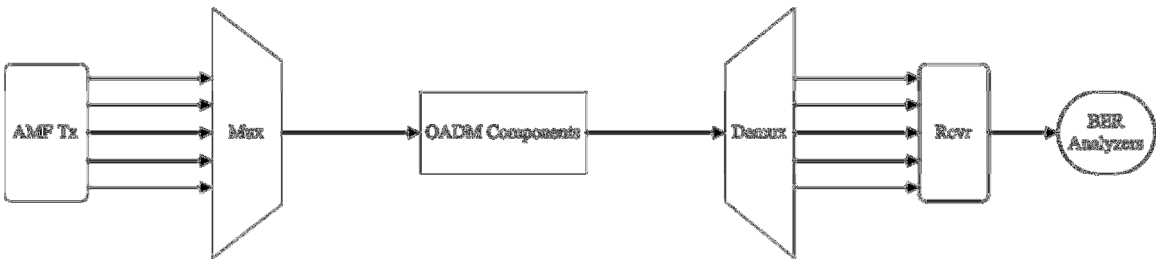

Figure 5.7 Configuration for multiplexed simulation

In all four categories of simulations with thirteen different modulation formats were designed to access the robustness of each modulation formats studied. Three of the categories of simulations each accessed the formats at a SE of 0.4 with the Bitrate equal to 40 GHZ and $\Delta\lambda$ equal to 100GHz, a SE of 0.8 where the bitrate was 40 GHz and the $\Delta\lambda$ equal to 50GHz, and a SE also equal to 0.8 with a different bitrate of 100GHz and a $\Delta\lambda$ equal to 100GHz. Based upon the results of the three previous simulations the most robust and best performing formats where then tested one last time. The results of the simulations will be presented in Chapter 6.

Chapter 6

RESULTS

This chapter presents the results of the simulations developed and implemented in this thesis. Thirteen modulation formats where assessed under three different set of conditions for a total of 234 sets of results. The results were plotted in a bar graph format in order to facilitate the analysis. In order to ensure consistency between the different modulation formats, all simulations were run with a laser transmitter power of 0dBm.

6.1 Repeated Filtering

After collecting data using the simulation configuration described in Section 5.1, the results obtained were ranked by the number of OADM sets the format was capable of traversing successfully at the receiving terminal of the transmission link. The Log(BER), the Log(FEC BER) and the number of OADM sets were plotted as bar graphs and the three best performing modulation formats were identified.

6.1.1 Filter Narrowing Caused by the Two Filter Adjacent Channels

The bar graphs contain the results for the filter narrowing simulation. The spectral efficiency (SE) was established at 0.4 with a wavelength separation of 100GHz and a

bitrate of 40 GHZ as was described in Section 2.6. The filter bandwidth of the optical add drop multiplexers was set at 100GHz.

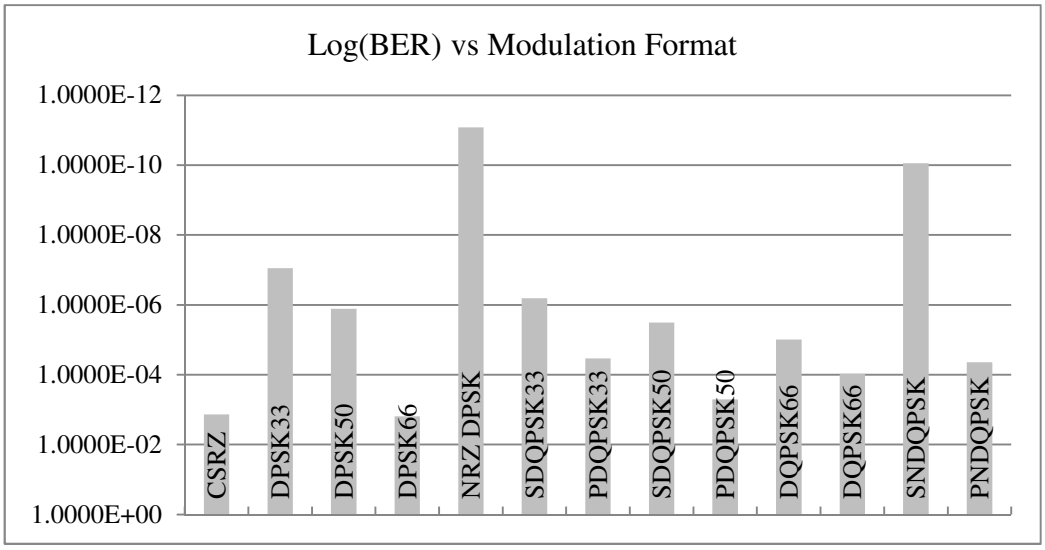

(a)

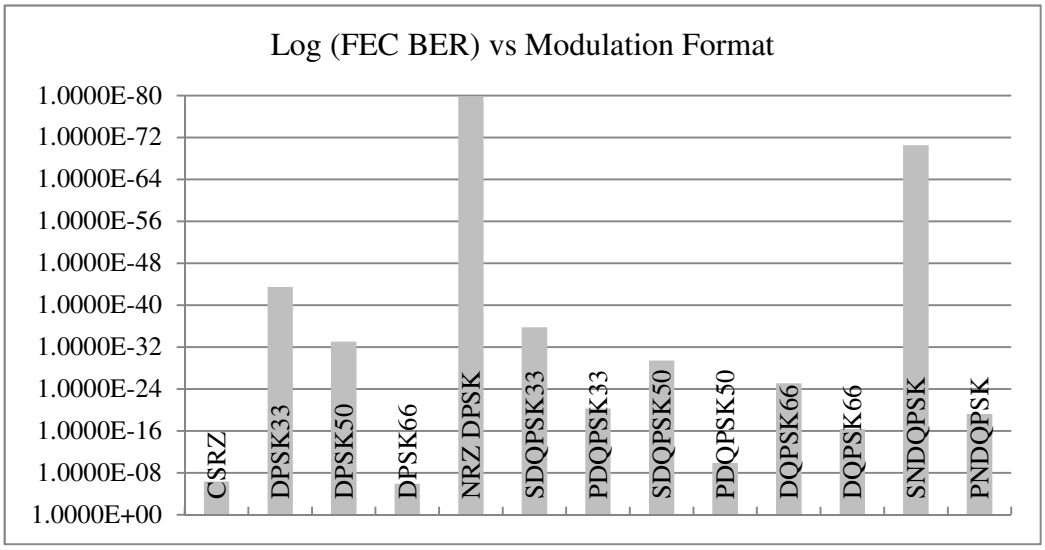

(b)

Figure 6.1 (a) Log(BER) and (b) Log(FEC BER) vs. modulation format

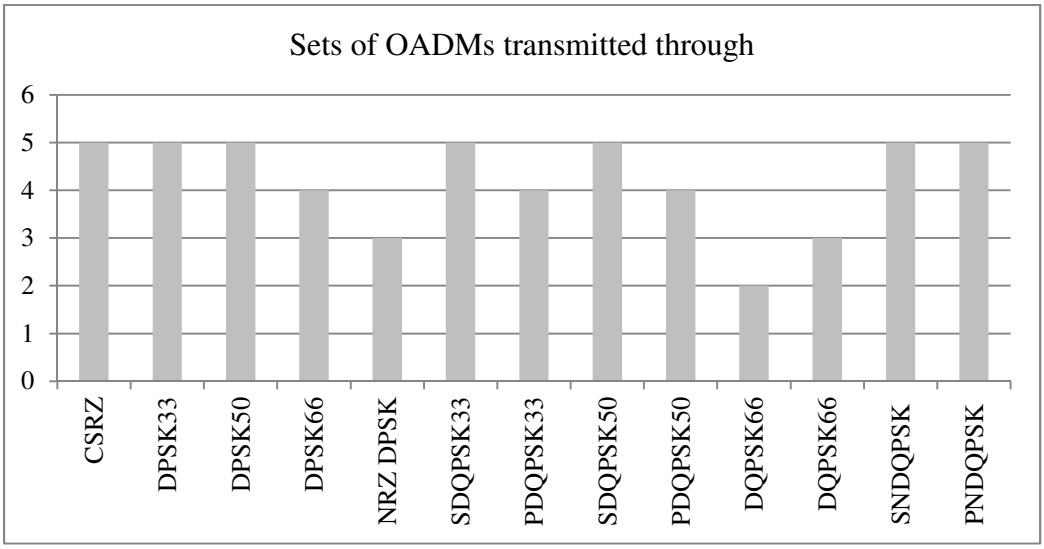

Figure 6.2 Sets of OADMs transmitted through

Figure 6.1(a) and (b) display the Log(BER) and the Log(FEC BER) respectively versus the modulation format. NRZ DPSK, NRZ DQPSK (series) then DPSK 33% produced the lowest BERs. Figure 6.2 shows the number of sets of OADM filters that transmission was possible as described in Section 5.1. All thirteen formats were able to transmit through at least two sets of OADMs and achieve a BER less than the maximum, seven of the formats were able to transmit through five sets of OADMs and exit with a BER lower than the maximum permissible. Application of the Reed Solomon FEC to the seven formats that passed through five sets of OADMs, resulted in NRZ DQPSK (series) format having the most improvement decreasing BER from 10^{-11} to 10^{-71}. Overall NRZ DQPSK (series) performed the best.

Figure 6.3 and Figure 6.4 contain the results for the filter narrowing simulation where the spectral efficiency (SE) was established at 0.4 with a wavelength separation of 100GHz

and a bitrate of 40 GHZ as described in Section 2.6. The filter bandwidth of the optical add drop multiplexers was set at 50GHz.

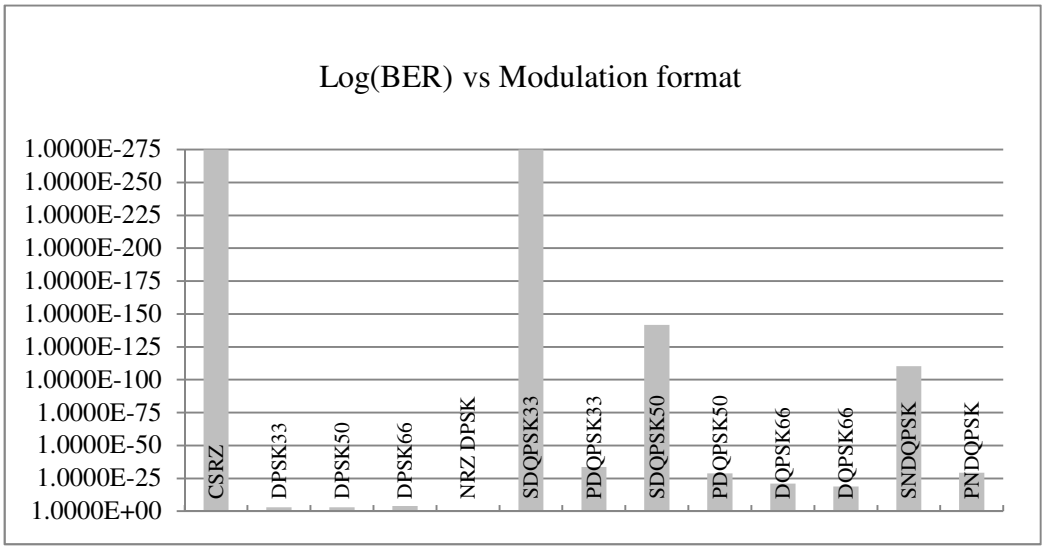

(a)

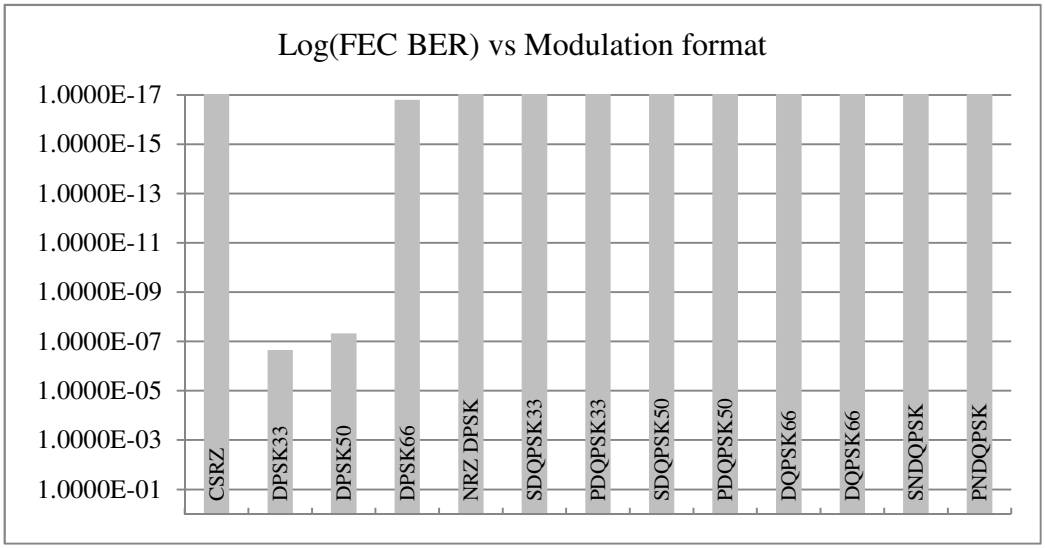

(b)

Figure 6.3 (a) Log(BER) and (b) Log(FEC BER) vs. modulation format

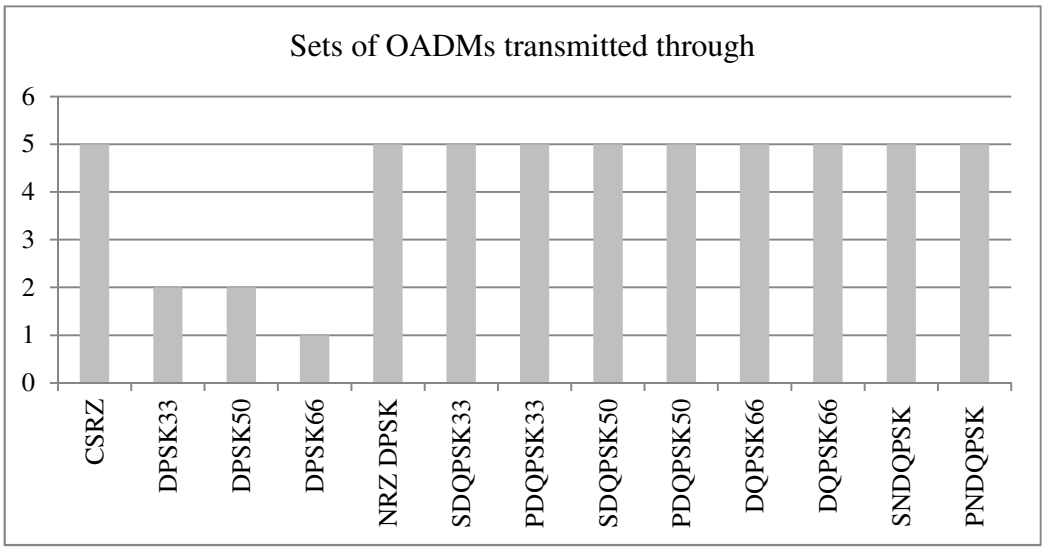

Figure 6.4 Sets of OADMs transmitted through

Figure 6.3(a) and (b) display the Log(BER) and the Log(FEC BER) respectively versus the modulation format. NRZ DPSK followed by NRZ DQPSK (series) produced the best BER results. Figure 6.4 shows the number of sets of OADM filters that transmission was possible as described in Section 5.1. All thirteen formats successfully passed through at least one set of OADMs with a BER less than the maximum permissible. Ten of the formats were able to transmit through five sets of OADMs and exit with a BER lower than the maximum permissible. RZ DQPSK 33%, followed by NRZ DPSK and then CSRZ obtained approximately zero BER after passing through five sets of OADMs. The application of the Reed Solomon FEC resulted in formats with a BER less than 10^{-19} correcting to approximately zero BER. Overall DQPSK 33% (series), NRZ DPSK and CSRZ performed the best.

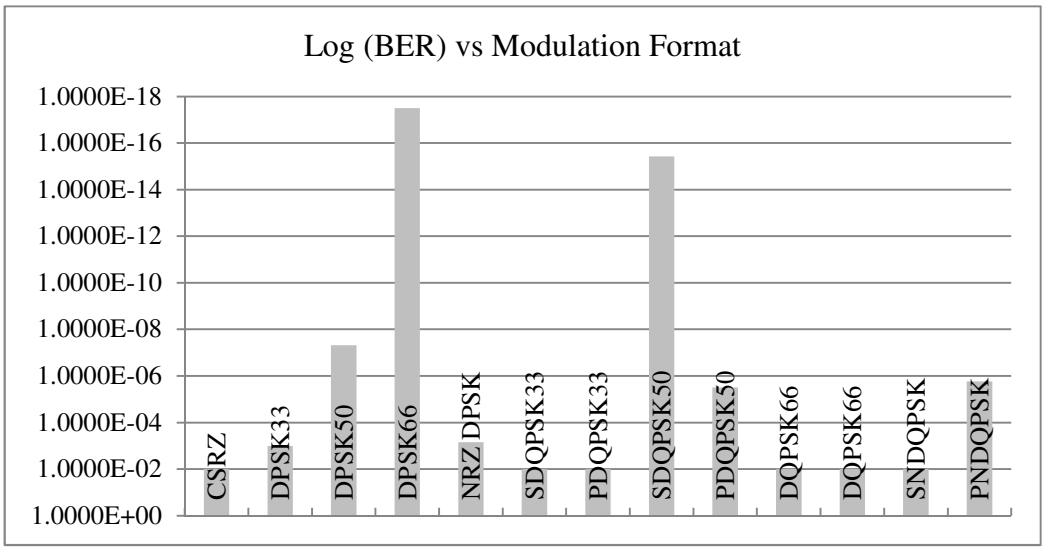

(a)

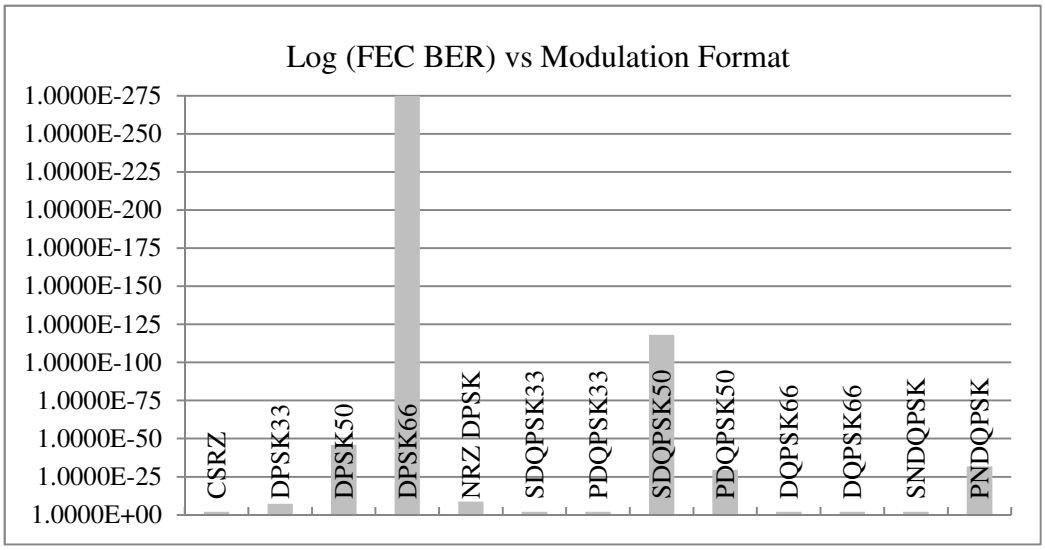

(b)

Figure 6.5 (a) Log(BER) and (b) Log(FEC BER) vs. Modulation format

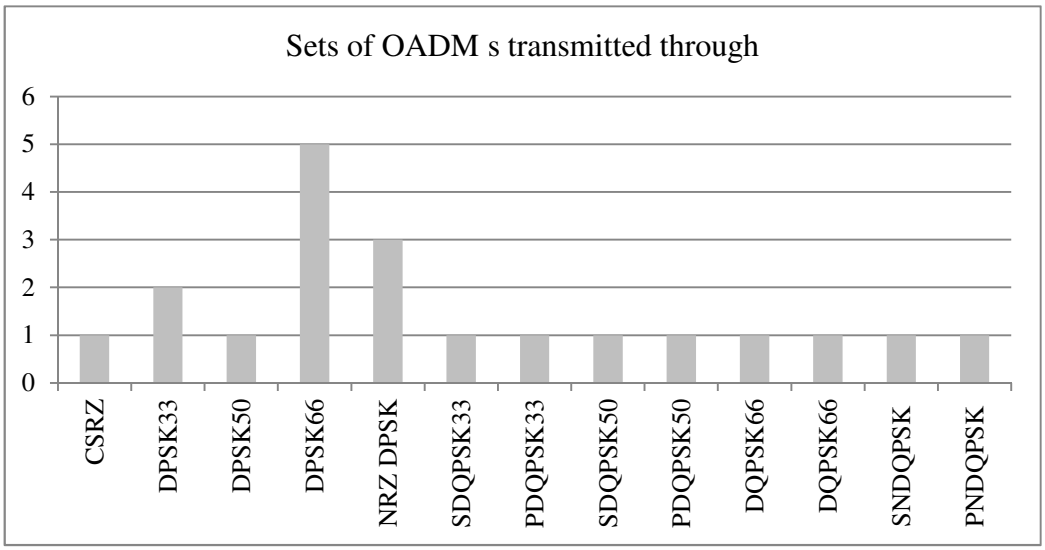

Figure 6.6 Sets of OADMs transmitted through

Figure 6.5(a) and (b) respectively display the Log(BER) and Log(FEC BER) versus modulation. NRZ DPSK, CSRZ and DPSK 66% produced the lowest BERs. Figure 6.6 shows the number of sets of OADM filters that transmission was possible as described in Section 5.1. Seven formats were able to transmit through at least one set of OADMs and achieve a BER at or above the maximum correctable level. DPSK 66% passed through five sets of OADMs and exit with a BER lower than the maximum permissible. The application of the Reed Solomon FEC to the DPSK 66% format resulted in an improvement of BER from 10^{-18} to approximately zero. Overall DPSK 66% performed the best.

The graphs shown in Figure 6.7 and 6.8 contain the results for the filter narrowing simulation. The spectral efficiency (SE) established at 0.8 with a wavelength separation of 80GHz and a bitrate of 100 GHz as was described in Section 2.6. The filter bandwidth of the optical add drop multiplexers was set at 50GHz.

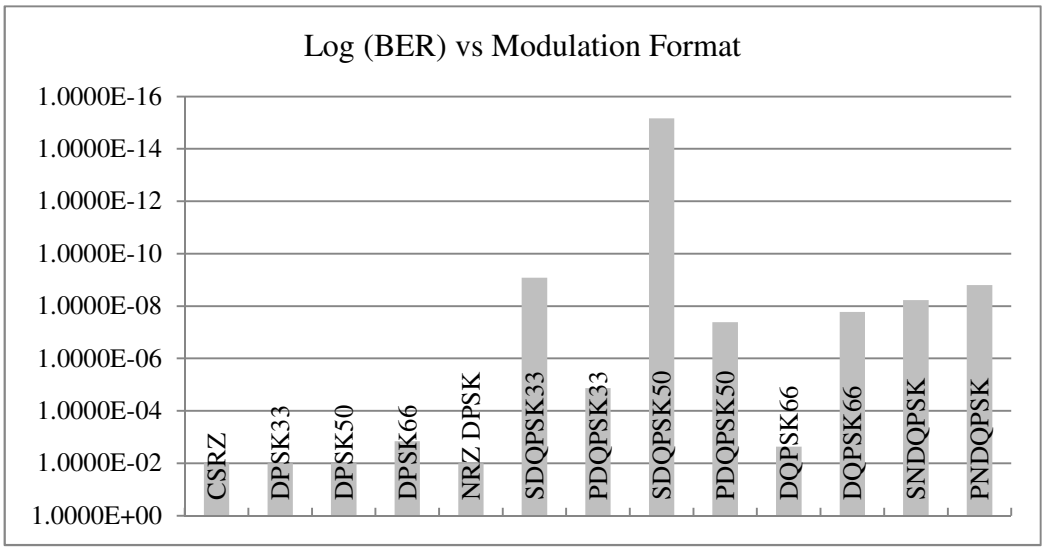

(a)

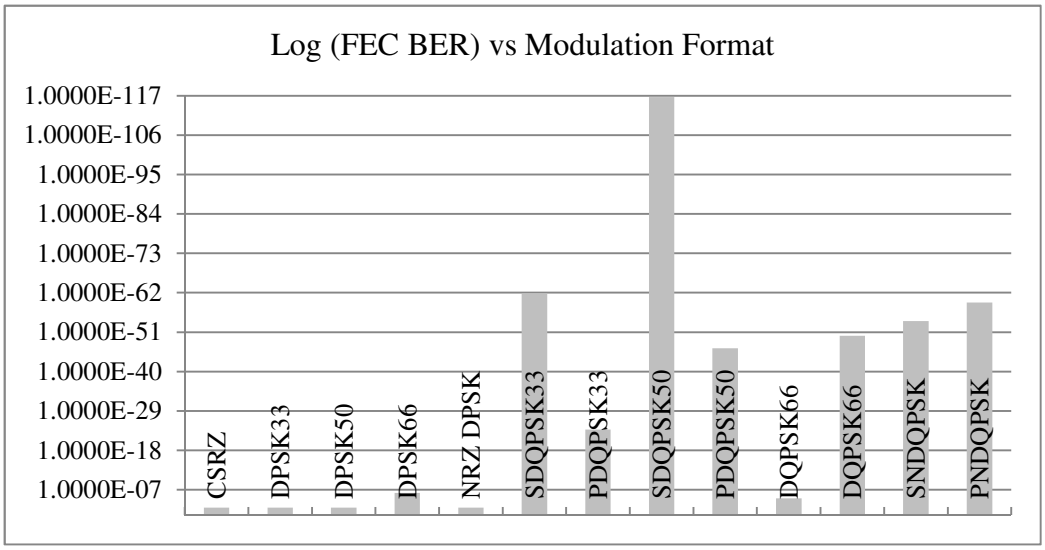

(b)

Figure 6.7 (a) Log(BER) and (b) Log(FEC BER) vs. modulation format

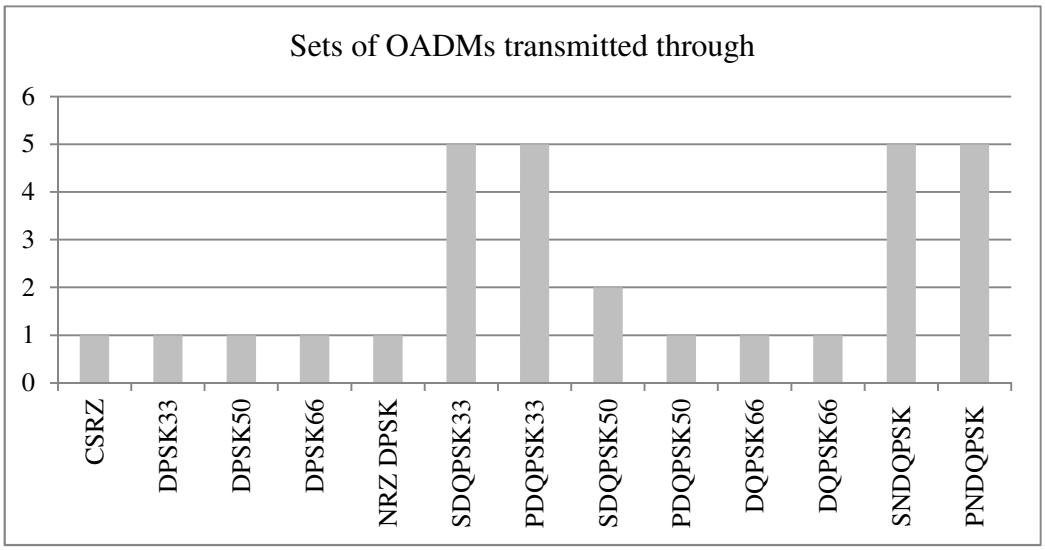

Figure 6.8 Sets of OADMs transmitted through

Figure 6.7(a) and (b) display the Log(BER) and the Log(FEC BER) respectively versus the modulation format. DQPSK 33% (series), DQPSK 50% (series) NRZ DQPSK (series) performed the best. Four formats transmitted through the maximum of five sets of OADMs while nine formats successfully passed through at least one set of OADMs with a BER less than the maximum permissible. RZ DQPSK 33% (series), NRZ DQPSK (parallel), NRZ DQPSK (series) and RZ DQPSK 33% (parallel) passed through five sets OADM filters and obtained a correctable BER. The application of the Reed Solomon FEC resulted in RZ DQPSK 33% (series) correcting from 10^{-10} to 10^{-62}.

The graphs shown in Figure 6.9 and 6.10 contain the results for the filter narrowing simulation where the spectral efficiency (SE) was established at 0.8 with a wavelength separation of 50GHz and a bitrate of 40 GHZ as was described in Section 2.6. The filter bandwidth of the optical add drop multiplexers was set at 100GHz.

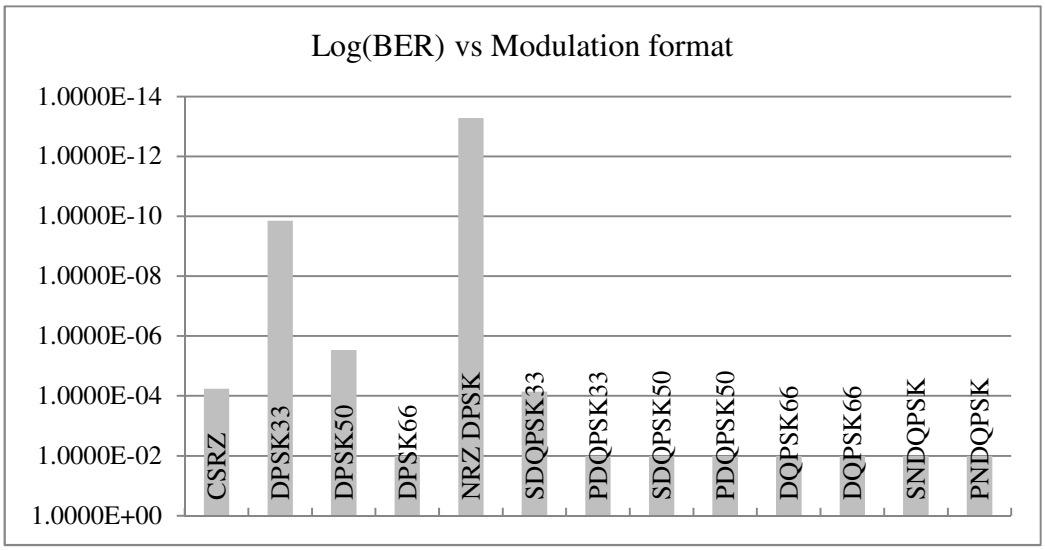

(a)

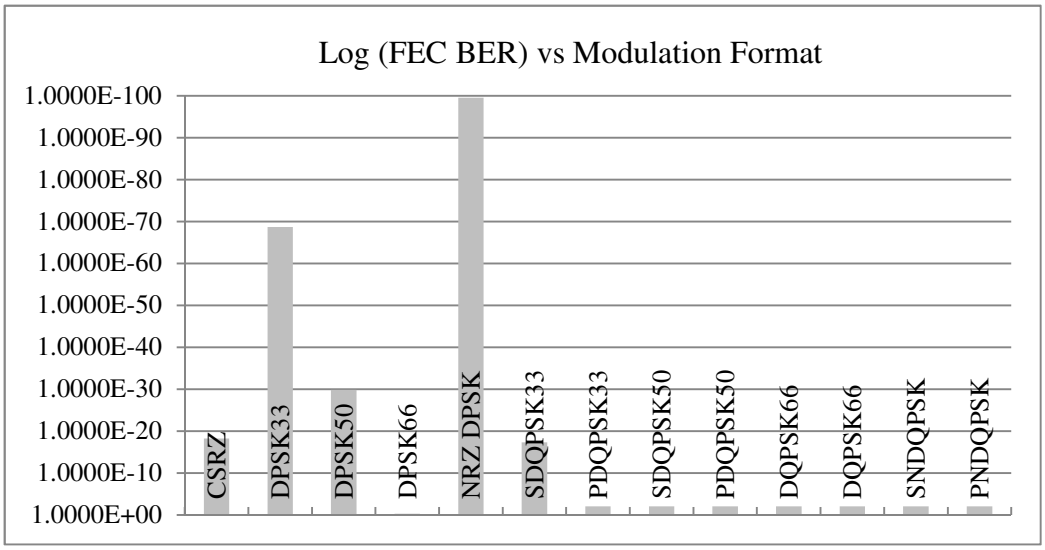

(b)

Figure 6.9 (a) Log(BER) and (b) Log(FEC BER) versus the modulation format.

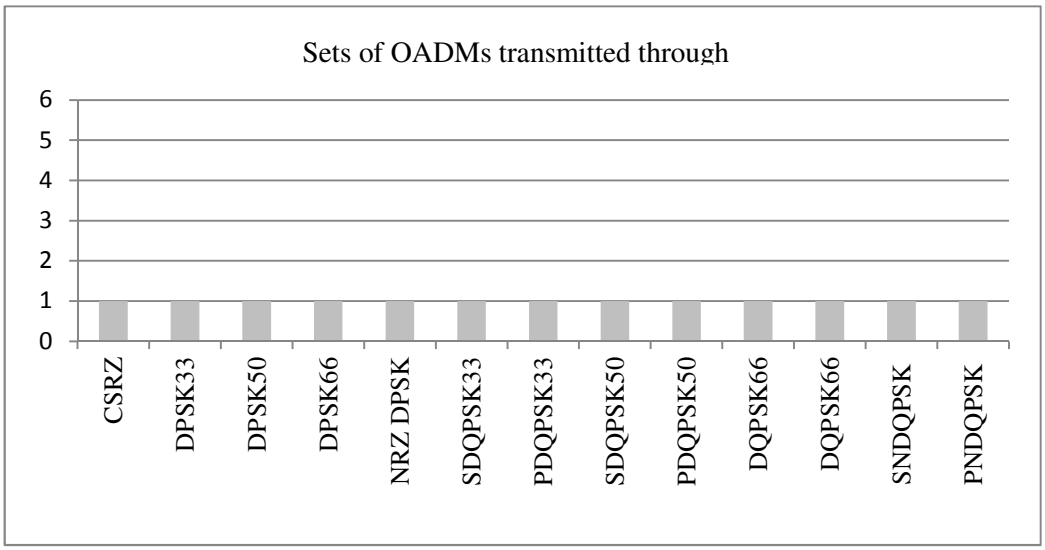

Figure 6.10 Sets of OADMs transmitted through

Figure 6.9 and (a) and (b) display the Log(BER) and Log(FEC BER) respectively versus the modulation format. NRZ DPSK, DPSK 33% and DPSK 50% produced the lowest BERs. Figure 6.10 shows the number of sets of OADMs through which transmission was possible as described in Section 5.1. Five formats passed through one set of OADMs and obtained a correctable BER. The maximum number of BER sets transmitted through was one. The application of the Reed Solomon FEC did not result in DPSK 33% correcting from 10^{-10} to 10^{-69}. Overall NRZ DPSK performed the best.

The graphs shown Figure 6.11 and 6.12 contain the results for the filter narrowing simulation where the spectral efficiency (SE) established at 0.8 with a wavelength separation of 50GHz and a bitrate of 40 GHZ as was described in Section 2.6. The filter bandwidth of the optical add drop multiplexer was set at 50GHz.

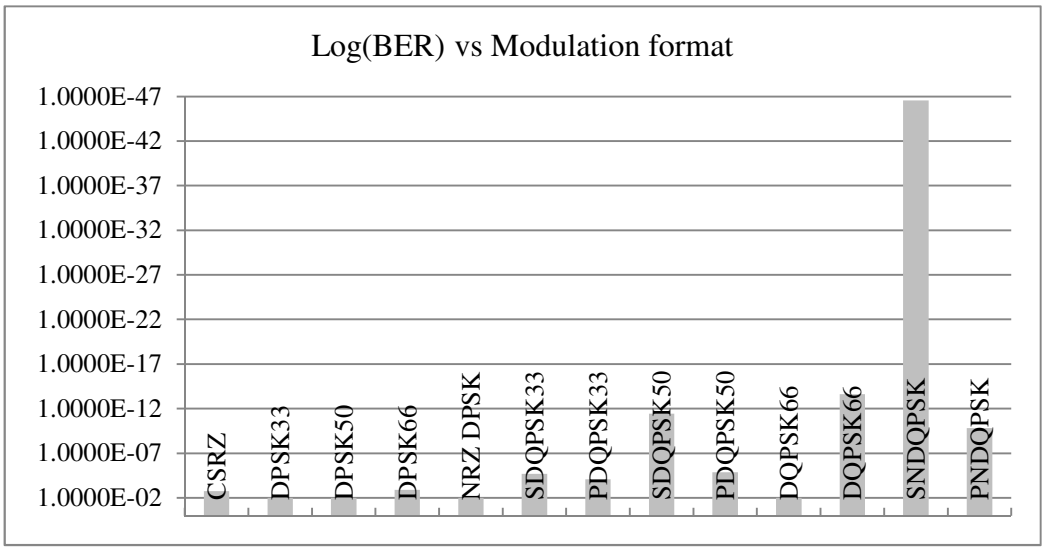

(a)

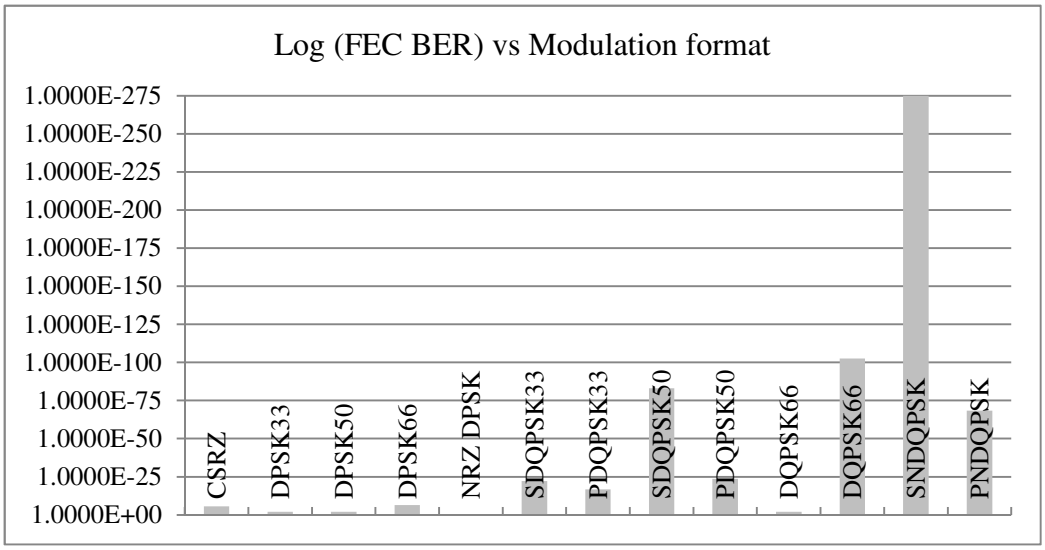

(b)

Figure 6.11 (a) Log(BER) and (b) Log(FEC BER) vs. modulation format

Figure 6.11(a) and (b) display the Log(BER) and the Log(FEC BER) respectively versus the modulation format. RZ DQPSK 33% (series), followed by CSRZ and then NRZ DQPSK (parallel) produced the lowest BER. Figure 6.12 shows the number of sets of OADMs through which transmission was possible as described in Section 5.1. Nine

formats were able to successfully pass through at least two sets of OADMs at a BER of 10^{-3} or less. The application of the Reed Solomon FEC resulted in NRZ DQPSK (series) being corrected to approximately zero BER also DQPSK 66% (parallel) corrected from 10^{-14} to 10^{-103}. Overall DQPSK 33% (series) performed the best.

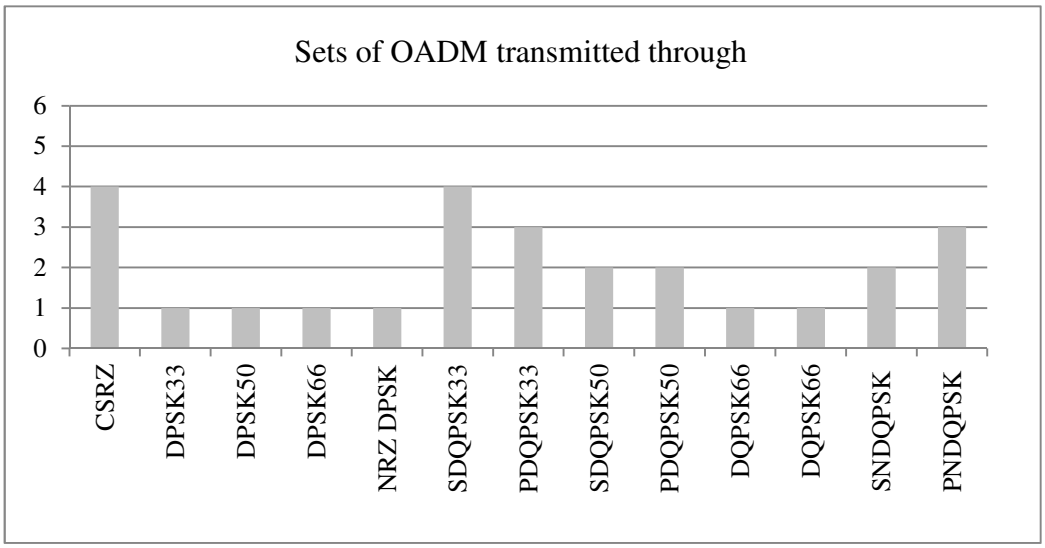

Figure 6.12 Sets of OADMs transmitted through

6.1.2 Filter Narrowing Caused by Single Channel Repeated Filtering

After collecting data using the simulation configuration described in Section 5.2, the results obtained were ranked by the number of OADM sets the format was capable of traversing successfully as well as the BER at the receiving terminal of the transmission link. The Log(BER), the Log(FEC BER) and the number of OADM sets were plotted as bar graphs and the three best performing modulation formats were identified.

Figure 6.13 and Figure 6.14 contain the results for the filter narrowing simulation where the spectral efficiency (SE) established at 0.4 with a wavelength separation of 100GHz and a bitrate of 40 GHZ as was described in Section 2.6. The filter bandwidth of the optical add drop multiplexers was set at 100GHz.

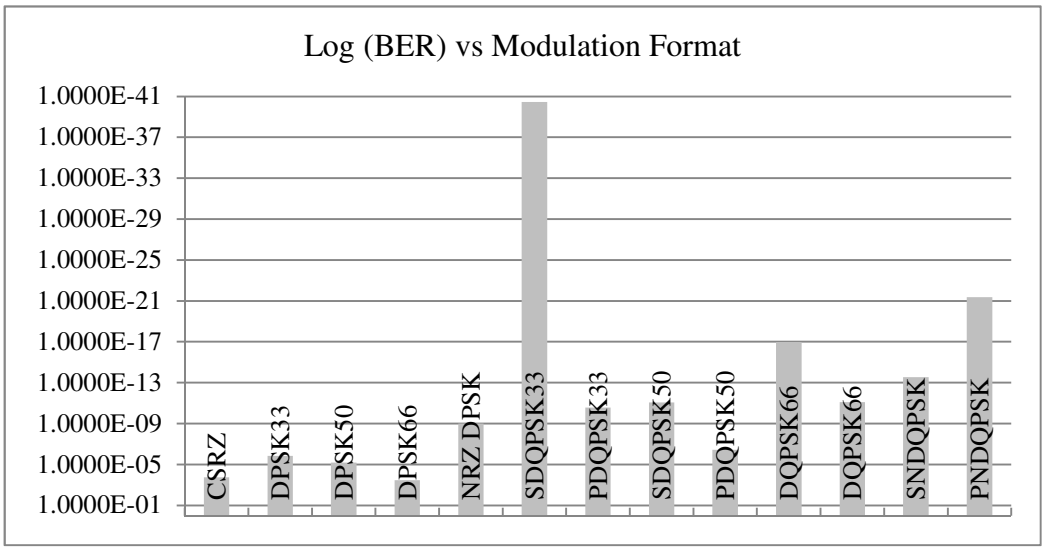

(a)

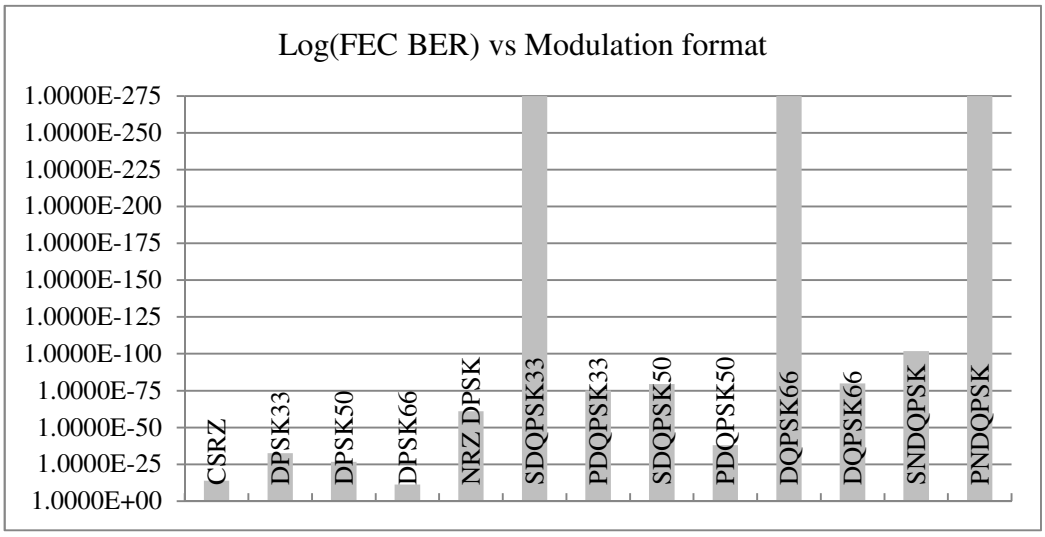

(b)

Figure 6.13 (a) Log(BER) and (b) Log(FEC BER) vs. modulation format

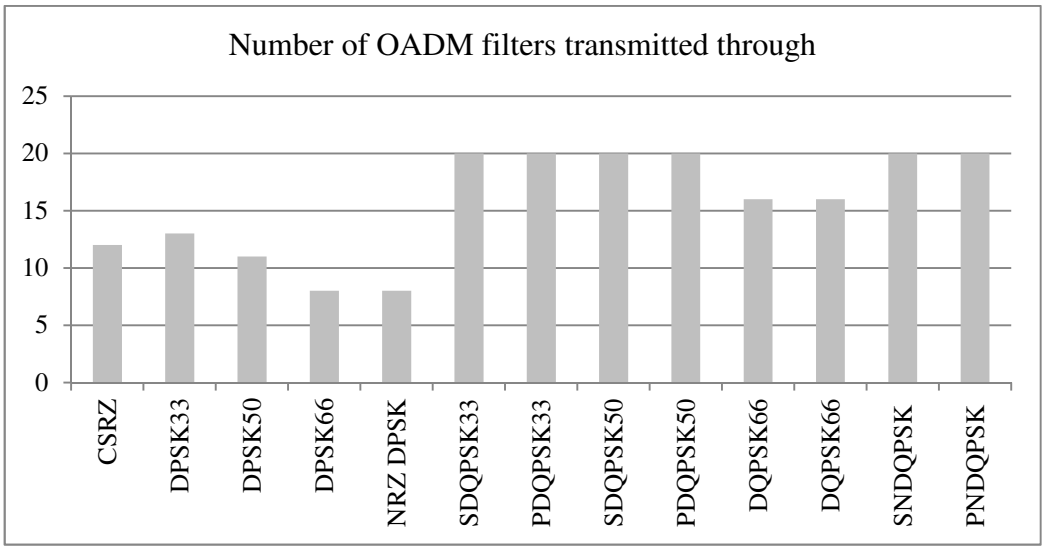

Figure 6.14 Number of OADM filters transmitted through

Figure 6.13(a) and (b) display the Log(BER) and the Log(FEC BER) respectively versus the modulation format. RZ DPSK 33% (series), NRZ DQPSK (parallel) produced the lowest BERs. Figure 6.14 shows the number of sets of OADM filters that transmission was possible as described in Section 5.1. Thirteen formats transmitted through at least eight OADM filters. Six formats transmitted through the maximum number of twenty. Application of the Reed Solomon FEC resulted in the RZ DQPSK 33% (parallel) correcting from 10^{-11} to 10^{-65}. Overall RZ DQPSK 33% (series) performed the best.

Figure 6.15 and Figure 6.16 contain the results for the filter narrowing simulation where the spectral efficiency (SE) of 0.4 with a wavelength separation of 100GHz and a bitrate of 40 GHZ as was described in Section 2.6. The filter bandwidth of the optical add drop multiplexers was set at 50GHz.

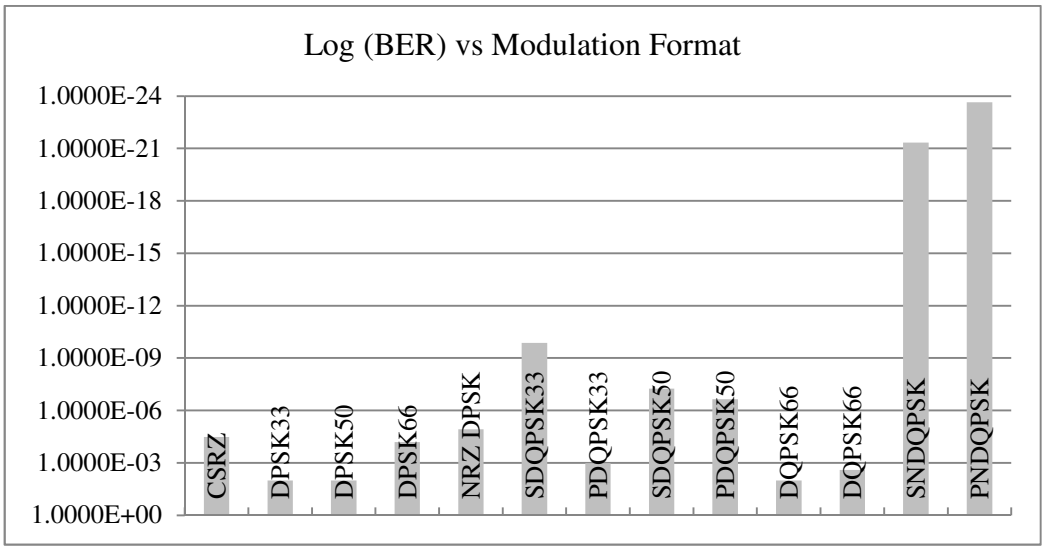

(a)

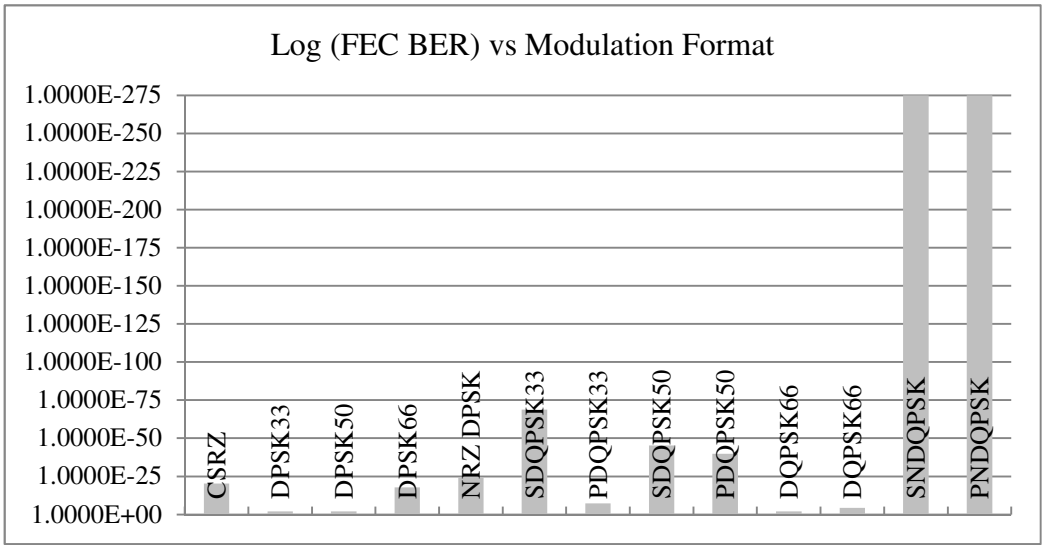

(b)

Figure 6.15 (a) Log(BER) and (b) Log(FEC BER) vs. modulation format

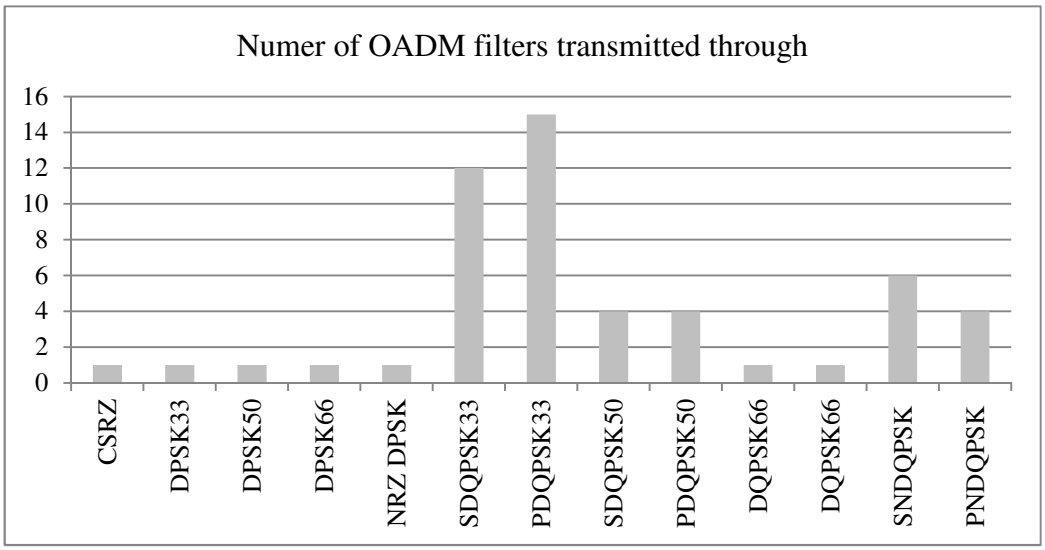

Figure 6.16 Number of OADM filters transmitted through

Figure 6.15(a) and (b) display the Log(BER) and the Log(FEC BER) respectively versus the modulation format. RZ DQPSK 33% (series) and (parallel) produced the lowest BER. Figure 6.16 shows the number of OADM filters through which transmission was possible as described in Section 5.2. Ten formats passed through at least one OADM filter and achieve a BER less than the maximum, and RZ DQPSK 33% (parallel) was able to transmit through fifteen OADM filters and exit with a BER lower than the maximum permissible. Application of the Reed Solomon FEC resulted in the RZ DQPSK 33% (series) demonstrating the best FEC result improving from 10^{-10} to 10^{-69}. Overall RZ DQPSK 33% was the best format under these circumstances.

Figure 6.17 and Figure 6.18 contain the results for the filter narrowing simulation where the spectral efficiency (SE) was established at 0.8 with a wavelength separation of 80GHz and a bitrate of 100 GHZ as was described in Section 2.6. The filter bandwidth of the optical add drop multiplexers was set at 100GHz.

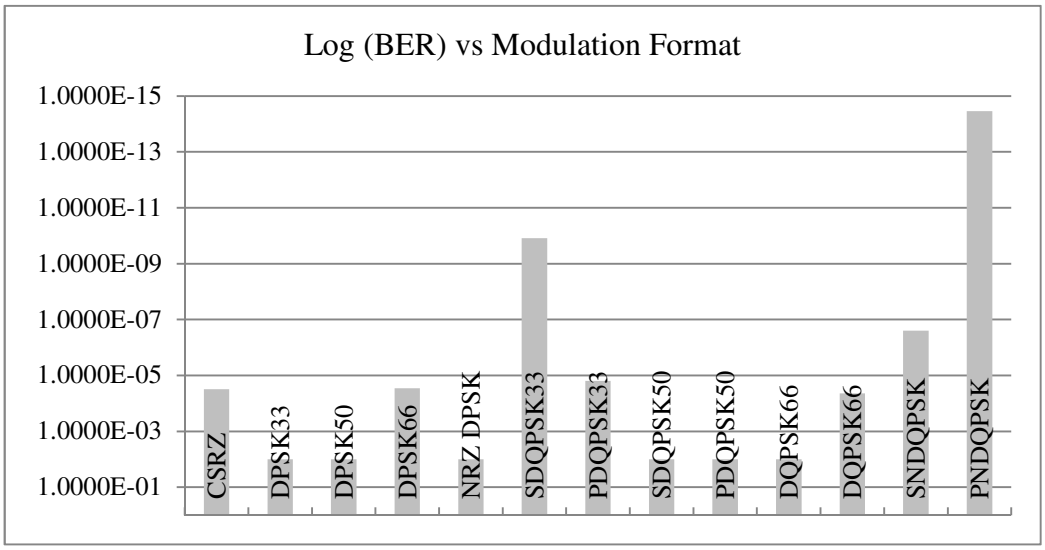

(a)

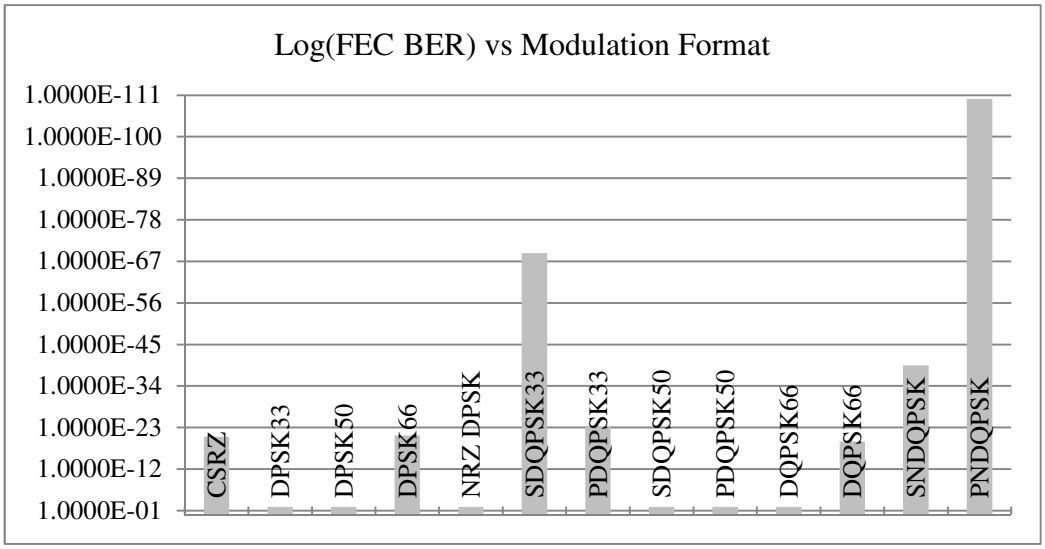

(b)

Figure 6.17 (a) Log(BER) and (b) Log(FEC BER) vs. modulation format

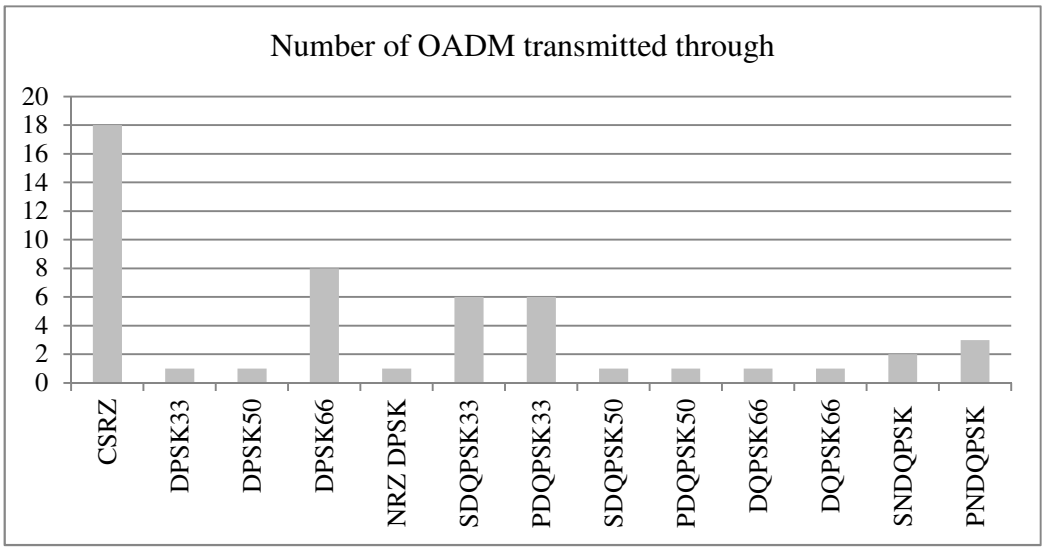

Figure 6.18 Number of OADMs transmitted through

Figure 6.17(a) and (b) display the Log(BER) and the Log(FEC BER) respectively versus the modulation format. NRZ DQPSK (parallel) produced the lowest BER. Figure 6.18 shows the number of sets of OADM filters that transmission was possible as described in Section 5.1. Seven of the formats were able to travel through at least one filter and obtain a correctable BER. The CSRZ format was able to transmit through 18 filter and produced a BER less than the maximum of 10^{-3}. Application of the Reed Solomon FEC resulted in the RZ DQPSK 33% format showing the best improvement for the lowest uncorrected BER of 10^{-10} to 10^{-70}. Overall CSRZ produced the best results.

For the next dataset, spectral efficiency (SE) was established at 0.8 with a wavelength separation of 80GHz and a bitrate of 100 GHZ as was described in Section 2.6. The filter bandwidth of the optical add drop multiplexers was set at 50GHz.

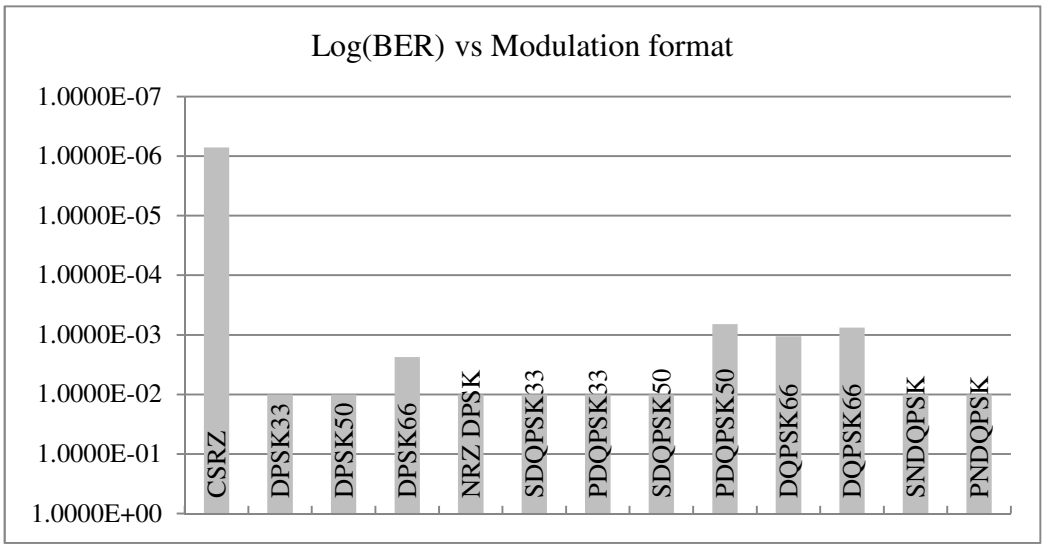

(a)

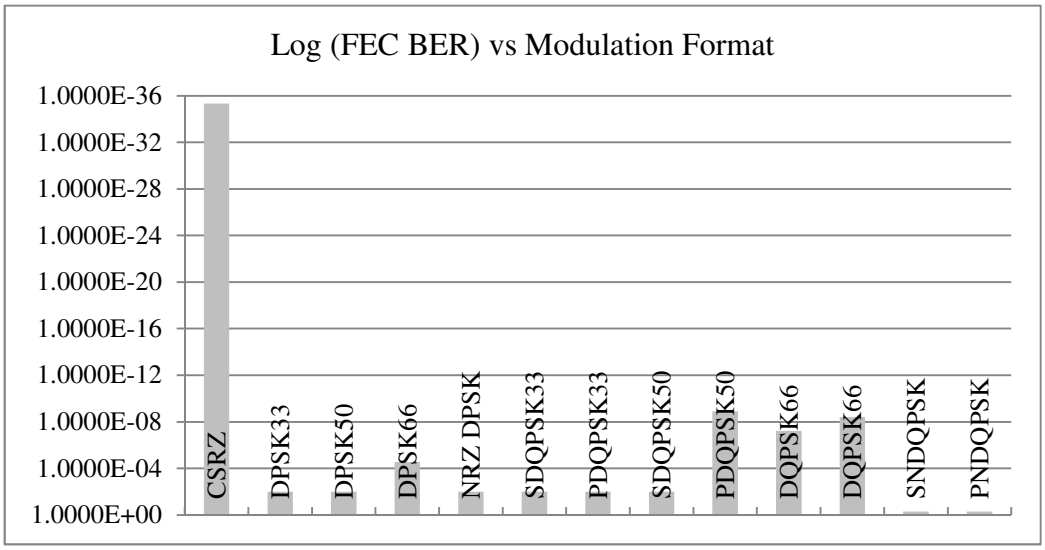

(b)

Figure 6.19 (a) Log(BER) and (b) Log(FEC BER) vs. modulation format

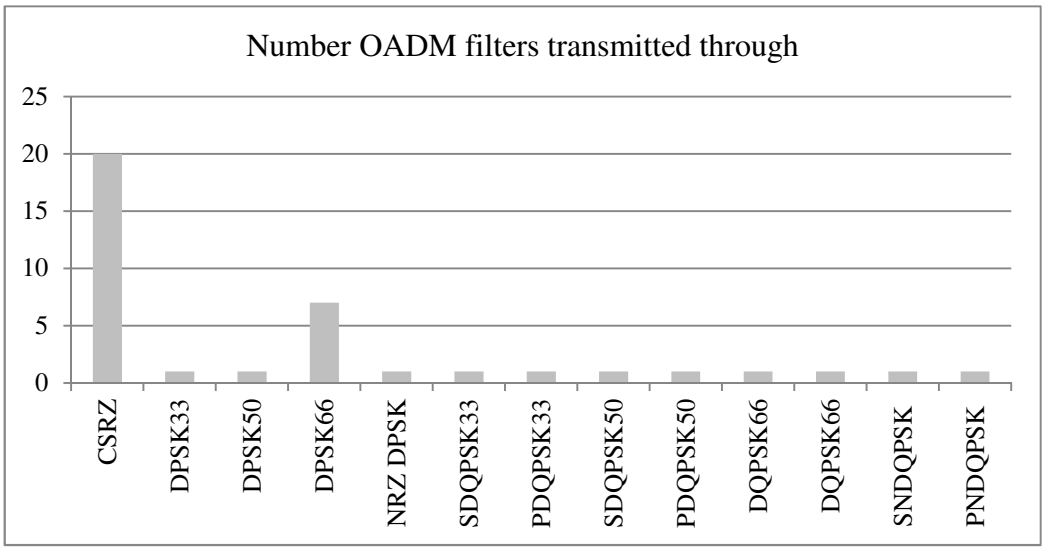

Figure 6.20 Number of OADMs transmitted through

Figure 6.19(a) and (b) show the Log(BER) and the Log(FEC BER) respectively versus the modulation format. CSRZ format finished with the lowest BER. Figure 6.20 shows the number of OADM filters through which transmission was possible as described in Section 5.2. Five of the formats successfully passed through at least one OADM filter with a BER less than the maximum permissible. The application of the Reed Solomon FEC resulted in the CSRZ format decreasing its BER from 10^{-7} to 10^{-36}. Overall the CSRZ format outperformed the other twelve formats.

The next set of filter narrowing simulations, spectral efficiency (SE) was established at 0.8 with a wavelength separation of 50GHz and a bitrate of 40 GHZ as was described in Section 2.6. The filter bandwidth of the OADM was set at 100GHz.

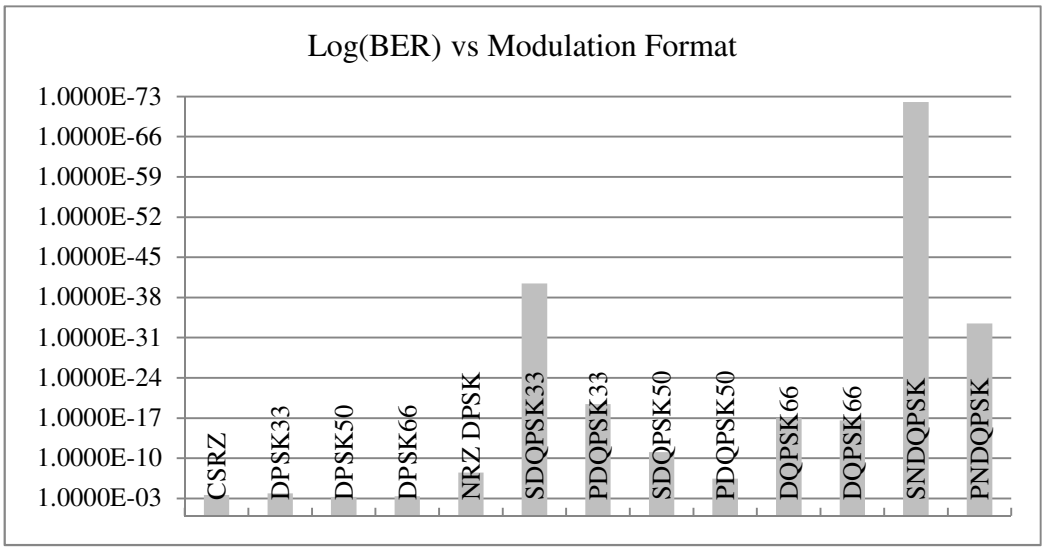

(a)

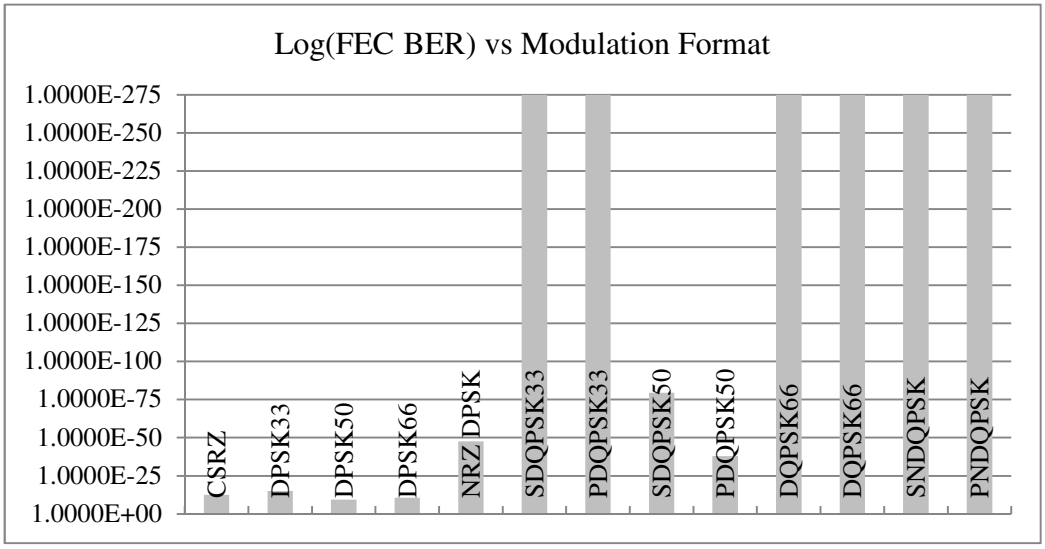

(b)

Figure 6.21 (a) Log(BER) and (b) Log(FEC BER) vs. modulation format

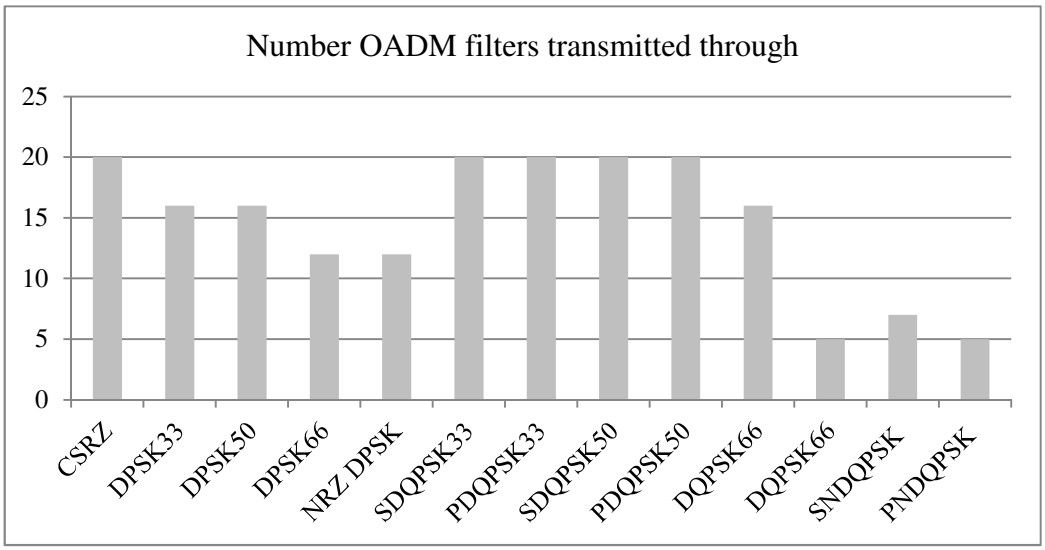

Figure 6.22 Number of OADM filters transmitted through

Figure 6.21(a) and (b) show the Log(BER) and the Log(FEC BER) respectively versus the modulation format. Six formats produced BER of approximately zero. Figure 6.22 shows the number of OADM filters through which transmission was possible as described in Section 5.2. All thirteen formats were able to navigate at least 5 filters and exit with a BER less than 10^{-3}. Five formats CSRZ, RZ DQPSK 33 (series) and (parallel) along with RZ DQPSK 50% (series) and (parallel) traveled through 20 filters. The application of the Reed Solomon FEC produced an improvement from $10^{—12}$ to 10^{-80} with the RZ DQPSK 50% (series) format. Overall the RZ DQPSK 33% (series) outperformed all the other formats.

Next, the spectral efficiency (SE) was established at 0.8 with a wavelength separation of 50GHz and a bitrate of 40 GHZ as was described in Section 2.6. The filter bandwidth of the OADM was set at 50GHz. Figures 6.23 and 6.24 contain those results.

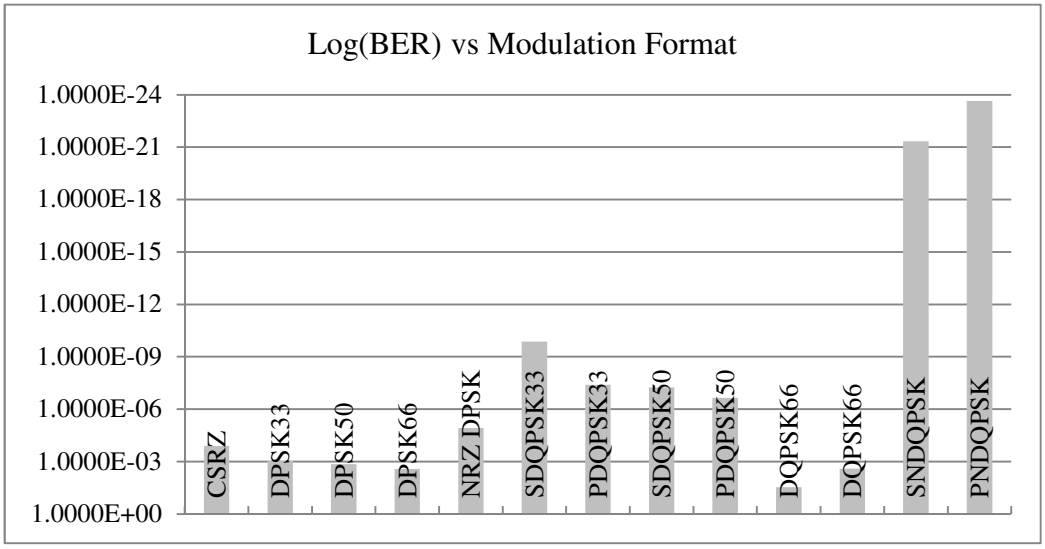

(a)

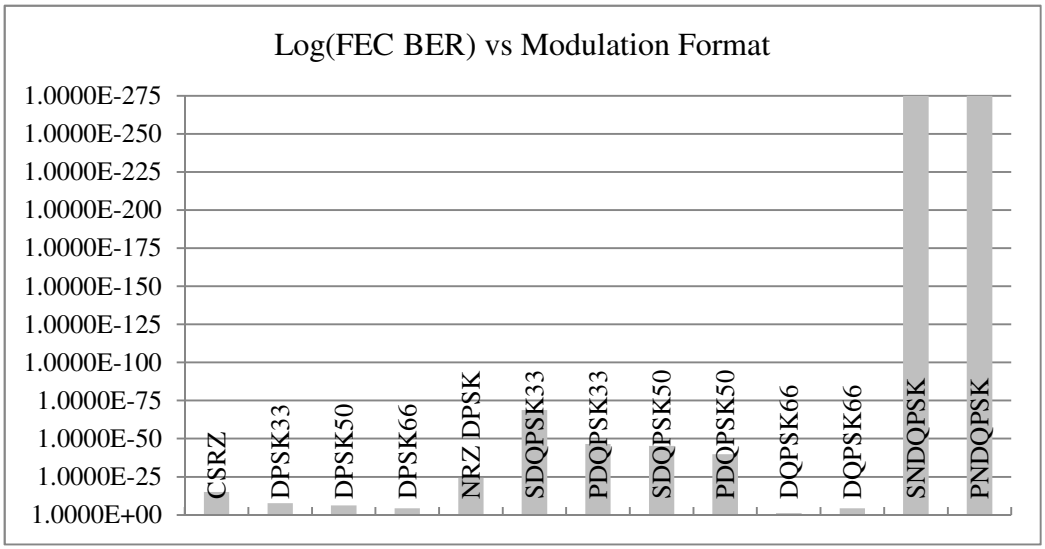

(b)

Figure 6.23 (a) Log(BER) and (b) Log(FEC BER) vs. modulation format

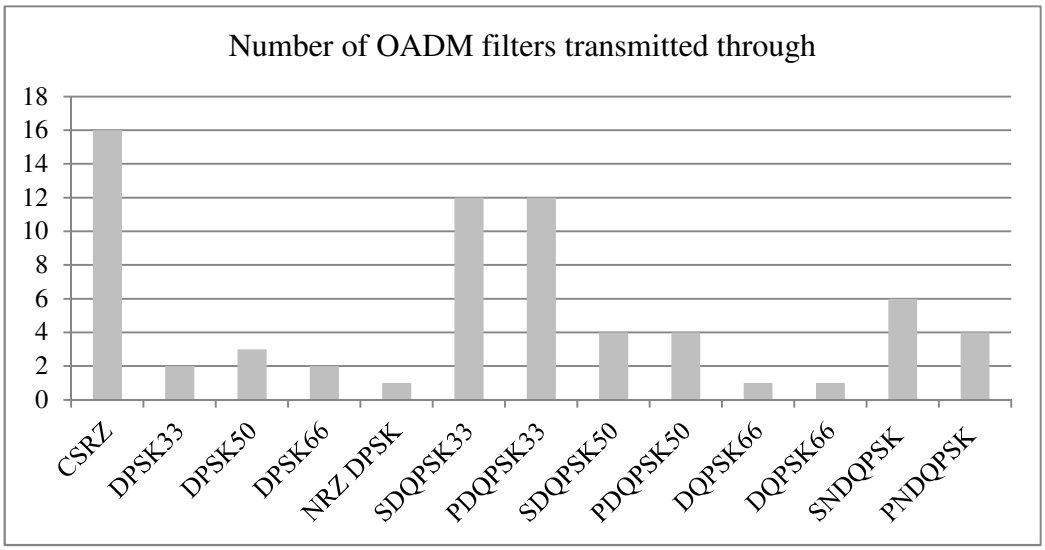

Figure 6.24 Number of OADM filters transmitted through

Figure 6.23(a) and (b) display the Log(BER) and the Log(FEC BER) respectively versus the modulation format. NRZ DQPSK (parallel) produced the lowest BERs. Figure 6.24 shows the number of sets of OADM filters that transmission was possible as described in Section 5.1. Twelve of the formats were able to transmit through at least one filter. One format CSRZ was able to transmit through sixteen filters and two other managed twelve filters. The application of the Reed Solomon FEC resulted in two formats being corrected to the approximately zero BER. RZ DQPSK 33% (series) had the best improvement with the lowest BER from 10^{-10} to 10^{-69}. Overall the CSRZ format produced the best results.

6.2 OADM Crosstalk

In order to investigate crosstalk, the results were ranked by the BER of each modulation format obtained after experiencing the adverse effects of the OADM and the crosstalk from the adjacent signals. The BER and the FEC BER received at the end of the

transmission was recorded. The BER the FEC BER were plotted as bar graphs and the three best performing modulation formats were identified and recorded in the tables by simulation.

The spectral efficiency (SE) was established at 0.4 with a wavelength separation of 100GHz and a bitrate of 40 GHZ as was described in Section 2.6. The filter bandwidth of the OADM was set at 100GHz.

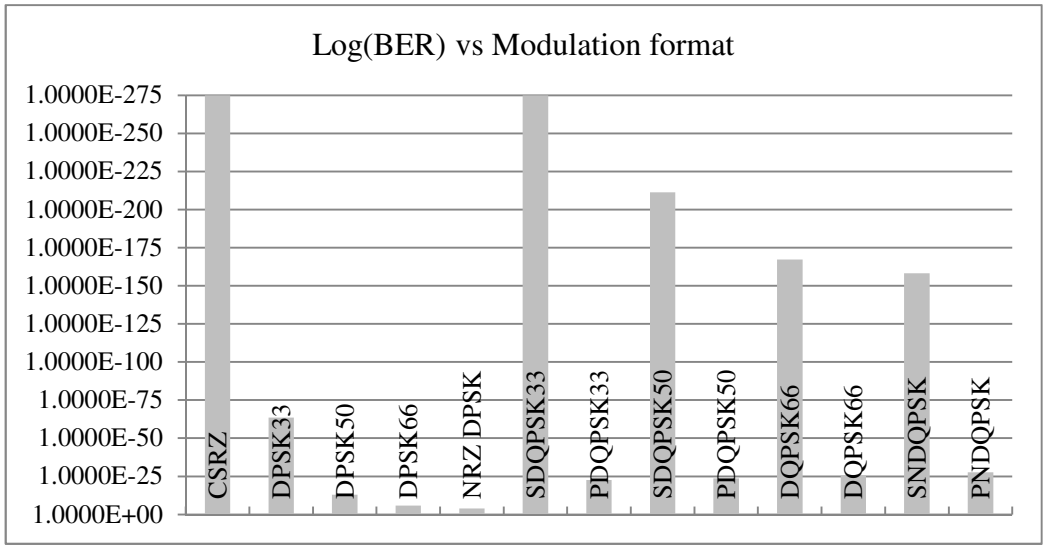

(a)

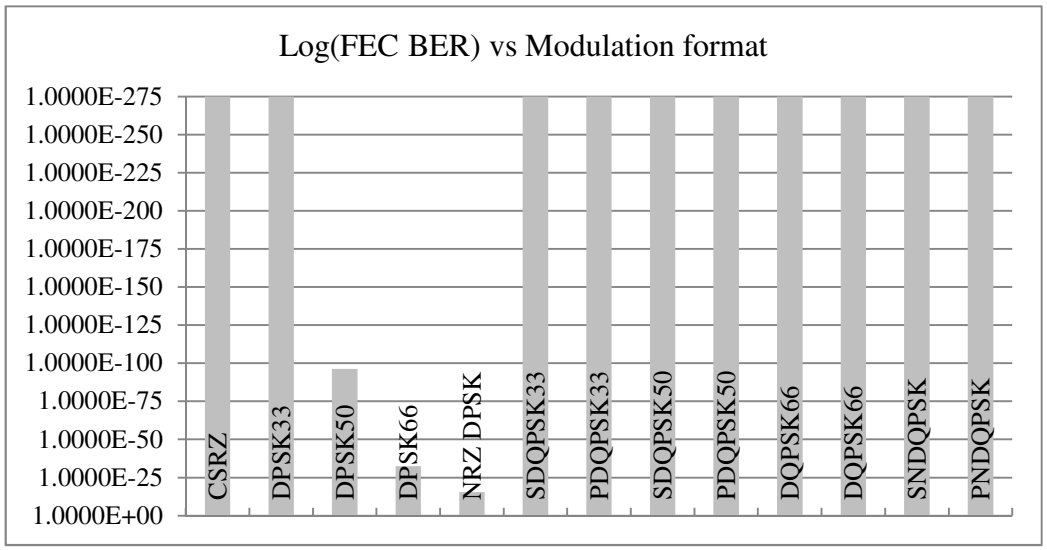

(b)

Figure 6.25 (a) Log(BER) and (b) Log(FEC BER) vs. modulation format

Figure 6.25(a) and (b) show the Log(BER) and the Log(FEC BER) respectively versus the modulation format. All of the formats successfully passed through the three optical nodes in the simulation with a BER less than the maximum permissible. RZ DQPSK 33% (series), CSRZ and RZ DQPSK 50% (series) obtained approximately zero BER. The application of the Reed Solomon FEC resulted in ten of the formats being corrected to approximately zero BER.

Next, the spectral efficiency (SE) was established at 0.4 with a wavelength separation of 50GHz and a bitrate of 40 GHZ as was described in Section 2.6. The filter bandwidth of the optical add drop multiplexers was set at 50GHz.

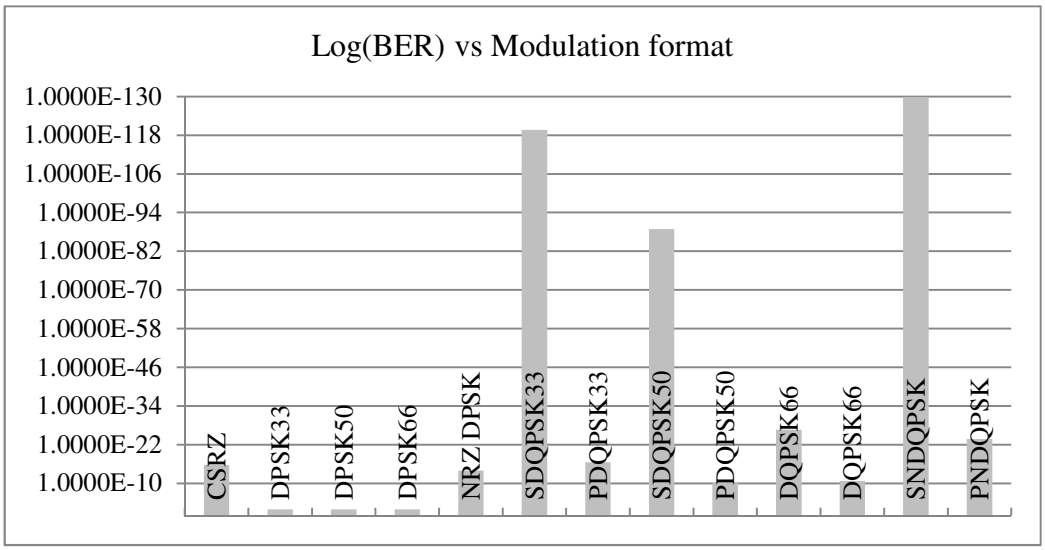

(a)

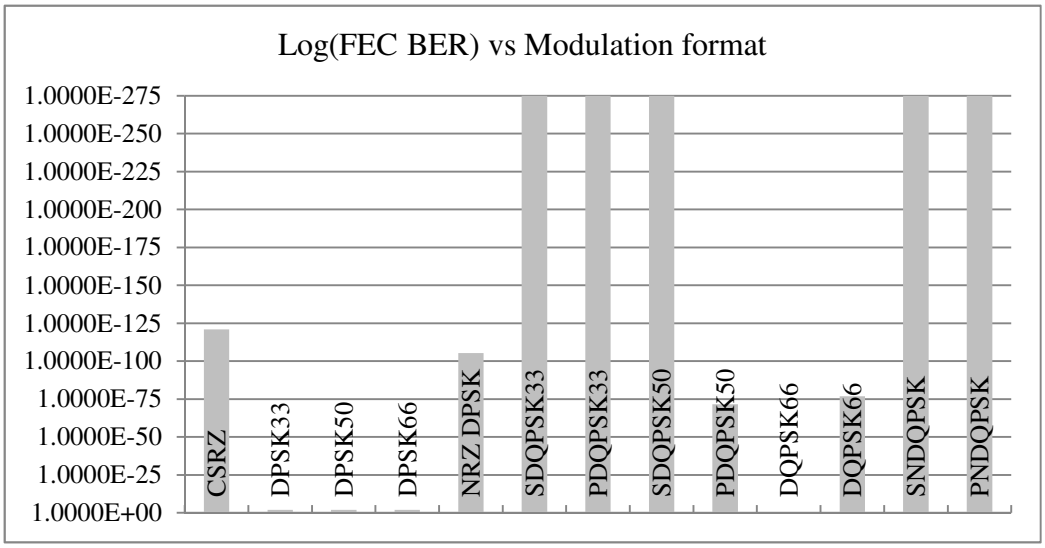

(b)

Figure 6.26 (a) Log(BER) and (b) Log(FEC BER) vs. modulation format

Figure 6.26 (a) and (b) show the Log(BER) and the Log(FEC BER) respectively versus the modulation format. Ten of the formats successfully passed through the three optical nodes in the simulation with a BER less than the maximum permissible. NRZ DQPSK (series), RZ DQPSK 33% (series) and RZ DQPSK 50% (series) obtained BERs of 10^{-130},

10^{-120}, 10^{-89} respectively. The application of the Reed Solomon FEC resulted in five of the formats being corrected to approximately zero BER.

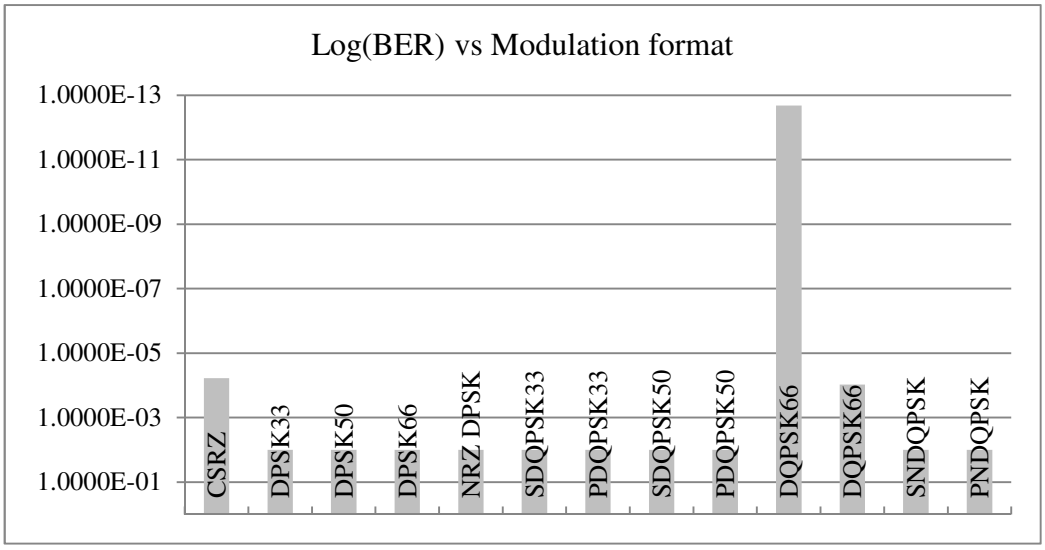

(a)

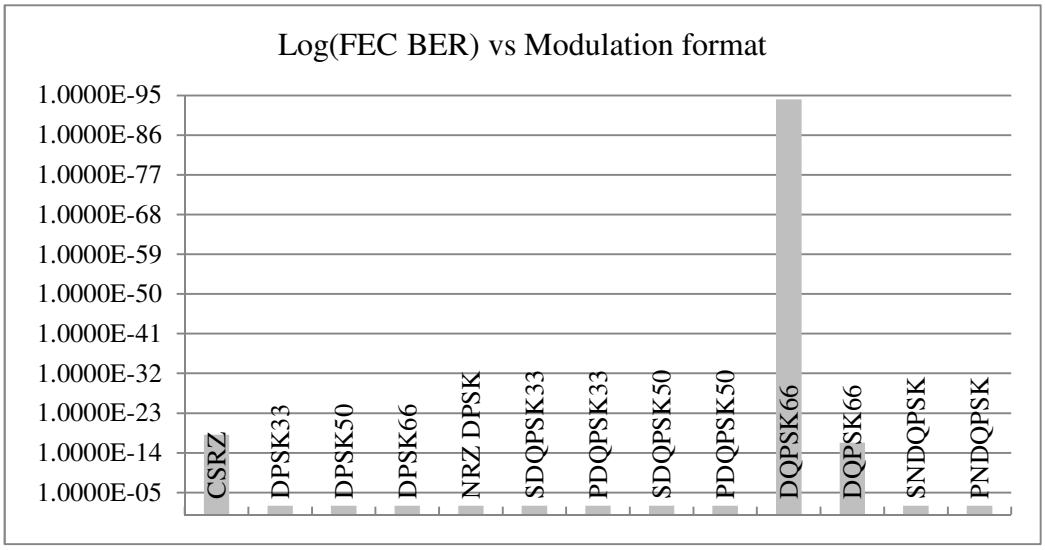

(b)

Figure 6.27 (a) Log(BER) and (b) Log(FEC BER) vs. modulation format

To continue investigating the effects of crosstalk, spectral efficiency (SE) was established at 0.8 with a wavelength separation of 80GHz and a bitrate of 100 GHZ as described in Section 2.6. The filter bandwidth of the optical add drop multiplexers was set at 100GHz.

Figure 6.27(a) and (b) show the Log(BER) and the Log(FEC BER) respectively versus the modulation format. Only three of the formats successfully passed through the three optical nodes in the simulation with a BER less than the maximum permissible. RZ DQPSK 66% (series), RZ DQPSK 66% (parallel), and CSRZ obtained correctable BERs. The application of the Reed Solomon FEC resulted in the RZ DQPSK 66% (series) format being corrected to 10^{-95} BER.

Next, the spectral efficiency (SE) was established at 0.8 with a wavelength separation of 80GHz and a bitrate of 100 GHZ as was described in Section 2.6. The filter bandwidth of the optical add drop multiplexers was set at 50GHz.

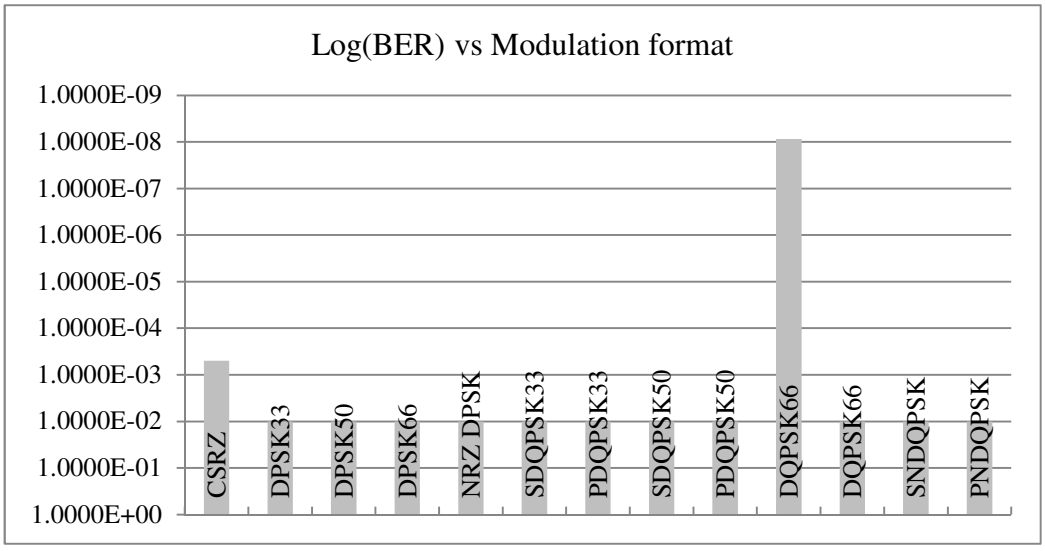

(a)

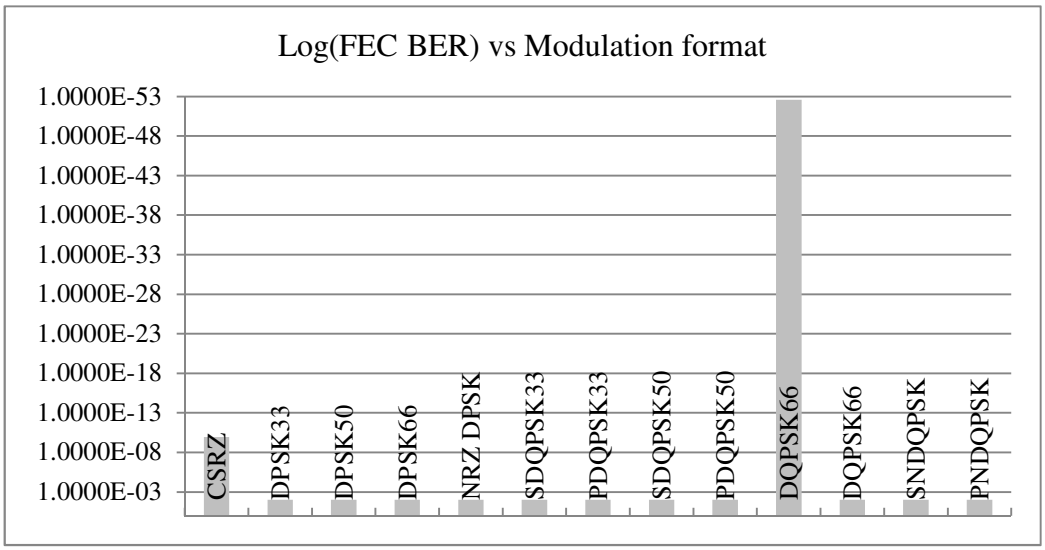

(b)

Figure 6.28 (a) Log(BER) and (b) Log(FEC BER) vs. modulation format

Figure 6.28(a) and (b) show the Log(BER) and the Log(FEC BER) respectively versus the modulation format. Only two of the formats successfully passed through the three optical nodes in the simulation with a BER less than the maximum permissible. RZ DQPSK 66% (series) and CSRZ obtained correctable BERs. The application of the Reed Solomon FEC resulted in the RZ DQPSK 66% (series) format being corrected to approximately 10^{-53} BER and the CSRZ to a 10^{-10} BER.

The spectral efficiency (SE) was then established at 0.8 with a wavelength separation of 50GHz and a bitrate of 40 GHZ as was described in Section 2.6. The filter bandwidth of the optical add drop multiplexers was set at 100GHz.

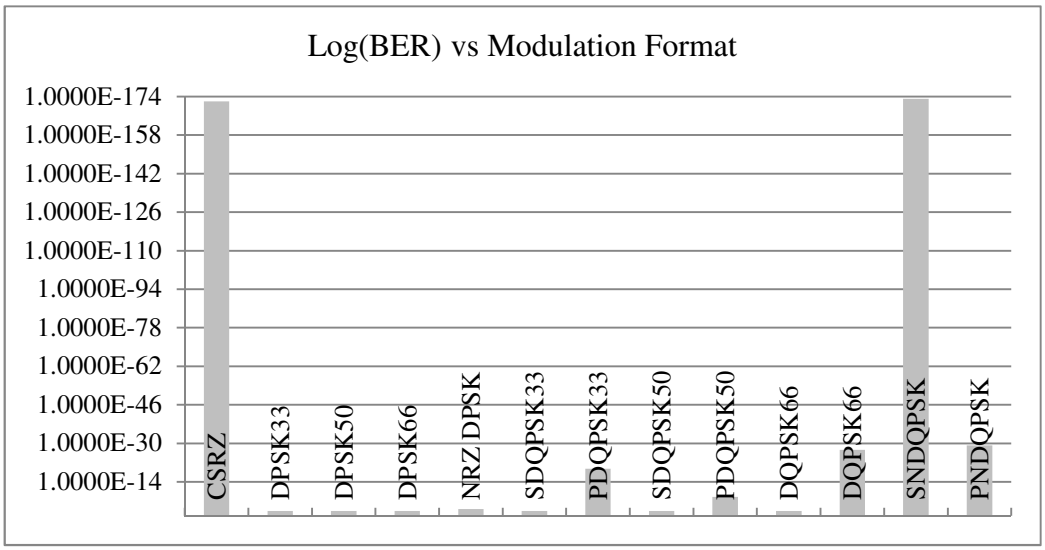

(a)

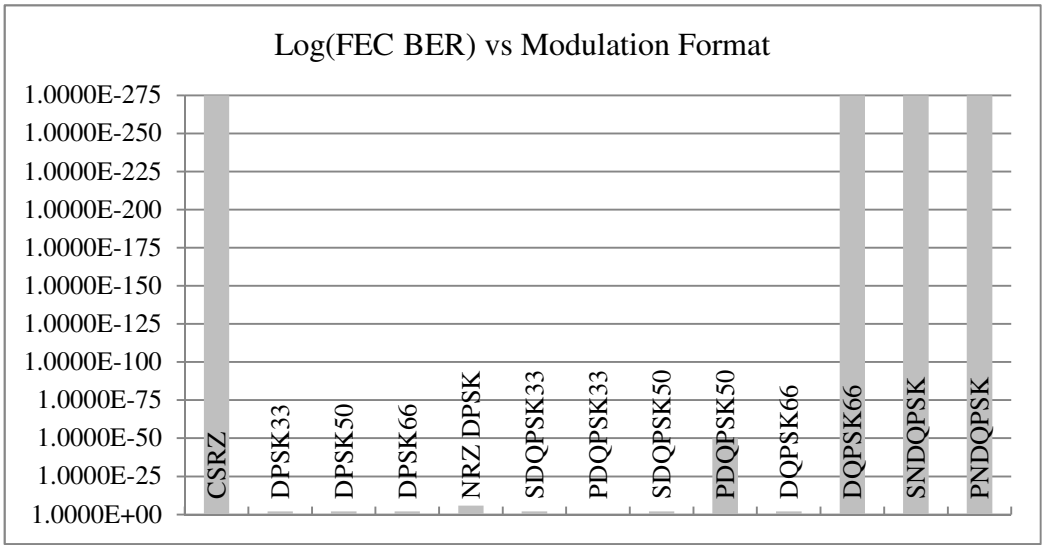

(b)

Figure 6.29 (a) Log(BER) and (b) Log(FEC BER) vs. modulation format

Figure 6.29 (a) and (b) shows the Log(BER) and the Log(FEC BER) respectively versus the modulation format. Seven of the formats successfully passed through the three optical nodes in the simulation with a BER less than the maximum permissible. NRZ DQPSK

(series) followed by CSRZ and then NRZ DQPSK(parallel) obtained lowest BERs respectively. The application of the Reed Solomon FEC resulted in the five formats being corrected to approximately zero BER.

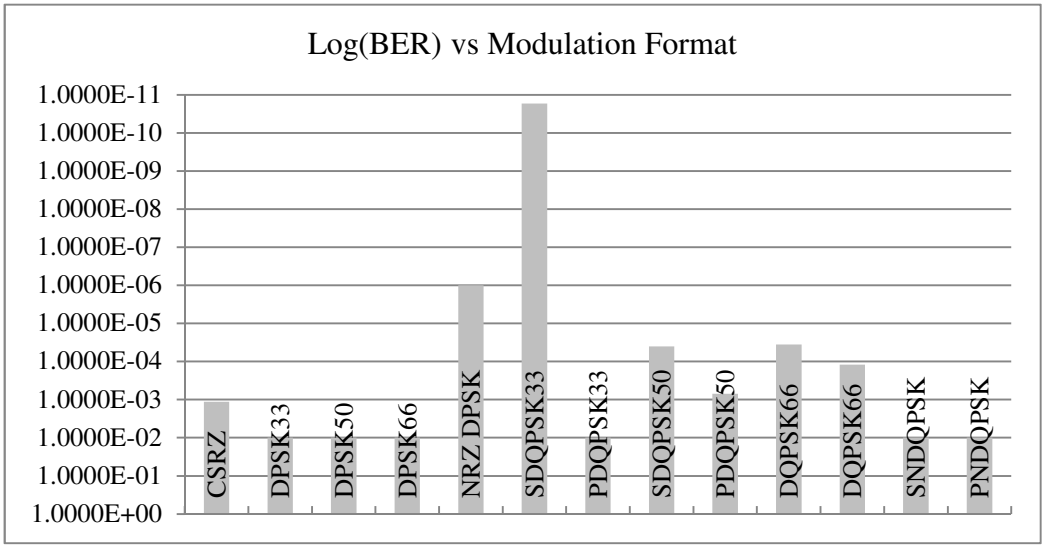

(a)

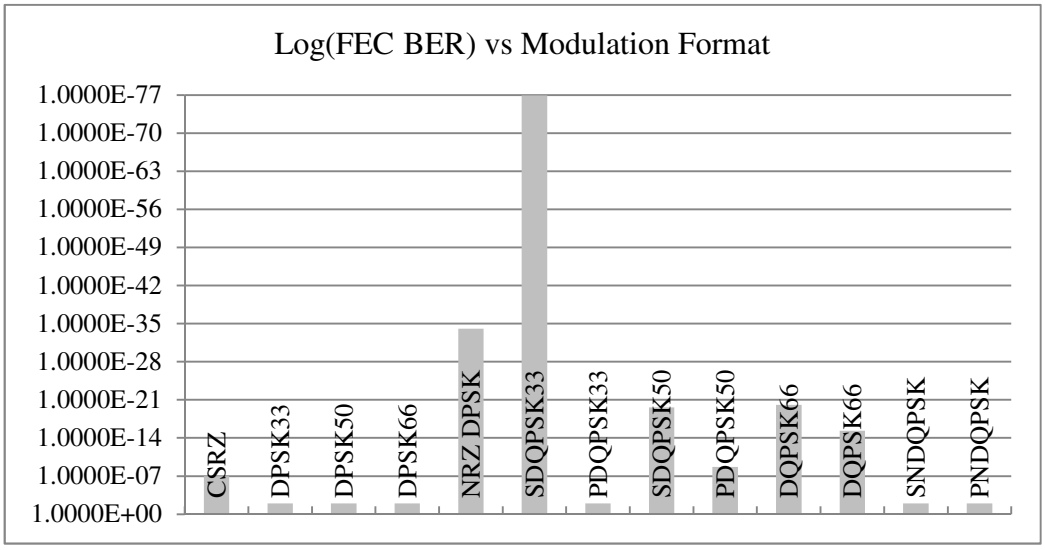

(b)

Figure 6.30 (a) Log(BER) and (b) Log(FEC BER) vs. modulation format

The spectral efficiency (SE) established at 0.8 with a wavelength separation of 50GHz and a bitrate of 40 GHZ as was described in Section 2.6. The filter bandwidth of the optical add drop multiplexers was set at 50GHz

Figure 6.30(a) and (b) show the Log(BER) and the Log(FEC BER) respectively versus the modulation format. Seven of the formats successfully passed through the three optical nodes in the simulation with a BER less than the maximum permissible. RZ DQPSK 33% (series) obtained the lowest BER followed by NRZ DPSK and then RZ DQPSK 66% (series). The application of the Reed Solomon FEC resulted in the RZ DQPSK 33% (series) format being corrected to approximately 10^{-77} BER and the NRZ DPSK to a 10^{-35} BER.

6.3 Summary of the Top Three Modulation Formats

After compiling the data obtained from all of the simulations performed in this thesis, the data was then analyzed to identify the top performing modulation formats. The results of this analysis are presented in this section. The analysis began by determining the number of times that each modulation format was one of the top three performers in each simulation.

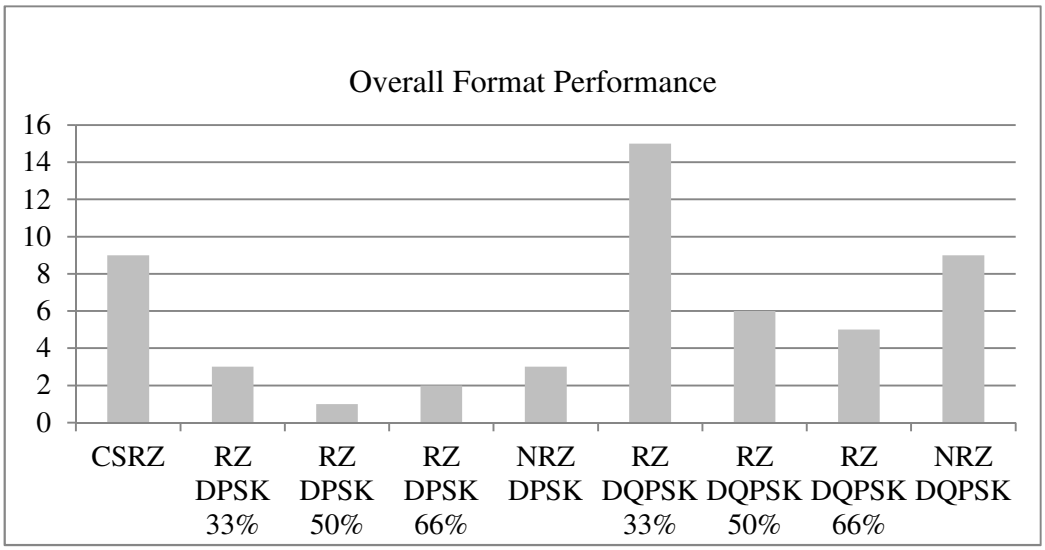

Figure 6.31 Top three performances by modulation format

This Figure 6.31 shows a comparison between the thirteen modulation formats and the total number of times the format appeared as one of three best. Overall RZ DQPSK 33%, NRZ DQPSK and CSRZ clearly outperformed the other formats, however, the DQPSK formats fall into two subcategories those that utilized either a series or parallel configuration of the MZM. Because DQPSK can fall into one of these two subcategories, further analysis was implemented to identify if one MZM configuration performed better than the other.

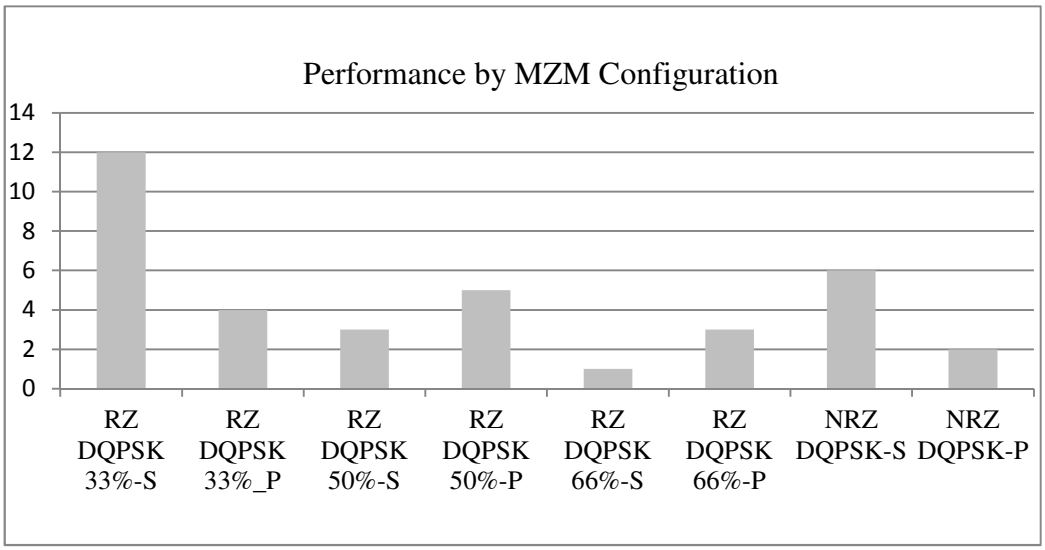

Figure 6.32 Performance of modulation formats by MZM configuration

Figure 6.32 is a comparison between the performance of the modulation formats based upon the configuration of their MZM, either series or parallel. The results were equally divided. However, two of the series configured formats NRZ DQPSK and RZ DQPSK 33% obtained more top three finishes than the other configured formats followed by the parallel configuration of RZ DQPSK 50%.

The next analysis identified the modulation format with the highest number of occurrences of the completing the simulation with the lowest BER.

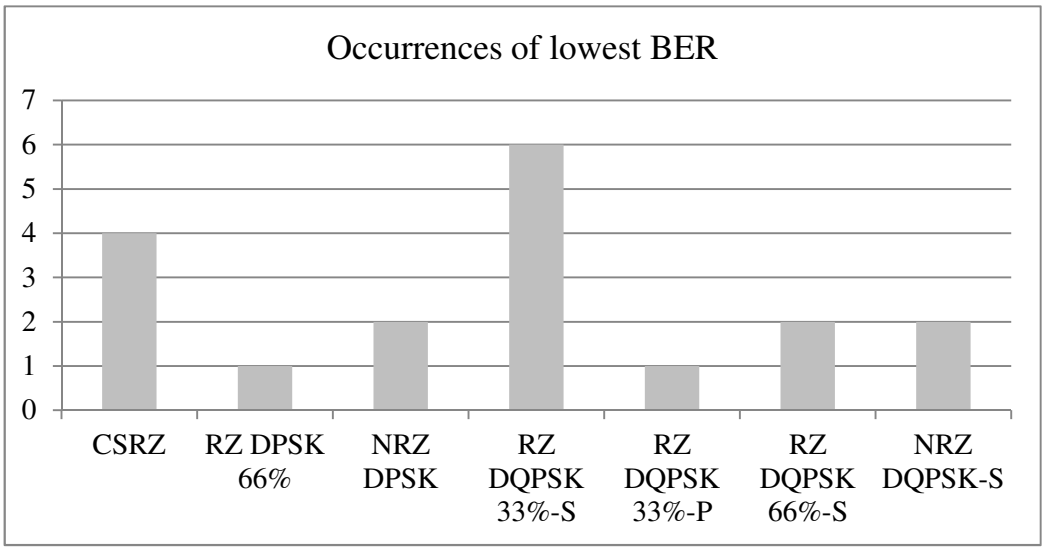

Figure 6.33 Number of best BER occurrences by modulation format

Figure 6.33 shows the results of this analysis. The formats with the lowest BER results in descending order were RZ DQPSK33% (series) with six, CSRZ with four, NRZ DQPSK (series), NRZ DPSK and NRZ DPSK 66% (series) with two and RZ DPSK 66% and RZ DQPSK 33% with one each.

Analyzing the data from Figures 6.31, 6.32 and 6.33 it was determined that the series configuration of the MZM outperformed the parallel configurations in the RZ DQPSK and NRZ DQPSK formats, furthermore RZ DQPSK 33% (series), CSRZ followed by NRZ DQPSK (series) performed better overall than NRZ DPSK and RZ DQPSK 66% (series). Based upon this assessment the best performing modulation formats were determined to be RZ DQPSK 33% (series), CSRZ and NRZ DQPSK (series) in that order. These three formats will used in the final simulation described in Section 6.1.4.

6.4 Multiplexed Simulation

In the final simulations RZ DQPSK 33% (series), CSRZ and NRZ DQPSK (series) formats were run through the simulated communication (Figure 5.8) link at a SE=0.8 a bitrate of 40GHz, channel separation of 50GHz and OADM filter bandwidths of 50GHz and 100GHz. The results are shown in Figure 6.34(a) and (b) respectively.

Both the RZ DQPSK 33% (series) and NRZ DQPSK (series) modulation format produced dramatically lower BERs than the CSRZ format with 50GHz filter bandwidth. With the application of the FEC algorithm the CSRZ obtained a BER of approximately 10^{-9} while the other two formats were corrected to approximately zero BER. With the filter bandwidths increased to 100GHz the RZ DQPSK 33% (series) signal became uncorrectable while the CSRZ format produced a correctable BER of 10^{-4} the NRZ DQPSK (series) formatted signal had a BER of 10^{-6}. The dramatic difference between these two formats occurs after the Reed Solomon FEC algorithm is applied. The BER of the CSRZ signal improves two orders of magnitude and corrects to 10^{-11} but the NRZ DQPSK (series) signal improves 15 orders of magnitude to a BER of 10^{-26}.

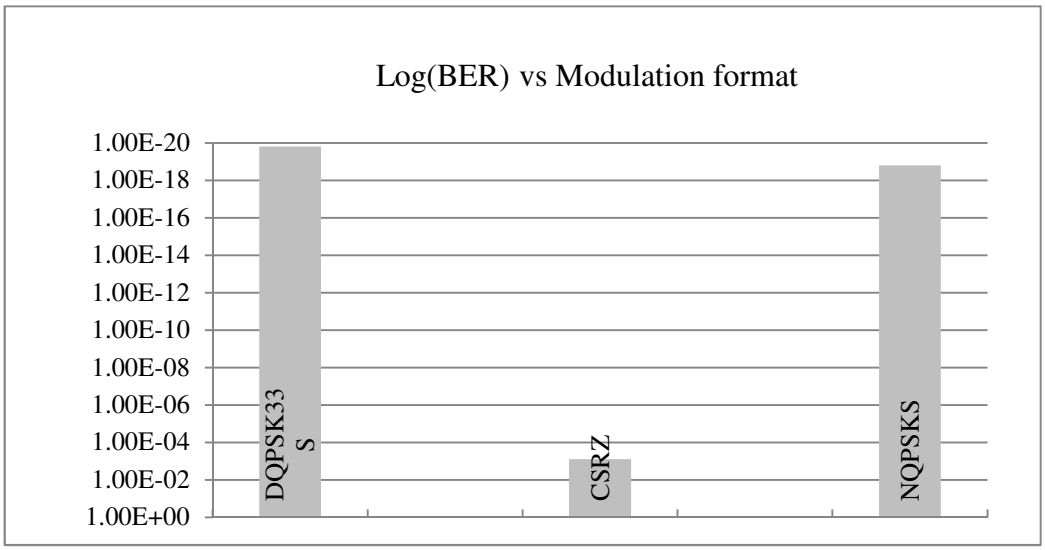

(a)

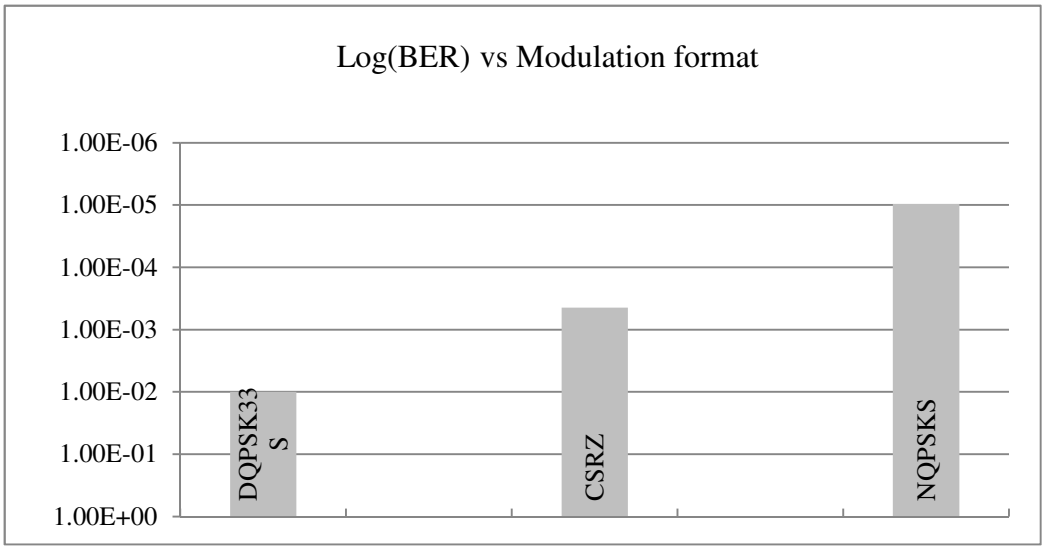

(b)

Figure 6.34 Results of multiplexed simulation (a) Log(BER) vs. modulation format (SE=0.8, B=40GHz, BW=50GHz) (b) Log(BER) vs. Modulation format (SE=0.8, B=40GHz, BW=100GHz)

Next the RZ DQPSK 33% (series), CSRZ and NRZ DQPSK (series) formats were run through the simulated communication link as was described in Figure 5.8 with a SE of 0.8, a bitrate of 100GHz and OADM filter bandwidths of 50 and 100GHz. The results for BW=100GHz did provide a correctable BER for any of the modulation formats, the results for the 50GHz OADM filter bandwidth are shown in Figure 6.35.

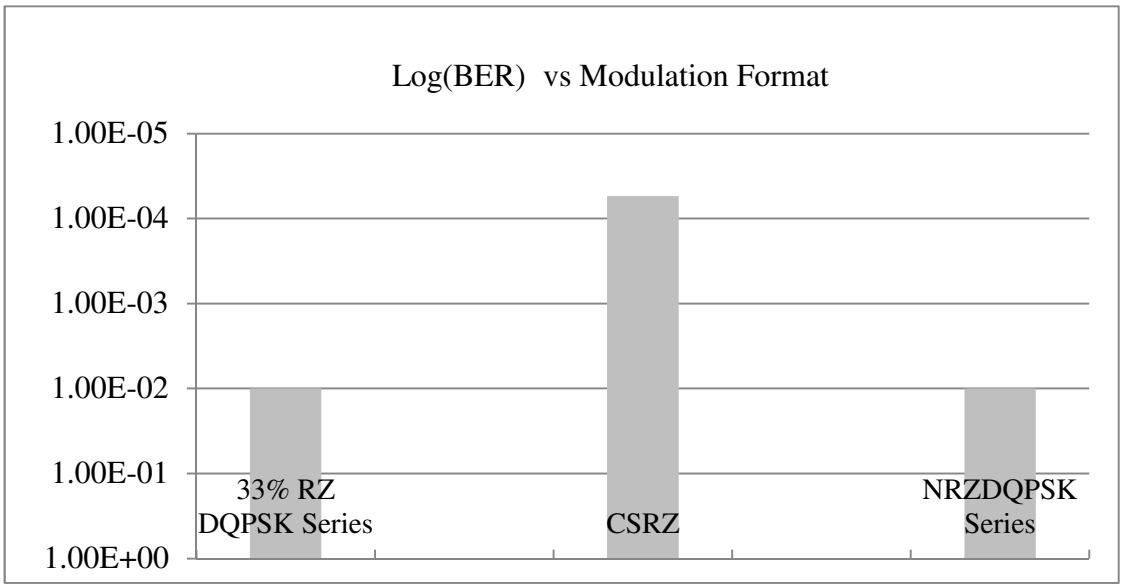

Figure 6.35 Results of multiplexed simulation Log(BER) vs. modulation format (SE=0.8, B=100GHz, BW=50GHz)

6.5 Summary

The result of the final simulation, the multiplexed simulation, was not completely indicative of the overall results of the first three simulations. Based upon the results from the simulations at a SE of 0.8 it was expected that both the CSRZ and RZ DQPSK 33% (series) would outperform the NRZ DQPSK format, this was not the case. While the RZ DQPSK 33% (series) was slightly better than the NRZ DQPSK (series) they were both

clearly better that the CSRZ signal at a bitrate of 50GHz and OADM filter bandwidth of 50GHz, it was definitely not the case when the bandwidth was increased to 100GHz. At a filter bandwidth of 100GHz the NRZ DQRSK (series) produced a BER approximately two orders of magnitude better than CSRZ format but corrected to fifteen orders of magnitude greater than the CSRZ format. The CSRZ format was the only signal that was able to generate a correctable BER at the 100GHz bitrate.

While the first three simulations the RZ DQPSK 33% (series) format did not perform better than all the other memoryless formats combined, it did achieve the best results in six of eighteen simulations whereas the next closest format only performed best in two of eighteen simulations. Overall RZ DQPSK33% (series) demonstrated good resistance to crosstalk and filter narrowing. This can be attributed to phase shifts not intensity levels determining bit change and the ability to transmit two bits at the same rate as other formats. This translates into lower launch powers, a decrease in linewidth tolerance and therefore less expensive laser transmitters.

The NRZ DQPSK (series) signal was clearly superior to the other signals at the 40GHz bitrate it operated well at both filter bandwidths and demonstrated the ability to be manipulated by the Reed Solomon algorithm. NRZ formats also do not need a pulse carver to generate its signal therefore this format not only performs as well as the RZ DQPSK 33% (series) format but as has been shown to out performs it in other scenarios. The NRZ DQPSK (series) has the same benefits as the RZ DQPSK 33% (series) it does

so at an even lower cost because it uses one less MZM in its design, making it the format of choice at a bitrate of 40GHz.

The modulation format CSRZ, a format with pseudo-memory, provided an excellent standard to compare the memoryless formats to. It consistently appeared as one of the three best performing formats and in the final simulation, and demonstrated correctable bit rates at 40GHz at both filter bandwidths as well as at a bitrate of 100GHz and filter bandwidth of 50GHz.

Chapter 7

CONCLUSIONS AND FUTURE WORK

7.1 Conclusions

The research presented in this thesis has focused on the use of FEC correction in conjunction with advanced modulation formats used in fiber optic communication links.

The results obtained through a theoretical analysis and simulation techniques have shown that RZ DQPSK 33% and NRZ DQPSK in the series configuration are well suited and very tolerant to the adverse effects from repeated optical filtering and OADM crosstalk when compared to other memoryless optical advanced modulation formats. Optical communication links have many inherent benefits that are needed to meet the needs of today's communication environment. As the need for faster and more reliable communication increases a key to a cost effective solution is a modulation format that can efficiently utilize the existing infrastructure demonstrate the ability to withstand transmission impairments and be responsive to FEC algorithms. Some of the inherent benefits to optical networks are:

- Optical fiber's transmission capacity in far superior to either coaxial cable or copper wire.
- All of the information transmitted over fiber is contained within the fiber.

- Fiber is more readily installed in existing infrastructure than either coaxial cable or copper wire.
- Optical communication links are highly immune to electromagnetic radiation and radio frequency interference.
- Fiber networks offer excellent network security.
- Maintenance can be performed while the network is operational.

The contributions of this thesis work and conclusions that follow indicate that RZ DQPSK 33% and NRZ DQPSK modulation formats could be used to help bridge the gap and facilitate the increase in efficiency of many communicate systems.

A study through the use of simulation software was performed. The performance of differential memoryless advanced modulation formats shown in Figure 3.5(b) was analyzed, compared to other memoryless formats and one format with pseudo-memory. This resulted in the following observations:

- AMF transmitters that utilized MZM in series outperformed transmitters with MZM nested in parallel.
- RZ DQPSK 33% (series) and NRZ DQPSK (series) clearly outperformed CSRZ at a SE equal to 0.8 generated at a bitrate of 40GHz and OADM filter bandwidths on the order of 50GHz.
- NRZ DQPSK (series) out performed both RZ DQPSK 33% (series) and CSRZ where OADM filter bandwidths were 100GHz.

- The CSRZ format was able to generate correctable BERs at a bite of 100GHz while NRZ DQPSK (series) and RZ DQPSK 33% (series) did not.

7.2 Future Work

This investigation has led to several ideas for future research. First would be to investigate whether other FEC algorithms increase format performance more than the Reed-Solomon FEC code. Second whether complex codes could provide an increase in BER that justifies their complexity. Furthermore, which FEC code provides the largest increase in BER based upon specific modulation format and network wide impairments. The investigation into the benefits of memoryless modulation formats, particularly DQPSK formats is a current topic of active research and future investigation.

REFERENCES

[1] J. C. Palais, "Fiber optic communications," pp. 441, 2005.

[2] G. Keiser, *Optical Fiber Communications.* New York: McGraw-Hill, 2011.

[3] T. E. Stern and G. B. Ellinas Krishna, *Multiwavelength Optical Networks Architecture, Design, and Control.* New York, NY, USA: Cambridge University Press, 2009.

[4] G. P. 1. (. P.). Agrawal , "Nonlinear fiber optics," pp. 466, 2001.

[5] Becker, P. C. Olsson, N. A. Simpson,J.R., (Jay R.) and ScienceDirect (Online service), "Erbium-doped fiber amplifiers fundamentals and technology," pp. 460, 1999.

[6] E. Desurvire and 1955-, "Erbium-doped fiber amplifiers : device and system developments," pp. 763, 2002.

[7] P. J. Winzer, M. Pfennigbauer and R. -. Essiambre, "Coherent crosstalk in ultradense WDM systems," *Lightwave Technology, Journal of,* vol. 23, pp. 1734-1744, 2005.

[8] P. J. Winzer and R. -. Essiambre, "Advanced Optical Modulation Formats," *Proceedings of the IEEE,* vol. 94, pp. 952-985, 2006.

[9] A. Yariv, H. Blauvelt and S. -. Wu, "A reduction of interferometric phase-to-intensity conversion noise," *Lightwave Technology, Journal of,* vol. 10, pp. 978-981, 1992.

[10] I. FIS. Polarization-mode-dispersion-pmd-testing. *2011(July),* pp. 1. 2010. Available: http://www.fiberinstrumentsales.com/blog/2010/06/17/polarization-mode-dispersion-pmd-testing/.

[11] Stern, Thomas E. Ellinas,Georgios.Bala, Krishna., "Multiwavelength optical networks : architectures, design, and control," pp. 966, 2009.

[12] J. J. O. Pires and L. G. C. Cancela, "Theoretical Insights Into the Impact of Coherent and Incoherent Crosstalk on Optical DPSK Signals," *Lightwave Technology, Journal of,* vol. 28, pp. 2766-2774, 2010.

[13] A. Hodzic, M. Winter, B. Konrad, S. Randel and K. Petermann, "Optimized filtering for 40-gb/s/ch-based DWDM transmission systems over standard single-mode fiber," *Photonics Technology Letters, IEEE,* vol. 15, pp. 1002-1004, 2003.

[14] S. Suzuki and Y. Kokubun, "Design rule of wavelength filter bandwidth and pulsewidth for ultimate spectral efficiency limited by crosstalk in DWDM systems," *Photonics Technology Letters, IEEE,* vol. 15, pp. 1645-1647, 2003.

[15] M. Pfennigbauer and P. J. Winzer, "Choice of MUX/DEMUX filter characteristics for NRZ, RZ, and CSRZ DWDM systems," *Lightwave Technology, Journal of,* vol. 24, pp. 1689-1696, 2006.

[16] J. G. Proakis and M. Salehi, *Digital Communications.* Boston: McGraw-Hill, 2008.
[17] J. M. Kahn and Keang-Po Ho, "Spectral efficiency limits in DWDM systems," in *Optical Communication, 2005. ECOC 2005. 31st European Conference on,* 2005, pp. 843-846 vol.4.

[18] Keang-Po Ho and J. M. Kahn, "Channel capacity of WDM systems using constant-intensity modulation formats," in *Optical Fiber Communication Conference and Exhibit, 2002. OFC 2002,* 2002, pp. 731-733.

[19] Version 9.0, "OptiSystem - Optical Communication System Design Software for Systems Engineers - Fiber Optics - DWDM - PON Design - Optical Networks," vol. 2011.

[20] S. Walklin and J. Conradi, "Multilevel signaling for increasing the reach of 10 Gb/s lightwave systems," *Lightwave Technology, Journal of,* vol. 17, pp. 2235-2248, 1999.

[21] R. A. Griffin and A. C. Carter, "Optical differential quadrature phase-shift key (oDQPSK) for high capacity optical transmission," in *Optical Fiber Communication Conference and Exhibit, 2002. OFC 2002,* 2002, pp. 367-368.

[22] M. Ohm, "Optical 8-DPSK and receiver with direct detection and multilevel electrical signals," in *Advanced Modulation Formats, 2004 IEEE/LEOS Workshop on,* 2004, pp. 45-46.

[23] B. Vasic, V.S. Rao, I.B. Djordjevic, R.K. Kostuk and I. Gabitov, "Ghost-pulse reduction in 40-Gb/s systems using line coding," *Photonics Technology Letters, IEEE,* vol. 16, pp. 1784-1786, 2004.

[24] J. B. Stark, J. E. Mazo and R. Laroia, "Phased amplitude-shift signaling (PASS) codes: Increasing the spectral efficiency of DWDM transmission," in *Optical Communication, 1998. 24th European Conference on,* 1998, pp. 373-374 vol.1.

[25] E. Forestieri and G. Prati, "Novel optical line codes tolerant to fiber chromatic dispersion," *Lightwave Technology, Journal of,* vol. 19, pp. 1675-1684, 2001.

[26] D. J. Costello Jr., J. Hagenauer, H. Imai and S. B. Wicker, "Applications of error-control coding," *Information Theory, IEEE Transactions on,* vol. 44, pp. 2531-2560, 1998.

[27] S. Bigo, "Multiterabit/s DWDM terrestrial transmission with bandwidth-limiting optical filtering," *Selected Topics in Quantum Electronics, IEEE Journal of,* vol. 10, pp. 329-340, 2004.

[28] M. Birk, D. Fishman and P. Magill, "Field trial of end-to-end OC-768 transmission using 9 WDM channels over 1000 km of installed fiber," in *Optical Fiber Communications Conference, 2003. OFC 2003,* 2003, pp. 290-291 vol.1.

[29] A. H. Gnauck and P. J. Winzer, "Optical phase-shift-keyed transmission," *Lightwave Technology, Journal of,* vol. 23, pp. 115-130, 2005.

[30] G. Jacobsen, *Noise in Digital Optical Transmission Systems.* Norwood,MA: Artech house, 1994.

[31] Gitlin, Richard D. Hayes,Jeremiah F., and S. B. 1934- Weinstein, "Data communications principles," pp. 733, 1992.

[32] P.J. Winzer, S. Chandrasekhar and Hoon Kim, "Impact of filtering on RZ-DPSK reception," *Photonics Technology Letters, IEEE,* vol. 15, pp. 840-842, 2003.

[33] Hoon Kim and P. J. Winzer, "Nonlinear phase noise in phase-coded transmission," in *Optical Fiber Communication Conference, 2005. Technical Digest. OFC/NFOEC,* 2005, pp. 3 pp. Vol. 4.

[34] N. Yoshikane and I. Morita, "1.14 b/s/Hz spectrally efficient 50×85.4-Gb/s transmission over 300 km using copolarized RZ-DQPSK signals," *Lightwave Technology, Journal of,* vol. 23, pp. 108-114, 2005.

[35] Ying Jiang, Xuefeng Tang, J. C. Cartledge and K. Roberts, "Electronic Pre-Compensation of Narrow Optical Filtering for OOK, DPSK and DQPSK Modulation Formats," *Lightwave Technology, Journal of,* vol. 27, pp. 3689-3698, 2009.

[36] A. H. Gnauck, P. J. Winzer, S. Chandrasekhar, X. Liu, B. Zhu and D. W. Peckham, "Spectrally Efficient Long-Haul WDM Transmission Using 224-Gb/s Polarization-Multiplexed 16-QAM," *Lightwave Technology, Journal of,* vol. 29, pp. 373-377, 2011.

[37] Jin Wang and J. M. Kahn, "Impact of chromatic and polarization-mode dispersions on DPSK systems using interferometric demodulation and direct detection," *Lightwave Technology, Journal of,* vol. 22, pp. 362-371, 2004.

[38] D.M. Gill, A.H. Gnauck, Xiang Liu, Xing Wei, D.S. Levy, S. Chandrasekhar and C.R. Doerr, "42.7-Gb/s cost-effective duobinary optical transmitter using a commercial 10-Gb/s Mach-Zehnder modulator with optical filtering," *Photonics Technology Letters, IEEE,* vol. 17, pp. 917-919, 2005.

[39] J. G. S. Proakis Masoud., "Communication systems engineering," pp. 801, 2002.

[40] C. E. Shannon, "A mathematical theory of communication," *Bell Syst. Tech. J.,* vol. 27, pp. 379-423-623-656, 1948.

APPENDIX A

List of Acronyms

ACRZ - Alternate-chirp return-to-zero
AMI - Alternate-mark inversion
ASE - Amplified spontaneous emission
BER - Bit-error ratio
CD - Chromatic dispersion
C-NRZ - Chirped nonreturn-to-zero
CRZ Chirped return-to-zero
CSRZ - Carrier-suppressed return-to-zero
DB - Duobinary
DCF - Dispersion-compensating fiber
DCS - Duobinary carrier suppressed
DFB - Distributed feedback laser
DGD - Differential group delay
DI - Delay interferometer
DM - Data modulation
DMF - Data modulation format
DML - Directly modulated laser
DPSK - Differential phase shift keying
DQPSK - Differential quadrature phase shift keying
DST - Dispersion-supported transmission
EAM - Electroabsorption modulator
EML - Electroabsorption modulated laser
EPD - Electronic predistortion
FEC - Forward error correction
FM - Frequency modulation
FWM - Four-wave mixing
GVD - Group velocity dispersion
IFWM - Intrachannel four-wave mixing
ISD - Information spectral density
ISI - Intersymbol interference
ITU - International telecommunication union
IXPM - Intrachannel cross-phase modulation
M-ASK - Multilevel amplitude shift keying
MI - Modulation instability
MLSE - Maximum-likelihood sequence estimator
MPI - Multipath interference
MZM - Mach–Zehnder modulator
NL - Nonlinearity
NRD - Net residual dispersion
NRZ - Nonreturn-to-zero

NZDF - Nonzero dispersion shifted fiber
OA - Optical amplifier
OADM -Optical add/drop multiplexer
OOK - On/off keying
OSNR - Optical signal-to-noise ratio
OXC - Optical crossconnect
PASS - Phased amplitude shift signaling
PMD - Polarization-mode dispersion
Pol-SK - Polarization shift keying
PSBT - Phase-shaped binary transmission
IFWM - Intrachannel four-wave mixing
ISD - Information spectral density
ISI - Intersymbol interference
ITU - International telecommunication union
IXPM - Intrachannel cross-phase modulation
M-ASK - Multilevel amplitude shift keying
MI - Modulation instabilit
MLSE - Maximum-likelihood sequence estimator
MPI - Multipath interference
MZM - Mach–Zehnder modulator
NL - Nonlinearity
NRD - Net residual dispersion
NRZ - Nonreturn-to-zero
NZDF - Nonzero dispersion shifted fiber
OA - Optical amplifier
OADM - Optical add/drop multiplexer
OOK - On/off keying
OSNR - Optical signal-to-noise ratio
OXC - Optical crossconnect
PASS - Phased amplitude shift signaling
PMD - Polarization-mode dispersion
Pol-SK - Polarization shift keying
PSBT - Phase-shaped binary transmission
PSP - Principal state of polarization
RDPS - Residual dispersion per span
RF - Radiofrequency
ROADM - Reconfigurable OADM
RX - Receiver
RZ - Return-to-zero
SE - Spectral efficiency
SPM - Self-phase modulation
SSB - Single sideband
SSMF - Standard single-mode fiber
TX - Transmitter
VSB - Vestigial sideband
WDM - Wavelength division multiplexing

APPENDIX B

Crosstalk

SE = 0.4 Δλ = 0.1 THz B=40GHz Insertion loss= 0dB Attenuation= 0dB		BW=100GHz	BW=100GHz
Crosstalk		BER	FEC BER
CSRZ		0.0000E+00	0.0000E+00
DPSK33		2.3798E-64	0.0000E+00
DPSK50		1.2382E-13	6.5748E-97
DPSK66		1.4820E-06	3.2903E-33
NRZ DPSK		1.1837E-04	3.9174E-16
SDQPSK33		0.0000E+00	0.0000E+00
PDQPSK33		1.9952E-23	0.0000E+00
SDQPSK50		4.9527E-212	0.0000E+00
PDQPSK50		2.2315E-24	0.0000E+00
DQPSK66		5.9443E-168	0.0000E+00
DQPSK66		3.0615E-26	0.0000E+00
SNDQPSK		7.5543E-159	0.0000E+00
PNDQPSK		2.5608E-28	0.0000E+00

SE = 0.4 Δλ = 0.1 THz B=40GHz Insertion loss= 0dB Attenuation= 0dB		BW=50GHz	BW=50GHz
Crosstalk		BER	FEC BER
CSRZ		1.7969E-16	1.2536E-121
DPSK33		1.0000E-02	1.0000E-02
DPSK50		1.0000E-02	1.0000E-02
DPSK66		1.0000E-02	1.0000E-02
NRZ DPSK		1.1984E-14	4.8946E-106
SDQPSK33		2.0745E-120	0.0000E+00
PDQPSK33		2.6871E-17	0.0000E+00
SDQPSK50		1.1743E-89	0.0000E+00
PDQPSK50		6.5524E-11	2.1272E-72
DQPSK66		1.9557E-27	0.0000E+00
DQPSK66		1.7194E-11	1.2549E-77
SNDQPSK		1.4216E-130	0.0000E+00
PNDQPSK		1.5202E-24	0.0000E+00

SE = 0.8 Δλ = 0.08 THz B=100GHz Attenuation= 0dB Insertion loss = 0dB			
		BW=100GHz	BW=100GHz
Crosstalk		0 dBm BER	0 dBm FEC BER
CSRZ		5.9040E-05	7.8966E-19
DPSK33		1.0000E-02	1.0000E-02
DPSK50		1.0000E-02	1.0000E-02
DPSK66		1.0000E-02	1.0000E-02
NRZ DPSK		1.0000E-02	1.0000E-02
SDQPSK33		1.0000E-02	1.0000E-02
PDQPSK33		1.0000E-02	1.0000E-02
SDQPSK50		1.0000E-02	1.0000E-02
PDQPSK50		1.0000E-02	1.0000E-02
DQPSK66		2.1056E-13	7.7526E-95
DQPSK66		9.4462E-05	5.2550E-17
SNDQPSK		1.0000E-02	1.0000E-02
PNDQPSK		1.0000E-02	1.0000E-02

SE = 0.8 Δλ = 0.08 THz B=100GHz Attenuation= 0dB Insertion loss = 0dB			
		BW=50GHz	BW=50GHz
Crosstalk		0 dBm BER	0 dBm FEC BER
CSRZ		5.0051E-04	1.2007E-10
DPSK33		1.0000E-02	1.0000E-02
DPSK50		1.0000E-02	1.0000E-02
DPSK66		1.0000E-02	1.0000E-02
NRZ DPSK		1.0000E-02	1.0000E-02
SDQPSK33		1.0000E-02	1.0000E-02
PDQPSK33		1.0000E-02	1.0000E-02
SDQPSK50		1.0000E-02	1.0000E-02
PDQPSK50		1.0000E-02	1.0000E-02
DQPSK66		8.6904E-09	2.7013E-53
DQPSK66		1.0000E-02	1.0000E-02
SNDQPSK		1.0000E-02	1.0000E-02
PNDQPSK		1.0000E-02	1.0000E-02

SE = 0.8 Δλ = 0.05 THz B=40GHz Attenuation= 0dB Insertion loss= 0dB			
		BW=100GHz	BW=100GHz
Crosstalk		0 dBm BER	0 dBm FEC BER
CSRZ		1.1370E-172	0.0000E+00
DPSK33		1.0000E-02	1.0000E-02
DPSK50		1.0000E-02	1.0000E-02
DPSK66		1.0000E-02	1.0000E-02
NRZ DPSK		1.6337E-03	1.8376E-06
SDQPSK33		1.0000E-02	1.0000E-02
PDQPSK33		3.4517E-20	0.0000E+00
SDQPSK50		1.0000E-02	1.0000E-02
PDQPSK50		1.6931E-08	1.0922E-50
DQPSK66		1.0000E-02	1.0000E-02
DQPSK66		5.4138E-28	0.0000E+00
SNDQPSK		8.8433E-174	0.0000E+00
PNDQPSK		7.5055E-30	0.0000E+00

SE = 0.8 Δλ = 0.05 THz B=40GHz Attenuation= 0dB Insertion loss= 0dB			
		BW=50GHz	BW=50GHz
Crosstalk		0 dBm BER	0 dBm FEC BER
CSRZ		1.1308E-03	1.0481E-07
DPSK33		1.0000E-02	1.0000E-02
DPSK50		1.0000E-02	1.0000E-02
DPSK66		1.0000E-02	1.0000E-02
NRZ DPSK		9.8974E-07	8.7002E-35
SDQPSK33		1.7012E-11	1.1400E-77
PDQPSK33		1.0000E-02	1.0000E-02
SDQPSK50		3.9911E-05	2.3680E-20
PDQPSK50		7.0180E-04	2.1002E-09
DQPSK66		3.5579E-05	8.4543E-21
DQPSK66		1.2129E-04	4.8668E-16
SNDQPSK		1.0000E+00	5.0000E-01
PNDQPSK		1.0000E+00	5.0000E-01

Filter narrowing single channel

SE = 0.4 Δλ = 0.1 THz B=40GHz Insertion loss= 0dB Attenuation= 0dB
BW=100GHz

Filter Narrowing all OADM's @ 193.4	# OADM	BER	FEC BER
CSRZ	12	1.7962E-04	1.5815E-14
DPSK33	13	1.4297E-06	2.3818E-33
DPSK50	11	6.6698E-06	2.4811E-27
DPSK66	8	3.3929E-04	4.1945E-12
NRZ DPSK	8	9.9012E-10	8.7381E-62
SDQPSK33	20	3.5044E-41	0.0000E+00
PDQPSK33	20	2.7140E-11	7.6338E-76
SDQPSK50	20	8.7794E-12	2.9608E-80
PDQPSK50	20	3.6156E-07	1.0086E-38
DQPSK66	16	1.0258E-17	0.0000E+00
DQPSK66	16	7.9090E-12	1.1569E-80
SNDQPSK	20	2.8997E-14	1.4243E-102
PNDQPSK	20	4.3115E-22	0.0000E+00

SE = 0.4 Δλ = 0.1 THz B=40GHz Insertion loss= 0dB Attenuation= 0dB
BW=50GHz

Filter Narrowing all OADM's @ 193.4	# OADM	BER	FEC BER
CSRZ	1	3.3050E-05	4.3631E-21
DPSK33	1	1.0000E-02	1.0000E-02
DPSK50	1	1.0000E-02	1.0000E-02
DPSK66	1	6.5209E-05	1.9207E-18
NRZ DPSK	1	1.1957E-05	4.7222E-25
SDQPSK33	12	1.3492E-10	1.4152E-69
PDQPSK33	15	1.0355E-03	5.1667E-08
SDQPSK50	4	5.6374E-08	5.4940E-46
PDQPSK50	4	2.2829E-07	1.6090E-40
DQPSK66	1	1.0000E-02	1.0000E-02
DQPSK66	1	2.5061E-03	4.0011E-05
SNDQPSK	6	4.5803E-22	0.0000E+00
PNDQPSK	4	2.2330E-24	0.0000E+00

SE = 0.8 Δλ = 0.08 THz B=100GHz Attenuation= 0dB Insertion loss = 0dB			
BW=100GHz			
Filter Narrowing all OADM's @ 193.4	# OADM	0 dBm BER	0 dBm FEC BER
CSRZ	18	3.1374E-05	2.7353E-21
DPSK33	1	1.0000E-02	1.0000E-02
DPSK50	1	1.0000E-02	1.0000E-02
DPSK66	8	2.8868E-05	1.2963E-21
NRZ DPSK	1	1.0000E-02	1.0000E-02
SDQPSK33	6	1.2396E-10	6.6043E-70
PDQPSK33	6	1.5658E-05	5.3288E-24
SDQPSK50	1	1.0000E-02	1.0000E-02
PDQPSK50	1	1.0000E-02	1.0000E-02
DQPSK66	1	1.0000E-02	1.0000E-02
DQPSK66	1	4.3404E-05	5.0229E-20
SNDQPSK	2	2.4792E-07	3.3802E-40
PNDQPSK	3	3.5059E-15	8.6150E-111

SE = 0.8 Δλ = 0.08 THz B=100GHz Attenuation= 0dB Insertion loss = 0dB			
BW=50GHz			
Filter Narrowing all OADM's @ 193.4	# OADM	0 dBm BER	0 dBm FEC BER
CSRZ	20	7.1419E-07	4.6159E-36
DPSK33	1	1.0000E-02	1.0000E-02
DPSK50	1	1.0000E-02	1.0000E-02
DPSK66	7	2.3703E-03	2.7307E-05
NRZ DPSK	1	1.0000E-02	1.0000E-02
SDQPSK33	1	1.0000E-02	1.0000E-02
PDQPSK33	1	1.0000E-02	1.0000E-02
SDQPSK50	1	1.0000E-02	1.0000E-02
PDQPSK50	1	6.5883E-04	1.2360E-09
DQPSK66	1	1.0586E-03	6.1729E-08
DQPSK66	1	7.5993E-04	4.0807E-09
SNDQPSK	1	1.0000E+00	5.0000E-01
PNDQPSK	1	1.0000E+00	5.0000E-01

SE = 0.8 Δλ = 0.05 THz B=40GHz			
BW=100GHz			
Filter Narrowing all OADM's @ 193.4	# OADM	0 dBm BER	0 dBm FEC BER
CSRZ	20	2.5117E-04	3.0316E-13
DPSK33	16	1.2965E-04	8.7977E-16
DPSK50	16	5.6733E-04	3.4930E-10
DPSK66	12	4.0513E-04	1.9508E-11
NRZ DPSK	12	3.1577E-08	2.9819E-48
SDQPSK33	20	3.5044E-41	0.0000E+00
PDQPSK33	20	3.6818E-20	0.0000E+00
SDQPSK50	20	8.7794E-12	2.9608E-80
PDQPSK50	20	3.6156E-07	1.0086E-38
DQPSK66	16	1.0258E-17	0.0000E+00
DQPSK66	5	2.6502E-17	0.0000E+00
SNDQPSK	7	9.5643E-73	0.0000E+00
PNDQPSK	5	3.4641E-34	0.0000E+00

SE = 0.8 Δλ = 0.05 THz B=40GHz			
BW=50GHz			
Filter Narrowing all OADM's @ 193.4	# OADM	0 dBm BER	0 dBm FEC BER
CSRZ	16	1.2811E-04	7.9122E-16
DPSK33	2	9.2554E-04	2.0749E-08
DPSK50	3	1.3799E-03	5.0359E-07
DPSK66	2	2.6344E-03	5.6047E-05
NRZ DPSK	1	1.1957E-05	4.7222E-25
SDQPSK33	12	1.3492E-10	1.4152E-69
PDQPSK33	12	4.02E-08	2.6359E-47
SDQPSK50	4	5.6374E-08	5.4940E-46
PDQPSK50	4	2.2829E-07	1.6090E-40
DQPSK66	1	2.9114E-02	5.5588E-02
DQPSK66	1	2.5061E-03	4.0011E-05
SNDQPSK	6	4.5803E-22	0.0000E+00
PNDQPSK	4	2.2330E-24	0.0000E+00

Filter narrowing adjacent channels

SE = 0.4 Δλ = 0.1 THz B=40GHz Insertion loss= 0dB Attenuation= 0dB			
BW=100GHz			
Filter Narrowing 193.2 to 193.6	# sets OADM	BER	FEC BER
CSRZ	5	1.3560E-03	4.3955E-07
DPSK33	5	8.9878E-08	3.6564E-44
DPSK50	5	1.2864E-06	9.2059E-34
DPSK66	4	1.5422E-03	1.1860E-06
NRZ DPSK	3	8.3125E-12	1.8104E-80
SDQPSK33	5	6.4196E-07	1.7683E-36
PDQPSK33	4	3.4096E-05	5.7699E-21
SDQPSK50	5	3.2328E-06	3.6739E-30
PDQPSK50	4	5.1034E-04	1.4180E-10
DQPSK66	2	9.9178E-06	8.7919E-26
DQPSK66	3	9.2963E-05	4.5566E-17
SNDQPSK	5	8.8096E-11	3.0535E-71
PNDQPSK	5	4.4013E-05	5.6911E-20

SE = 0.4 Δλ = 0.1 THz B=40GHz Insertion loss= 0dB Attenuation= 0dB			
BW=50GHz			
Filter Narrowing 193.2 to 193.6	# sets OADM	BER	FEC BER
CSRZ	5	0.0000E+00	0.0000E+00
DPSK33	2	1.2444E-03	2.2412E-07
DPSK50	2	1.0244E-03	4.7333E-08
DPSK66	1	8.2516E-05	1.5732E-17
NRZ DPSK	5	0.0000E+00	0.0000E+00
SDQPSK33	5	1e-321	0.0000E+00
PDQPSK33	5	2.6320E-34	0.0000E+00
SDQPSK50	5	1.9060E-142	0.0000E+00
PDQPSK50	5	1.7733E-29	0.0000E+00
DQPSK66	5	9.8241E-22	0.0000E+00
DQPSK66	5	1.4537E-19	0.0000E+00
SNDQPSK	5	5.9372E-111	0.0000E+00
PNDQPSK	5	5.2002E-30	0.0000E+00

SE = 0.8 Δλ = 0.08 THz B=100GHz Attenuation= 0dB Insertion loss = 0dB			
BW=100GHz			
Filter Narrowing 193.24, 193.32, 193.48, 193.56	# sets OADM	0 dBm BER	0 dBm FEC BER
CSRZ	1	1.0000E-02	1.0000E-02
DPSK33	2	1.0333E-03	5.0796E-08
DPSK50	1	4.7567E-08	1.1912E-46
DPSK66	5	3.1210E-18	0.0000E+00
NRZ DPSK	3	6.8771E-04	1.7721E-09
SDQPSK33	1	1.0000E-02	1.0000E-02
PDQPSK33	1	1.0000E-02	1.0000E-02
SDQPSK50	1	3.7532E-16	6.4187E-119
PDQPSK50	1	3.1156E-06	2.6356E-30
DQPSK66	1	1.0000E-02	1.0000E-02
DQPSK66	1	1.0000E-02	1.0000E-02
SNDQPSK	1	1.0000E-02	1.0000E-02
PNDQPSK	1	1.7259E-06	1.2961E-32

SE = 0.8 Δλ = 0.08 THz B=100GHz Attenuation= 0dB Insertion loss = 0dB			
BW=50GHz			
Filter Narrowing 193.24, 193.32, 193.48, 193.56	# sets OADM	0 dBm BER	0 dBm FEC BER
CSRZ	1	1.0000E-02	1.0000E-02
DPSK33	1	1.0000E-02	1.0000E-02
DPSK50	1	1.0000E-02	1.0000E-02
DPSK66	1	1.4344E-03	6.7984E-07
NRZ DPSK	1	1.0000E-02	1.0000E-02
SDQPSK33	5	8.1854E-10	1.5761E-62
PDQPSK33	5	1.3468E-05	1.3763E-24
SDQPSK50	2	6.7740E-16	2.4675E-117
PDQPSK50	1	4.1364E-08	3.3867E-47
DQPSK66	1	2.3236E-03	2.3786E-05
DQPSK66	1	1.6701E-08	9.6593E-51
SNDQPSK	5	5.9269E-09	8.6224E-55
PNDQPSK	5	1.5557E-09	5.0996E-60

SE = 0.8 Δλ = 0.05 THz B=40GHz Attenuation= 0dB Insertion loss= odB			
BW=100GHz			
Filter Narrowing 193.3, 193.35, 193.45, 193.5	# sets OADM	0 dBm BER	0 dBm FEC BER
CSRZ	1	5.7445E-05	6.1801E-19
DPSK33	1	1.4206E-10	2.2509E-69
DPSK50	1	2.9064E-06	1.4103E-30
DPSK66	1	1.0000E+00	5.0000E-01
NRZ DPSK	1	5.2791E-14	3.0716E-100
SDQPSK33	1	7.2720E-05	5.0888E-18
PDQPSK33	1	1.0000E-02	1.0000E-02
SDQPSK50	1	1.0000E-02	1.0000E-02
PDQPSK50	1	1.0000E-02	1.0000E-02
DQPSK66	1	1.0000E-02	1.0000E-02
DQPSK66	1	1.0000E-02	1.0000E-02
SNDQPSK	1	1.0000E-02	1.0000E-02
PNDQPSK	1	1.0000E-02	1.0000E-02

SE = 0.8 Δλ = 0.05 THz B=40GHz Attenuation= 0dB Insertion loss= 0dB			
BW=50GHz			
Filter Narrowing 193.3, 193.35, 193.45, 193.5	# sets OADM	0 dBm BER	0 dBm FEC BER
CSRZ	4	1.7483E-03	3.0554E-06
DPSK33	1	1.0000E-02	1.0000E-02
DPSK50	1	1.0000E-02	1.0000E-02
DPSK66	1	1.3073E-03	3.3033E-07
NRZ DPSK	1	1.0000E+00	5.0000E-01
SDQPSK33	4	2.0458E-05	5.8879E-23
PDQPSK33	3	8.4365E-05	1.9171E-17
SDQPSK50	2	3.6037E-12	9.7958E-84
PDQPSK50	2	1.3899E-05	1.8259E-24
DQPSK66	1	1.0000E-02	1.0000E-02
DQPSK66	1	2.4564E-14	3.2069E-103
SNDQPSK	2	2.7372E-47	0.0000E+00
PNDQPSK	3	1.5518E-10	4.9844E-69